Tryptophan and proline scanning mutagenesis:
A tool to study the aggregation of tau protein into
Alzheimer paired helical filaments

Doctoral thesis submitted to the

Department of Biology, Hamburg University

Presented by

Li Li

From P. R. China

Hamburg, 2003

Genehmigt vom
Fachbereich Biologie der
Universität Hamburg
auf Antrag von Herrn Professor Dr. E. MANDELKOW

Weitere Gutachter der Dissertation:
Herr Priv.-Doz. Dr. H. QUADER

Tag der Disputation: 10. Januar 2003

Hamburg, den 10. Dezember 2002

Professor Dr. U. Wienand
Dekan

Table of contents

Acknowledgements

I am grateful to Prof. Dr. Eckhard Mandelkow and Dr. Eva Maria Mandelkow who introduced me to the reasearch field, provided this interesting theme and constant advice throughout this work.

I would also like to thank Prof. Dr. H. Quader for surveying my thesis.

I owe special thanks to Dr. Martin von Bergen who provided many suggestions and expert advice throughout this thesis.

I want to thank Dr. Jacek Biernat, Dr. Stefan Barghorn, Dr. Claire Goldsbury for many insightful suggestions, help and critical reading of this thesis.

Many other colleagues kindly helped me in many ways whose names cannot be listed here. They all gave me a pleasant working environment, warmhearted help, and I am happy to be one of this group.

I. Introduction

1. Alzheimer's Disease (AD)

In 1907, Alois Alzheimer published a case of a 51-year old female patient, who suffered from strong feelings of jealousy, increased memory impairment, disorientation, hallucinations, and often loud and aggressive behaviour. After four and a half years of rapidly deteriorating mental illness, she died in a completely demented state (Alzheimer, 1907). Now this disease carries the doctor's name – Alzheimer's disease.

Alzheimer's disease (AD) is an age-related brain disorder that is characterized by a slow progressive loss of memory and other cognitive functions and a deterioration of behaviour and social adaptation. AD is the most common cause of dementia among people 65 years of age and older. In most people with AD, symptoms first appear after age 60, the earliest symptoms characteristically include loss of recent memory, later compounded by faulty judgement, and changes in personality. On average, patients with AD live for 8 to 10 years after they are diagnosed, though the disease can last for up to 20 years. Most commonly, people with AD die of pneumonia.

Scientists estimate that in worldwide, up to 15 million people currently suffer from Alzheimer's disease (Ernst and Hay, 1994) and the prevalence (the number of people with the disease at any one time) doubles every 5 years beyond age 65. It is also estimated that approximately 360 000 new cases (incidence) will occur each year and this number will increase as the population ages (Brookmeyer et al., 1998).

The certainty of a diagnosis of AD, in its sporadic form, can be established at the present time only by a post-mortem pathologic examination, while during the life of the patient, only a diagnosis at best probable, can be established after a neuropsychological and behavioural evaluation (Growdon, 1999; Ritchie and Touchon, 2000). Biopsies performed ante-mortem pose ethical problems and are very often non-informative.

Post-mortem studies of brains from AD patients show cortical atrophy with loss of 8 to 10% of the brain weight every 10 years of disease progression. Through post-mortem identification of the location of the damaged neurons and the severity of the pathology, six stages in the evolution of the neurological changes can be differentiated (Braak et al., 1994; Braak and Braak, 1997; Braak and Braak, 1991; Hyman, 1998; Hyman and Trojanowski, 1997; Nagy et al., 1997; Samuel et al., 1997; Samuel et al., 1996). With the degeneration of the neocortex, patients become severely demented, and major disturbances of autonomic functions reflect the far-reaching devastation of the limbic loop centers.

Two abnormal structures in the brain are the hallmarks of AD: amyloid plaques and neurofibrillary tangles (NFTs)(Fig. 1)(Hauw et al., 1996). The amyloid plaques are extracellular deposits mainly localized in the cortex. They contain degenerated neurites and a 39-43 amino acid peptide called β-amyloid (Aβ), which has a natural tendency to form insoluble fibrils (Vickers et al., 2000). NFTs are intraneuronal filamentous deposits consisting largely of hyperphosphorylated tau proteins. NFTs form intracellulary, and the cells containing NFTs have lost the rest of their characteristic cytoskeleton (Gray et al., 1987). Electron microscopy analysis shows that NFTs are composed of filamentous structures called paired helical filaments (PHFs) and are associated with ubiquitin. These lesions are accompanied by deterioration of the neuronal system, and their distribution is correlated with multiple deficits of the neurotransmitters implicated in cholinergic, monoaminergic, and peptidergic systems (Moller, 1999; Sirvio, 1999).
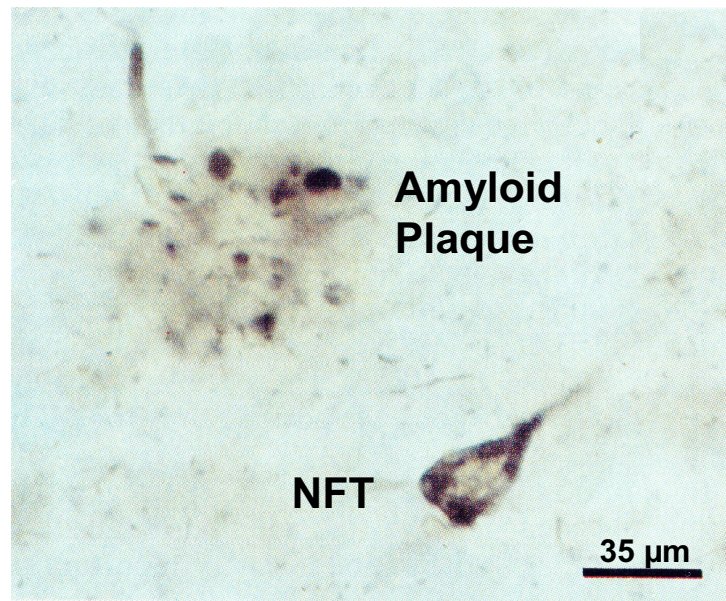
Fig. 1: Immunohistochemical staining of the two hallmarks in AD: a NFT and an amyloid plaque, which obtained from an Alzheimer patient brain (from Spillantini et al., 1990, modified).

It has been known that clinically typical AD can cluster in families and can specifically be inherited in an autosomal dominant fashion. In the last 15 years significant advances in genetic mapping and positional cloning approaches have clarified the genetic contribution to AD, providing evidence that even in the relatively small subgroup of familial AD (FAD) there are probably several different abnormally expressed genes and thus FAD is a genetically heterogeneous disorder. The gene defects responsible for early-onset FAD (<65 year) are presenilin 2 (PS2), presenilin 1 (PS1), amyloid β protein precursor (APP), and apolipoprotein E (Apo-E) gene for late-onset FAD respectively (for review, see Selkoe, 2001; Sorbi et al., 2001).

1.1 Amyloid plaques

In Alzheimer's disease, amyloid plaques consist of insoluble fibrillar deposits and can be 5 to 200 μm in diameter. The major component of the deposits is the Aβ peptide – derived from a transmembrane glycoprotein precursor produced by neurons and glial cells: the Aβ precursor protein (βAPP). The physiological pathway of maturation of

βAPP – the secretory pathway – leads, under the action of a α-secretase, to the release of soluble peptide fragments deprived of amyloid-forming capacity. A minor metabolic pathway, the endosomal-lysosomal pathway, leads to the formation of amyloid peptides 39/40 or 42/43 amino acids long according to their neuronal or vascular localization, respectively. The endosomal-lysosomal pathway has recently been shown to depend on a transmembrane aspartic protease named BACE (β-site APP-cleaving enzyme) (Bennett et al., 2000; Farzan et al., 2000; Greenfield et al., 2000; Haniu et al., 2000; Sauder et al., 2000). *In vitro* studies showed that the soluble, α-helical form of Aβ has a strong tendency to form an insoluble β-sheet, which is neurotoxic (Pitschke et al., 1998). The demonstration of the association of heparan sulfate proteoglycans with amyloid deposits and neurofibrillary tangles suggests that these molecules may contribute to the formation of the amyloid deposits (Castillo et al., 1999; McLaurin et al., 1999).

It has been suggested that the formation of neurofibrillary tangles, the other characteristic lesion in AD, could be mediated by amyloid deposit toxicity (Delacourte, 1998). However, the observation, in some patients, of diffuse Aβ deposits without senile plaques nor syndromes of dementia (Berr et al., 1994) and the presence of neurofibrillary tangles in very old AD patients without amyloid deposits (Bancher and Jellinger, 1994) limits the range of the Aβ hypothesis. Recent transgenic experiments and studies of a variant form of FAD suggest that Aβ deposition may not be sufficient to cause AD (Shastry and Giblin, 1999).

1.2 Pathological aggregation of tau proteins

One of the best markers of Alzheimer's disease is the deposition of tau in neurofibrillary aggregates in the brain, in the form of paired helical filaments (PHFs). Changes such as aggregation, hyperphosphorylation, loss of microtubule binding, glycation, proteolysis, or ubiquitination are most prominent in Alzheimer tau (Friedhoff and Mandelkow, 1999). Until recently, it was thought that abnormal phosphorylation of tau proteins was responsible for their aggregation in AD. However, normal tau proteins are also

phosphorylated in fetal and adult brain, and they do not aggregate to form filamentous inclusions. Moreover, non-phosphorylated recombinant tau proteins can form filamentous structures under physiological conditions *in vitro*, implying that the hyperphosphorylation of tau in Alzheimer's disease may not be directly responsible for the pathological aggregation into PHFs. On the contrary, phosphorylation may be protective against aggregation (Schneider et al., 1999), and could simply reflect an altered balance between kinases and phosphatases (Anderton et al., 1995). On the other hand, oxidative stress is likely to contribute to PHF assembly since disulfide bridge formation promotes tau dimerization and hence filament assembly (Schweers et al., 1995). Other factors important in PHF assembly are acidic cofactors such as heparin, RNA (Goedert et al., 1996; Kampers et al., 1996; Perez et al., 1996), or lipids (Wilson and Binder, 1997). All these data suggest that, in addition to phosphorylation, other mechanisms may be involved in the formation of pathological tau filaments, but whether the accumulation of intracellular tau aggregates or paired helical filaments (PHFs) is toxic is not clear at present.

Although the neurofibrillary pathology of tau is most obvious in Alzheimer's disease, it occurs in other diseases as well, such as Parkinson's disease, Pick's disease, Creutzfeldt-Jacob's disease, Downs syndrome and inclusion-body myositis. The diversity of diseases suggests that neurofibrillary pathology involving tau protein may be the consequence of different causative factors. The possibility that the aggregation of tau is one of the factors leading to cell death is left open.

1.2.1 Tauopathies and FTDP-17 mutations

A group of heterogeneous dementias and movement disorders that are characterized neuropathologically by prominent intracellular accumulations of abnormal filaments formed by the microtubule associated protein tau appears to share common mechanisms of disease. They are collectively known as neurodegenerative tauopathies. Despite their diverse phenotypic manifestations, brain dysfunction and degeneration in tauopathies is linked to the progressive accumulation of filamentous tau inclusions, and this, together with the absence of other disease specific neuropathological abnormalities, provided

circumstantial evidence implicating abnormal tau in disease onset and/or progression. However, this view remained unproven and highly controversial until 1998, when multiple tau gene mutations were discovered in frontotemporal dementia and parkinsonism linked to chromosome 17 (FTDP-17)(Foster et al., 1997), thereby providing unequivocal evidence that tau abnormalities alone are sufficient to cause neurodegenerative disease (Hutton et al., 1998; Poorkaj et al., 1998; Spillantini et al., 1998). This seminal finding opened up new avenues for investigating the role of tau abnormalities in mechanisms of brain dysfunction and degeneration (for review, see Virginia M-Y Lee, 2001).

Frontotemporal dementia and parkinsonism linked to chromosome 17 (FTDP-17) is characterized by behavioural, cognitive and motor disturbances (Foster et al., 1997). Pathological changes in the brain include frontotemporal atrophy with neuronal loss, grey and white matter gliosis and superficial cortical spongiform. In addition, intraneuronal tau inclusions with the variable occurrence of glial inclusions are present in FTDP-17 brains (Dickson et al., 1995).

Two classes of FTDP-17 mutations are defined by *in vitro* functional analysis. One class affects tau-MT interaction properties, reducing the affinity of tau for MT and/or the ability of tau to stimulate MT polymerization (e.g. K257T, G272V, P310L, P301S, ΔK280, V337M, G389R, R406W) (Dayanandan et al., 1999; D'Souza et al., 1999; Murrell et al., 1999). Some of these mutations (P301L, ΔK280) also alter tau self aggregation properties, accelerating the *in vitro* formation of filaments (Barghorn et al., 2000; Goedert et al., 1999a). A second class of mutations alters the relative levels of four-repeat (4R) versus three-repeat (3R) tau by affecting alternative splicing of exon 10 (E10). These include missense mutations (N279K, N296H, and S305N), silent mutations (L284L, N296N, S305S) and deletion mutations (ΔK280, ΔN296) in E10 and intronic mutations (E10+3, E10+11, E10+12, E10+13, E10+14, E10+16) in intron 10 (I10). Most of these mutations increase the proportion of E10+ mRNA and thus the ratio of 4R to 3R tau isoforms (D'Souza and Schellenberg, 2002; Hong et al., 1998; Spillantini et al., 1998). Increasing the ratio of 4R forms of tau to 3R forms of tau by as little as two-fold results in FTDP-17, however, the mechanism by which this shift in ratio leads to neurodegeneration remains unclear. In contrast, the ΔK280 mutation

reduces the proportion of E10+ transcripts in exon trapping assays indicate that production of 4R forms of tau is significantly reduced (D'Souza et al., 1999; Rizzu et al., 1999). The mechanism by which this common variability in the tau gene influences the development of these neurodegenerative diseases is unclear, however, it further suggests a central role for tau in the pathogenesis of several neurodegenerative conditions including Alzheimer's disease.

1.2.2 Structure of paired helical filaments

PHFs have an appearance of two strands twisted around one another, such that the crossover repeats are around 75-80 nm and their apparent widths are 10-22 nm, as if each strand had a diameter of about 10 nm (Crowther and Wischik, 1985). A fraction of PHFs isolated from Alzheimer brain is not twisted but straight, as if the two protofibrils ran parallel to each other (Crowther, 1991). Other variants of tau filaments are observed in certain familial dementias, showing twisted ribbon-like filaments with an irregular periodicity of 90-130 nm (Goedert et al., 1999b; Ksiezak-Reding et al., 1994; Spillantini et al., 1997). Image reconstructions suggest that both appearances can be explained by a similar domain structure of the protofibrils (Crowther, 1991). The PHFs usually terminate in an abrupt fashion without fraying out, suggesting that the two strands are not separate entities on a molecular level. The main problem in all models of PHFs thus far is that their protein subunits cannot be clearly delineated so that the packing of molecules is still unknown.

It is widely accepted that all six tau isoforms occur in Alzheimer-PHFs (Jakes et al., 1991; Kosik et al., 1988). However, the state of isoform composition can be different in other dementias with tau pathology where 4R isoforms (e.g. PSP (Buee and Delacourte, 1999)) or 3R isoforms (e.g. Pick's disease (Delacourte et al., 1996)) predominate. Important constraints for structural models of tau filaments come from proteolytic cleavage and antibody labelling experiments, suggesting that the structural core of PHFs contains the equivalent of 3R (Novak et al., 1993; Wischik et al., 1988a). Recent data shows that a short hexapeptide stretch at the beginning of the second (^{275}VQIINK^{280})

and the third repeat (^{306}VQIVYK^{311}) induces PHF aggregation by forming β-structure (von Bergen et al., 2001; von Bergen et al., 2000).

1.2.3 Microtubule-associated protein tau

Tau proteins belong to the microtubule-associated proteins (MAP) family (Weingarten et al., 1975), tau is mainly expressed in neurons where they play an important role in the assembly of tubulin subunits into microtubules to constitute the neuronal microtubule network. Non-neuronal cells usually have only trace amounts. For instance, tau proteins can be expressed in glial cells mainly in pathological conditions (Chin and Goldman, 1996), it is possible to detect tau mRNA and proteins in low amounts in several peripheral tissues such as heart, kidney, lung, muscle, pancreas, testis, as well as in fibroblasts (Gu et al., 1996; Ingelson et al., 1996; Vanier et al., 1998). In the human genome there is only one tau gene, located on chromosome 17 at band position 17q21(Neve et al., 1986), which contains 16 exons (Andreadis et al., 1992), with the major tau protein isoform being encoded by 11 exons. Exon 4A is found in bovine, human and rodent peripheral tissues with a high degree of homology. Tau mRNAs with exon 8 has not been described in humans, although some transcripts with exon 8 are found in bovine and rhesus monkey brains (Himmler, 1989b; Nelson et al., 1996). Exon -1 is part of the promoter and is transcribed but not translated, exon 14 is found in messenger RNA, but it is not translated into protein (Andreadis et al., 1992; Goedert et al., 1989a; Goedert et al., 1989b). By alternative splicing of exons 2, 3 and 10, six main isoforms of tau with 352-441 amino acid residues are produced (Goedert et al., 1989a; Himmler et al., 1989a; Lee et al., 1988) (Fig. 2). There are zero, one, or two inserts of 29 residues each near the N-terminus (exon 2 and 3), and three or four homologous stretches of 31or 32 amino acid residues each. The 'repeat' R2 in the C-terminal half (encoded by exon 10) may be missing. The longest isoform has four repeats and two inserts (htau 40) with 441 residues, and the shortest (fetal) isoform has three repeats and no insert (htau23) with 352 residues. A 'big' tau isoform containing ~300 additional residues (exon 4A) is expressed in peripheral nerves (Couchie et al., 1992; Goedert et al., 1992).

1.2.3.1 Structure of tau protein

Tau molecules have a rodlike structure as judged by electron microscopy (56.1±14.1 nm long) and associate *in vitro* with microtubules (MTs), forming armlike projections (18.7±4.8 nm long) (Hirokawa et al., 1988). In microtubule preparations saturated with bound tau the ratio is one tau molecule per approximately two tubulin dimers (Gustke et al., 1994).

In human brain, the molecular weight of six tau isoforms ranges from 45 to 65 kDa when run on polyacrylamide gel electrophoresis in the presence of sodium dodecyl sulfate (SDS-PAGE). Tau contains either one or two cysteine residues – Cys291 in R2 (present only in 4R isoforms) and Cys322 in R3 (always present). This difference has an influence on *in vitro* PHF assembly (4R tau has two cysteine residues – Cys291 and Cys322, which can form various dimeric forms and an internal disulfide bridge upon oxidation) and the balance between isoforms may be important within the adult brain. The amino acid composition of tau is dominated by hydrophilic and charged residues; two inserts near the N-terminus are highly acidic and are followed by a basic proline-rich region. The N-terminal part is referred to as the projection domain because it projects from the microtubule surface where it may interact with other cytoskeletal elements and the plasma membrane (Brandt et al., 1995; Hirokawa et al., 1988; Steiner et al., 1990). The C-terminal half of tau (repeats plus flanking regions) constitutes the microtubule binding domain (Butner and Kirschner, 1991; Goode et al., 1997; Gustke et al., 1994). The repeat region is flanked upstream by the basic proline-rich region (about 25% proline) and downstream by another basic stretch also containing several prolines. Adult tau isoforms with 4R are more efficient at promoting microtubule assembly than the isoform with 3R (Ackmann et al., 2000; Butner and Kirschner, 1991; Goedert and Spillantini, 1990; Gustke et al., 1994).

Tau has resisted all efforts of crystallization so far (precluding an X-ray crystallographic analysis), and it is too large for a structural analysis by magnetic resonance methods. Therefore, details of the folding of the polypeptide chain are unknown. Most of the available structural data come from electron microscopy, IR and CD spectroscopy, or small angle X-ray scattering of tau in solution (Crowther, 1991; Crowther and Wischik,

1985; Kirschner et al., 1986; Schweers et al., 1994; Weingarten et al., 1975; Wille et al., 1992). Additional information comes from hydrodynamic and light scattering measurements showing that the polypeptide chain has a highly asymmetric shape (axial ratio of >10 (Cleveland et al., 1977)). In summary, these data argue for a natively unfolded conformation of tau with little α-helix and β-sheet (Schweers et al., 1994; Wille et al., 1992). This loose, open structure may explain why tau is resistant to heat, denaturants, or acids, because these treatments destroy the compact folding of other proteins but apparently do not harm tau. These experimental data are corroborated by various secondary structure prediction methods, which yield little α- or β-structure (less than 10% (Friedhoff and Mandelkow, 1999)).
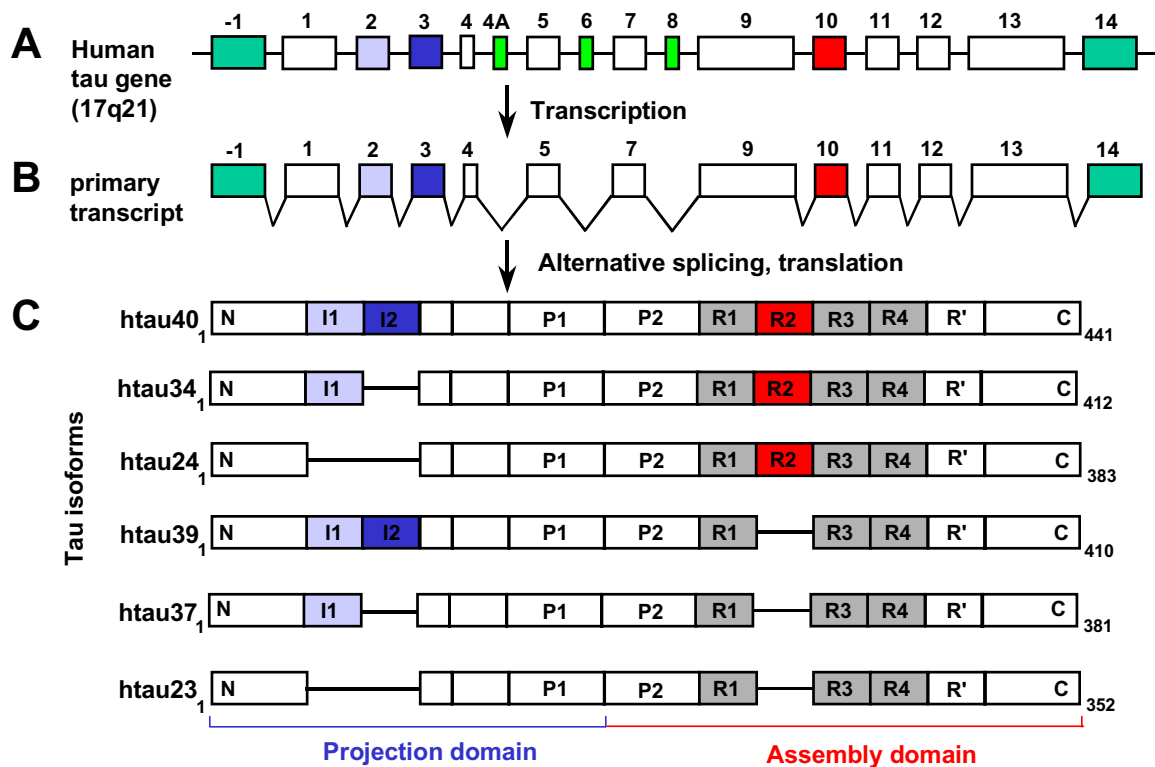
Fig. 2: Schematic representation of the human tau gene and the six tau isoforms.

(A): The human tau gene is located over 100 kb on the long arm of chromosome 17 at position 17q21. It contains 16 exons, with exon -1 being part of the promoter. Exons 6 and 8 are not transcribed in humans, exon 4A codes 254 additional residues in ´big` tau isoform, which is expressed only in peripheral nerves (light green).

(B): The tau primary transcript contains 13 exons; exons -1 and 14 are transcribed but not translated (dark green). Exons 1, 4, 5, 7, 9, 11, 12, 13 are constitutive (white), and exons 2, 3, 10 are alternatively spliced, giving rise to six different mRNAs that are to translate in six different tau isoforms. These isoforms differ by the absence or presence of one or two 29 amino acid inserts encoded by exon 2 (light blue) and 3 (dark blue) in the amino-terminal part, and the second repeat region R2 encoded by exon 10 (red) in the carboxy-terminal part.

(C): The six tau isoforms in the human central nervous system, with or without one or two N-terminal inserts (I1 = light blue, I2 = dark blue) and with three (R1, R3, R4 = grey) or four (R1, R3, R4 = grey, R2 = red) repeats in the C-terminal. Tau proteins can be separated by different domains. The projection domain (M1-Y197) contains boxes from N to P1, and the assembly domain contains boxes from P2 to C, which is the microtubule-binding domain. Boxes P1 and P2 are proline-rich regions, and R' is the pseudo-repeat region (Figure modified from Buee et al., 2000; Gustke et al., 1994).

1.2.3.2 Function of tau protein

The main functions of tau proteins are the stabilization of axonal microtubules affecting axonal transport (Drubin and Kirschner, 1986). Furthermore, tau proteins are known to promote tubulin polymerization *in vitro* (Brandt and Lee, 1993; Cleveland et al., 1977; Nixon and Sihag, 1991). They have been shown to increase the rate of microtubule

polymerization, and to inhibit the rate of depolymerization (Drechsel et al., 1992; Trinczek et al., 1995). Other functions include a role in signal transduction (Flanagan et al., 1997; Jenkins and Johnson, 1998), interaction with the actin cytoskeleton (Cunningham et al., 1997), neurite outgrowth (Biernat and Mandelkow, 1999; Esmaeli-Azad et al., 1994), interaction with the plasma membrane (Brandt et al., 1995; Lee et al., 1998), anchoring of enzymes such as protein kinases and phosphatases (Liao et al., 1998; Reszka et al., 1995; Sontag et al., 1996), and the regulation of intracellular vesicle transport (Ebneth et al., 1998)(for review, see Johnson and Hartigan, 1998; Mandelkow and Mandelkow, 1998).

1.2.3.3 Phosphorylation of tau protein

Tau proteins bind MTs through their microtubule-binding domains; however, MT assembly depends partially upon the phosphorylation state since phosphorylated tau proteins are less effective than non-phosphorylated tau proteins in promoting microtubule polymerization (Biernat et al., 1993; Bramblett et al., 1993; Cleveland et al., 1977). Tau phosphorylation is regulated physiologically, being higher during fetal and neonatal development than in the adult (Bramblett et al., 1993; Brion et al., 1999). Phosphorylation has been shown to be the key factor regulating MAP-microtubule interactions (Biernat et al., 1993; Drewes et al., 1997). Many of the identified phosphorylation sites are concentrated in the regions between amino acids 181 to 235, 396 to 422 and KXGS motifs within the repeat region. Most of these phosphorylation sites are Ser-Pro and Thr-Pro motifs and the different states of tau phosphorylation result from the activity of specific kinases and phosphatases towards these sites.

Most of the kinases involved in tau phosphorylation are proline-directed protein kinases (PDPK), which include mitogen activated protein kinase (MAPK) (Drewes et al., 1992; Goedert et al., 1997; Reynolds et al., 1997), glycogen synthase kinase 3 (GSK3)(Hanger et al., 1992; Mandelkow et al., 1992). Cyclin dependent kinases including cdc2 and cdk5 (Baumann et al., 1993) and stress-activated protein kinases (SAP kinase) act on tau and are involved in tau phosphorylation (Goedert et al., 1997; Jenkins and Johnson, 1998; Reynolds et al., 1997). There are still some other non Ser/Thr-Pro sites which can

be phosphorylated by non-proline-directed kinases, including microtubule-affinity regulating kinase (MARK)(Drewes et al., 1997), Ca^{2+}/calmodulin-dependent protein kinase II (CaMPK II) (Johnson, 1992; Steiner et al., 1990), cyclic-AMP-dependent kinase (PKA) (Drewes et al., 1995; Jicha et al., 1999b) and casein kinase II (Greenwood et al., 1994).

Taken together, phosphorylation in combination with the type of isoform can modulate the properties of tau proteins. In turn, tau proteins provide the microtubule with its own identity and physical characters (rigidity, length, stability, interactive capacity with other organelles). Therefore, by regulating microtubule assembly, tau proteins have a role in modulating the functional organization of the neuron, and particularly in axonal morphology, growth, and polarity (for review, see Buee et al., 2000; Lovestone and Reynolds, 1997).

1.2.3.4 *In vitro* assembly of tau protein into paired helical filaments

To understand the principles of tau aggregation, it is necessary to assemble the subunits into the fibers *in vitro* and study the structure both in the subunit and in the polymeric states. The progress in investigating PHF assembly has been slow, primarily because tau is soluble in most circumstances.

Bona fide PHFs, showing the appropriate diameter and periodicity, were first assembled from recombinant tau constructs containing essentially the repeats (Wille et al., 1992). Assembly was strongly promoted by the covalent dimerization of tau via Cys322 (Schweers et al., 1995). 3R tau constructs, having one cysteine, can be dimerized by oxidation and form PHFs readily, while 4R constructs tend to form intramolecular cross-bridges and do not readily dimerize and assemble. Nevertheless, even with dimerized 3R constructs the assembly was slow and inefficient. Moreover, the difficulty remained that full-length recombinant tau would not assemble, and that native PHFs contained both 3R and 4R isoforms. A further important step was the observation that several polyanionic cofactors greatly facilitate the formation of PHFs from tau protein *in vitro*. These polyanions can be sulfated glycosaminoglycans (such as heparin)

(Goedert et al., 1996; Perez et al., 1996), RNA (Kampers et al., 1996) or polyglutamic acid (Friedhoff et al., 1998b; Perez et al., 1996). A role of these substances in PHF formation is supported by the finding that both sulfated glycosaminoglycans (Perry et al., 1991; Snow et al., 1989; Snow et al., 1990) and RNA (Ginsberg et al., 1997; Ginsberg et al., 1998) are found to be associated with NFTs. These polyanionic cofactors stimulate the assembly of full-length tau, both with three and four repeats, within a few days.

The development of a quantitative assay for PHF formation using Thioflavine S (Friedhoff et al., 1998b), which is known to stain not only amyloid but also PHFs (Roher et al., 1988; Schweers et al., 1995; Wischik et al., 1988b), opened the way to a more detailed study of the mechanism of PHF formation. Using this assay, assembly studies revealed that even after formation of dimers and in the presence of polyanions a kinetic barrier existed, which prevented the rapid formation of filaments (Friedhoff et al., 1998b; Goedert et al., 1996). This suggested that a nucleation step beyond dimerization is rate limiting. (for review, see Friedhoff et al., 2000)

2. Aim of This Work

Tau is an unusually hydrophilic protein containing many polar and charged residues, and remains in solution even after heat and acid treatment (Cleveland et al., 1977; Lindwall and Cole, 1984). This slowed down the attempts to find conditions for aggregation *in vitro* and for studying the nature of the fibers. Certain domains of tau, and certain cofactors were necessary to make the aggregation process experimentally accessible. Recently it was realized that a small fraction of tau, the hexapeptide motif PHF6 ([306]VQIVYK[311]), is capable of inducing tau aggregation via formation of a β-sheet interaction (von Bergen et al., 2000). The assembly promoting hexapeptide motif PHF6 lies in R3, and the earlier results had been obtained with tau domains and peptides lacking R2. Therefore, the question was, whether 4R tau would obey similar principles of aggregation. In addition, because the extra repeat R2 can modify the rate

of aggregation in different ways, depending on aggregation conditions, it was unclear how the two hexapeptide motifs would interact with each other. In this thesis, it was shown that 4R tau isoforms contain another hexapeptide motif PHF6* (^{275}VQIINK^{280}), similar to PHF6 (^{306}VQIVYK^{311}), which promotes β-structure formation and aggregation. Moreover, in order to verify the importance of the hexapeptide PHF6 and PHF6* for the conformational change occurring during tau aggregation, proline mutants were generated in the region of PHF6 and PHF6*, since proline residues disrupt a potential β-strand (Wood et al., 1995).

Another problem was to monitor tau aggregation in real time and in solution *in vitro*, rather than just by electron microscopy. One solution is the Thioflavine S (ThS) assay (Friedhoff et al., 1998b), which is based on the fact that the fluorophore Thioflavine S, added to the aggregation solution, strongly increases its fluorescence yield when PHFs are formed. Although the ThS assay works reproducibly, it is conceptually not ideal because it relies on an exogenous reagent that could possibly alter features of the aggregation pathway. Therefore, in this thesis, a new assay was developed for PHF assembly, which is based on signals that are intrinsic to the tau protein. Tryptophan (Trp) fluorescence was used as a reporter to obtain new insights into the conformation of tau in the soluble state and after incorporation into PHFs. This opened the opportunity to study the stability of PHFs and the solvent accessibility of residues in tau polymers. Finally, the Trp fluorescence can be used to monitor the effects of compounds that act as PHF inhibitors.

II. Materials and Methods

1. Materials

1.1 Chemicals

All chemicals were purchased at analytical grade from following companies:

Amersham-Buchler	Merck
Amersham Pharmacia Biotech	New England Biolabs
AppliChem	Pharma-Waldhof
Biomol	Pierce
Boehringer-Mannheim	Promega
Fluka	Qiagen
Gerbu	Riedel-de-Haen
In ViTaq	Serva
Kodak	Sigma

1.2 Bacteria and plasmids

1.2.1 Bacteria

All plasmids were cloned in *E.coli* strain XL2-Blue (Bullock, 1987), and the proteins were expressed in *E.coli* strain BL21 (DE3) (Studier et al., 1990).

1.2.2 Plasmids

All *E.coli* clones containing genes of the recombinant human tau and tau constructs or mutants were generously provided by Dr. Jacek Biernat from our laboratory. The vector plasmid used is pNG2, which is 5.8 kb long.

1.3 Photomaterials

Photodeveloper Ilford 2000	Ilford
Fixer Ilford 2000	Ilford
Photopaper Ilfordspeed Multigrade III MGX 1M	Ilford
Hyperfilm ECL	Amersham Life Science
Röntgenfilm X-OMAT	Kodak
EM-Negative developer D-19	Kodak
Electron Image Film Estar Thick Base SO-163	Kodak

1.4 Equipments and accessories

Centrifuges:

Cold centrifuge J2-21 M/E	Beckman
Ultracentrifuge L8-70M	Beckman
Ultracentrifuge TL-100	Beckman
Table centrifuge 5402	Eppendorf
Table centrifuge 5415C	Eppendorf
Minifuge RF	Heraeus
Flowthrough Centrifuge 17RS	Heraeus

Rotors:

JA-10, JA-14, JA-20	Beckman
TLA-45, TLA-100.3	Beckman
TFT 45.94, TFT 70.38	Kontron
Flowthrough rotor 8575	Heraeus

FPLC system and corresponding accessories:

FPLC system	Pharmacia
Mono-S column HR10/10	Pharmacia
HiLoad™ 16/60 Superdex™ 200 or 75 prep grade	Pharmacia
Super loop 2 ml, 50 ml and 150 ml	Pharmacia

Electron microscopy and accessories:

Electron microscope CM12	Philips
Sample holder PW 6596-00	Philips
Power Supply TCP 300	Pfeiffer
Evaporation Control BSV 080	Balzers Union
Pivani-Cold Cathode Gauge Control PKG 020	Balzers Union

Other equipments and accessories:

French Press	Aminco
Gel dryer Model 583	Bio-Rad
Speed Vac Concentrator	Bachofer
Incubator Shaker innova 4300	New Brunswick Scientific
Fluoromax DM3000	Spex Industries
Fluoroskan Ascent	Labsystems
Novablot Electrophoretic Transfer Kit 2117-250	Pharmacia
UV/Visible Spectrophotometer Ultrospec 1000	Pharmacia
Fermenter Biostat B	Braun Biotech international

2. Methods

2.1 Molecular biology

2.1.1 Culture and storage of E.coli

E.coli XL2-blue and BL21 (DE3) cells were incubated overnight at 37°C in LB medium with shaking at 160-200 rpm. For storage purposes overnight cultures were supplemented with 30% glycerol and stored at -80°C. The *E.coli* cells were also cultured on agar plates overnight at 37°C. Agar plates were kept at 4°C for up to 2 weeks.

2.1.2 Preparation of plasmids

All plasmid mini-preparations were carried out with the NucleoSpin Plus Kit (Macherey-Nagel) following the user manual. All plasmid midi-preparations were carried out with the Nucleobond AX Kit (Macherey-Nagel) following the user manual.

2.1.3 Restriction analysis of DNA

The DNA sample solution was mixed with restriction enzyme and enzyme buffer in a reaction tube, the total volume of the reaction was 10 µl, the mixture was incubated for 1 hour at 37°C or the optimal temperature for the enzyme. The cut DNA was then directly supplemented with 6× DNA loading buffer and analyzed by agarose gel electrophoresis.

2.1.4 Electroporation

Electroporation is a highly efficient transformation method, for which the salt concentration in the transformation solution should be less than 1 mM otherwise the

efficiency of transformation will be decreased. The DNA solution (0.5 µl) was mixed well with 20 µl cooled electro-competent *E.coli* BL21 (DE3) cells. The electro-cell-manipulator 600 (BTX, Invitrogen) was used under the conditions of 2 500 voltages and 129 Ohm resistance.

2.1.5 DNA agarose gel electrophoresis

DNA loading buffer (6×) was added to DNA samples and 12 µl of the mixtures were applied in 1-2% agarose gels in Tris-acetate (TAE) buffer (0.04 M Tris-acetate, 0.001 M EDTA). The voltage was set to 100 V and the running time was about 45 minutes. DNA was stained with ethidiumbromide (4 µg/ml in H_2O) for 20 minutes and then destained with H_2O for 10 minutes. Pictures were recorded with the gel photo processor system (Photo PR SID, Mitsubishi).

2.1.6 Mutagenesis of tau protein

All of the plasmids of recombinant human tau isoforms, constructs and mutants described in this thesis were cloned in the pNG2 expression vector, which originated from the pET-3 vector (Studier et al., 1990). The mutations were created by site-directed mutagenesis, which was performed using the Quik Change Site-Directed Mutagenesis Kit (Stratagene)(for primer sequences see appendices). The PCR reaction system was listed below:

10× Pfu buffer	2.5 µl
ds DNA template	50 ng
Forward primer	125 ng
Reverse primer	125 ng
10 mM dNTPs mixture (2.5 mM each dNTP)	1 µl
Native Pfu DNA polymerase	1 µl
ddH$_2$O to a final volume of	25 µl

As a negative control, only the forward primer was present in the reaction system.

The PCR program was performed as below:

PCR-Phase	Temperature	Time	Cycles
0. Denaturing	95°C	30 sec	1
1. Denaturing	95°C	30 sec	
2. Annealing	55°C	1 min	16
3. Elongation	68°C	10 min	

After completion of the PCR program, 0.5 µl of Dpn I (New England Biolabs) restriction enzyme (10 U/µl) was added to the reaction solution and gently mixed. The reaction was incubated for 1 hour at 37°C and the step was repeated. Dpn I endonuclease is specific for methylated and hemimethylated DNA and was used to digest the parental DNA template to select for mutated synthesized DNA. After digestion, XL2-blue cells (Epicurian Coli XL2-blue MRF' Ultracompetent cells, Stratagene) were transformed with the PCR product. Therefore, 1 µl Dpn I digested DNA was gently mixed with 15 µl ultracompetent cells and incubated on ice for 30 minutes, pulse heated for 30 seconds at 42°C and finally incubated on ice for 2 minutes. 200 µl of pre-warmed (42°C) NZY+ medium was mixed with the transformation reaction, incubated at 37°C for 1 hour with shaking at 225-250 rpm in an incubator shaker (Innova 4300, New Brunswick Scientific). (the NZY+ medium contains per liter: 10 g NZ amine (casein hydrolysate), 5 g yeast extract, 5 g NaCl, after autoclaving, 12.5 ml 1 M $MgCl_2$, 12.5 ml 1 M $MgSO_4$, 10 ml 2 M filter-sterilized glucose solution were added in). A 250 µl aliquot of the transformation reaction was plated on LB-ampicillin (50 µg/ml) agar plates and incubated overnight at 37°C.

After overnight incubation, colonies were screened by restriction analysis. Therefore plasmid DNA was extracted with a mini-prep and the endorestriction enzyme was used whose recognition site was inserted as a silent mutation by the mutagenesis primer. To confirm the mutations, all plasmids were sequenced on both strands.

2.1.7 DNA sequencing

DNA sequencing reactions were performed using fluorescent dye labelling and the Sanger-Didesoxy-Method (Sanger et al., 1977) in a Robocycler Gradient 96

(Stratagene) PCR machine. The conditions of the temperature cycle program are summarized below. After the reaction, the mixture was supplemented with 100% ethanol to a final concentration of 70% in order to precipitate the DNA. The sample was incubated on ice for 10 minutes and centrifuged at 16 000 ×g for 30 minutes at 4°C. The supernatant was then discarded and the pellet was air-dried for 10 minutes, resuspended in 75 µl distilled water, heated to 80°C for 2 minutes and applied to the sequencing tube. The ABI PRISM 310 Genetic Analyser (PE Applied Biosystems) was used to sequence the DNA. NTI vector software (Informax) was used for the analysis of the sequencing results.

PCR reaction system:

Terminator Ready Reaction Mix	8 µl
ds DNA	200-500 ng
Sequencing primer (7.5 pmol/µl)	1 µl
ddH$_2$O to a final volume of	20 µl

PCR program for sequencing of DNA:

PCR-Phase	Temperature	Time	Cycles
1. Denaturing	96°C	10 sec	
2. Annealing	40°C	5 sec	25
3. Elongation	60°C	4 min	

2.2 Biochemical methods

2.2.1 SDS-polyacrylamide gel electrophoresis (SDS-PAGE)

SDS-PAGE was performed following a modified protocol in our laboratory (Laemmli, 1970; Mandelkow et al., 1985; Matsudaira and Burgess, 1978). The gels were 0.5 mm thick; the stacking gels contained an acrylamide concentration of 4% and the separation gels a concentration range from 8% to 17% (table 1).

Protein samples were 1:1 (v/v) diluted in 2× sample buffer (160 mM Tris, pH 6.8, 10% (w/v) SDS, 10% (w/v) glycerol, 2% (w/v) β-mercaptoethanol, 0.01% (w/v) bromphenolblue) and heated to 95°C for 5 minutes to denature the proteins. The electrophoresis was carried out at 250 Volts in SDS-PAGE running buffer (25 mM Tris-HCl, 190 mM glycin, 0.1% (w/v) SDS) at room temperature. The molecular weight marker proteins used are listed in table 2. The gels were stained with coomassie staining solution (see 2.2.2) and dried using a vacuum gel dryer (Model 583, Bio-Rad).

Table 1: Solutions for preparing SDS-PAGE gels

	Stacking gel (4%)	8%	10%	15%	17%
40% acrylamide/ Bis-acrylamide (38/1)	5.4 ml	12 ml	15 ml	22.6 ml	25.6 ml
1 M Tris-HCl pH 8.8	-	22 ml	22 ml	22 ml	22 ml
0.25 M Tris-HCl pH 6.8	27 ml	-	-	-	-
H$_2$O	20.9 ml	25 ml	22 ml	14.4 ml	11.4 ml
10% SDS	0.54 ml	0.6 ml	0.6 ml	0.6 ml	0.6 ml
TEMED	0.108 ml	0.12 ml	0.12 ml	0.12 ml	0.12 ml
10% APS	0.15 ml	0.065 ml	0.065 ml	0.065 ml	0.065 ml

Table 2: Molecular weight standard for SDS-PAGE

Protein	Molecular weight, kDa
β-galactosidase	116.0
Bovine serum albumin	66.2
Ovalbumin	45.0
Lactate dehydrogenase	35.0
Restriction endonuclease Bsp981	25.0
β-lactoglobulin	18.4
Lysozyme	14.4

2.2.2 Coomassie staining of protein gels

The gels were immersed in the staining solution (0.1% (w/v) coomassie brilliant blue R-250, 45% (v/v) methanol, and 9% (v/v) acetic acid) for 20 minutes and stirred on a slowly rotating platform. Afterwards the gels were destained in an intensive destaining solution (50% (v/v) methanol, 10% (v/v) acetic acid) for 20 minutes and for a minimum of 1 hour in a normal destaining solution (5% (v/v) methanol, 7.5% (v/v) acetic acid).

2.2.3 Determination of protein concentration

For full-length isoforms of tau, a modified BCA method (BCA protein assay reagent, Sigma) was used to determine the concentration of proteins. Protein samples (50 µl of 50-200 µg/ml) were mixed with 1 ml of reagent mixture (1 ml copper- (II) sulfate (Sigma) 4% (w/v), 50 ml bicinchoninic acid solution (Sigma)), the mixture was incubated at 60°C for 30 minutes, and the absorption was measured at 562 nm in a spectrophotometer (Ultrospec 3000 pro, Pharmacia Biotech). For the blank reference, H_2O was used instead of protein solution.

For short tau constructs (K18 and K19), UV absorption measurements at 214 nm were performed to determine the concentration of proteins. Protein samples (5 µl of 50-200 µg/ml) were mixed with 95 µl H_2O, transferred into a quartz microcuvette (3 mm $\times$ 3 mm, Hellma), and the absorption measured at 214 nm in the spectrophotometer (Ultrospec 3000 pro, Pharmacia Biotech). For the zero reference the corresponding buffer of the protein solution was used.

For both methods, the protein concentration was calculated from a BSA (1 mg/ml, Sigma) standard curve, which was recorded every time in parallel.

2.2.4 Expression of recombinant tau proteins in E.coli

The DNA plasmids decoding the protein of interest were transformed into *E.coli* expression strain BL21 (DE3) cells (Studier et al., 1990). 5-10 colonies were screened for the highest expression level of the desired protein. Aliquots of 5 ml LB medium containing 50 µg/ml ampicillin were inoculated with 100 µl overnight culture. The cells were grown in a shaking incubator at 190 rpm at 37°C until the optical density was (measured at 600 nm, OD_{600}) reached of 0.6-0.8. Isopropylthio-β-D-galactoside (IPTG) was then added to a final concentration of 0.4 mM to induce protein expression. The cultures were grown for another 2.5 hours before 1 ml aliquots cells were transferred into a microfuge tube and centrifuged at 16 000 $\times$g for 1 minute. The supernatant was removed and the pellet was resuspended in 70 µl SDS sample buffer and analyzed by SDS-PAGE.

Expression of high quantities of recombinant proteins was performed by fermentation, using a 10 l fermenter (Biostat B, B. Braun Biotech International). 10 l LB-medium containing ampicillin (50 µg/ml) was inoculated with 500 ml of overnight-cultured cells and incubated at 37°C with aeration until the OD_{600} reached 0.8-1.2, IPTG was then added to a final concentration of 0.4 mM and the cells were grown for another 3 hours. The parameters used for fermentation were: 37°C, pH 7.0, 600 rpm, filtered air. After induction, cells were harvested by a flowthrough centrifuge (Centrifuge 17 RS, Rotor HCT 22.300, Heraeus) at 10 000 rpm at 4°C. The cell pellet was resuspended in 100 ml resuspending buffer (20 mM MES, 1 mM EGTA, 0.2 mM $MgCl_2$, 5 mM DTT, 1 mM PMSF, 10 µg/ml leupeptin, 2 mM benzamindin, 10 µg/ml pepstatin A, pH 6.8) and kept on ice.

2.2.5 Isolation and purification of recombinant tau protein

The resuspended cells (see 2.2.4) were subjected to two French-Press (SLM Aminco, SLM Instruments Inc.) cycles. The cell lysate was centrifuged at 127000 ×g (Ultracentrifuge L8-70M, Beckman) for 40 minutes at 4°C. The supernatant was then transferred to a glass beaker and NaCl (5M stock solution) was added to a final concentration of 500 mM. The solution was heated to 100°C for 20 minutes, centrifuged again and the pellet was discarded. Because of tau protein's heat stability, tau protein stayed in the supernatant whereas most other proteins were denatured and were found in the pellet (Gustke et al., 1994; Herzog and Weber, 1978; Weingarten et al., 1975).

In preparations of the proteins for fluorescence spectroscopy experiments, the cell lysate was not incubated at 100°C because heating potentially disrupts the fluorescence intensity of the fluorophore (heating can activate the surrounding environment of fluorophores), but was enriched by fractionated ammonium sulfate precipitation. Ammonium sulfate (Sigma) was added to a concentration of 25%, the solution was centrifuged at 127 000 ×g for 30 minutes at 4°C (Ultracentrifuge L8-70M, Beckman), the pellet was discarded and ammonium sulfate was added to a final concentration of 55% in the supernatant, the solution was then centrifuged again, the supernatant removed and the pellet resuspended in 70 ml SP-Sepharose A buffer.

The supernatants from the heating-step and the solubilized proteins derived from the ammonium sulfate precipitation were dialyzed for 2 hours against 1 l SP-Sepharose buffer A (2 mM Na-MES pH 6.8, 0.1 mM PMSF, 2 mM DTT, 50 mM NaCl, 1 mM Na-EGTA, 1 mM $MgSO_4$) in a suitable dialysis bag (Peichelt Chemietechnik). The molecular weight cut-off used were 3.5 kDa for tau constructs K18 and K19 and 10 kDa for other tau isoforms. The dialysis buffer was changed one time.

After dialysis, the protein solution was centrifuged at 127 000 ×g for 30 minutes at 4°C, (Ultracentrifuge L8-70M, Beckman) and the supernatant was filtered through 0.45 µm Ready-To-Use filter holders (Schleicher & Schuell). For purification the solution was applied to a cation exchange column (SP-Sepharose, fast flow column material, XK 16 Column, Pharmacia). The column was equilibrated before use with 60 ml of SP-Sepharose buffer A. The flow rate was 2 ml/min and tau proteins were eluted by using a NaCl gradient elution buffer: SP-Sepharose buffer B (2 mM Na-MES pH 6.8, 0.1 mM PMSF, 2 mM DTT, 1 M NaCl, 1 mM Na-EGTA, 1 mM $MgSO_4$). All of these purification steps were performed on a FPLC system (Pharmacia, Sweden) at 4°C. The collected protein fractions were analyzed by SDS-PAGE. The suitable fractions were concentrated by using a centrifugal-filter device (Millipore, Cold centrifuge 5820 R, Eppendorf) to a final volume of 1 ml.

For further purification, the concentrated proteins were applied to a gelfiltration column (HiLoad 16/60 Superdex 200 for tau isoforms or Superdex 75 for tau constructs, prep grade. Pharmacia). The column was pre-equilibrated with PBS (137 mM NaCl, 3 mM KCl, 10 mM Na_2HPO_4, 2 mM KH_2PO_4, pH 7.4, with or without 1 mM DTT) on a FPLC system (Pharmacia) at 4°C. The protein was eluted with PBS at a flow rate of 0.5 ml/min. The protein fractions were collected and analyzed by SDS-PAGE. During this step, the degraded proteins were removed (Friedhoff et al., 1998a; von Bergen et al., 2000).

For separation of the dimeric and monomeric proteins of htau39, the pre-oxidized proteins were applied to a Superose 12 PC 3.2/30 column (Amersham Pharmacia) under control of the Smart-HPLC System (Amersham Pharmacia) with a flow rate of

50 µl/min. The fractions were analyzed by SDS-PAGE and the SDS-PAGE sample buffer contained no β-meracptoethanol.

2.3 Aggregation of recombinant tau protein *in vitro*

2.3.1 PHF assembly

Aggregation of tau isoforms and constructs was induced by incubating with the polyanionic cofactor heparin (MW ~3000 Da, Sigma). Tau protein concentrations between 50-100 µM in volumes of 20-500 µl at 37°C in PBS (pH 7.4) were used as described (Barghorn et al., 2000; Friedhoff et al., 1998a). Solution of tau isoforms contained protease inhibitors (final concentration: 1 mM PMSF, 1 mM EDTA, 1 mM EGTA, 1 µg/ml pepstatin A, 1 µg/ml leupeptin, 1 µg/ml Aprotenin). The incubation time varied between hours up to several days according to the isoforms or constructs which were used. The formation of aggregated PHFs was ascertained by the Thioflavine S fluorescence assay (Friedhoff et al., 1998b). Aliquots of the aggregation reactions were withdrawn and analyzed by electron microscopy in parallel.

2.3.2 Thioflavine S fluorescence spectroscopy of PHFs

The PHFs formed *in vitro* can be quantified by Thioflavine S (ThS) (Friedhoff et al., 1998b). Thioflavine S is a fluorescence dye whose fluorescence intensity is increased after binding to PHFs. Fluorescence was measured with a Fluoroskan Ascent Spectrofluorometer (Labsystems, Helsinki) with an excitation filter of 440 nm and an emission filter of 510 nm in a black 384 well plate (Cliniplate 384, Labsystems). Before the measurement, the samples in the plate were mixed for 5 seconds at 420 rpm (system control); the measurements were carried out at room temperature in PBS (pH 7.4) with 10 µM ThS unless stated otherwise for 15 minutes. Background fluorescence and light scattering of the samples without Thioflavine S were subtracted when needed.

2.3.3 Pelleting assay

The pelleting assay was performed for quantification of PHFs in the inhibitor compounds screening and PHF denaturation experiments. Pre-formed PHFs were incubated with varying concentrations of compounds or denaturants overnight at 37°C. The mixture was centrifuged at 100 000 ×g for 1 h at room temperature (bench top-centrifuge TL-100, Beckman). The PHF pellet was washed twice with PBS (pH 7.4), the resulting pellets and supernatants were dried and resuspened in SDS-PAGE sample buffer containing β-mercaptoethanol. Pellets and supernatants were boiled at 95°C for 5 minutes to dissolve PHFs and subjected to SDS-PAGE (17% acrylamide). Gels were stained with Coomassie brilliant blue R250.

2.3.4 Transmission electron microscopy

Electron microscopy (EM) was used to ascertain the structure of paired helical filaments formed by tau protein. The specimens for EM examination were placed on carbon-coated copper grids (600 mesh). The carbon film was produced by evaporation onto a freshly cleaved mica surface by using the high vacuum evaporator (BAE 080T, Balzer). The film was floated off the mica at an air-water interface and picked up from below on the EM grids. Before usage, the grids were glow discharged in a vacuum chamber of a vacuum evaporator (CTA 010, Balzer) for 30 seconds. The carbon-coated grids (carbon side down) were floated for 45 seconds on 5 µl of the diluted protein solutions (0.1-10 µM); the grids were washed with 2 drops of H_2O (filtered), and negatively stained for 1 minute with 2% (w/v) uranylacetate (pH 4.5, filtered).

The specimens were examined in a TEM CM12 (Philips) electron microscope operated at 100 kV. Images of the selected areas were taken at a magnification of 45 000. The electron image films (SO-163, Eastman Kodak Co. 8.3x10.2 cm) were developed in a full-strength developer (D19, Eastman Kodak Co.).

2.4 Light scattering for analysis of tau influence on microtubule assembly

The ability of tau to promote microtubule assembly was monitored by light scattering at an angle of 90 degrees and a wavelength of 350 nm on a Kontron spectrophotometer (Kontron Instruments). Tau protein (5 µM) was mixed with tubulin dimer (30 µM) and GTP (1 mM) at 4°C in polymerization buffer (100 mM Na-PIPES pH 6.9, 1 mM EGTA, 1 mM $MgSO_4$, 1 mM DTT) with a final volume of 120 µl. Tau was added as the last component. After rapid mixing, the samples were pipetted into a quartz cuvette (10 mm path length, Hellma), which was pre-warmed to 37°C. The reaction was started by raising the temperature to 37°C with defined heating rates (half-time ~4 s). The assembly of tubulin into microtubules was monitored over time by a change in light scattering at 90°. Three parameters were extracted from the obtained light scattering curves, the maximum assembly at steady state, the rate of assembly, and the lag time between the temperature jump and the start of the light scattering rise.

2.5 Fourier transform infrared spectroscopy

For studying the secondary structure of the soluble and aggregated tau protein, Fourier transform infrared spectroscopy (FTIR) was used. Instead of the wavelength λ, infrared spectra are expressed in terms of the wavenumber ($1/\lambda$). The amide I region from 1600 to 1700 cm^{-1} was used to investigate the secondary structure of the protein, which is mainly associated with the carbonyl stretching vibration (85%) of the backbone of the amino acids and is directly related to the backbone conformation and hydrogen-bonding pattern of the protein. Because water absorbs strongly in the important spectral region around 1640 cm^{-1}, studies were performed in deuterium oxide (D_2O).

To prepare the samples for FTIR analysis, soluble proteins were precipitated by 80% acetone, incubated at -20°C for 2-4 hours and centrifuged at 16 000 $\times$g for 10 minutes at 4°C, (Table centrifuge 5402, Eppendorf). The pellet was washed with 90% ethanol in

D_2O and dried by vacuum. The protein was dissolved in D_2O (Sigma). Pre-formed PHFs were centrifuged at 100 000 ×g for 30 minutes at room temperature (bench top-centrifuge TL-100, Beckman), the supernatant was discarded and the pellet was resuspended in 100 µl D_2O and incubated for at least 2 hours at 4°C before usage.

FTIR experiments were performed on a Jasco FT-IR 410 instrument (Jasco). Atmospheric water vapour was removed by flushing the spectrometer with nitrogen. Interferograms were recorded between 1700 and 1600 cm^{-1} at a spectral resolution of 1 cm^{-1}, and 128 spectra were averaged. They were acquired in the transition mode using CaF_2 cells, separated by spacers of different thickness (usually 25 µm). After recording a reference spectrum of the instrument and of the used D_2O lot the protein solutions were applied, and the absorbance spectrum of the sample was measured. The D_2O spectra and the sample spectra were first corrected for the vapour background before subtracting the D_2O spectra from the sample spectrum. To facilitate comparison the spectra were then normalized with respect to their maxima.

2.6 Tryptophan fluorescence spectroscopy

Proteins contain three amino acid residues that contribute to their ultraviolet fluorescence: tyrosine (Tyr, Y), tryptophan (Trp, W), and phenylalanine (Phe, F). Phenylalanine displays the shortest absorption and emission wavelength maxima. The emission maximum of tyrosine in water is at 303 nm and is relatively insensitive to solvent polarity. The emission maximum of tryptophan in water is near 350 nm and is highly dependent upon polarity and/or the local environment (Lakowicz, 1999). A valuable feature of intrinsic protein fluorescence is the high sensitivity of tryptophan to its local environment. One can frequently observe changes in emission spectra of tryptophan in response to protein conformational transitions or denaturation, which can affect the local environment surrounding the indole ring. For tryptophan in a completely apolar environment, the emission spectrum shows a blue-shift, when tryptophan moves towards hydrogen-bonding groups or becomes exposed to water, the emission spectrum

shifts to longer wavelengths (Shopova, 1983). Therefore the response of the tryptophan fluorescence was explored to monitor the process of the aggregation of tau into PHFs.

2.6.1 Tryptophan fluorescence spectroscopy

All of the fluorescence experiments were performed on a Spex Fluoromax spectrophotometer (Polytec) using 3 mm $\times$ 3 mm microcuvette from Hellma (Mühlheim) with 20 µl sample volumes. For tyrosine excitation spectra, scans ranged from 250-300 nm at a fixed emission wavelength of 310 nm, for emission spectra, scans ranged from 290-450 nm at a fixed excitation wavelength of 275 nm. For tryptophan excitation spectra, scans ranged from 210-310 nm at a fixed emission wavelength of 350 nm, for emission spectra, scans ranged from 300-400 nm at a fixed excitation wavelength of 290 nm. In all cases, the slit widths were 5 nm, the integration time was 0.25 second, and the photomultiplier voltage was 950 V.

In order to prepare the samples for tryptophan fluorescence spectra, the pre-formed PHFs were centrifuged at 100 000 $\times$g for 30 min at room temperature (bench top-centrifuge TL-100, Beckman). The pellet was resuspended in 20 µl PBS (pH 7.4).

2.6.2 Fluorescence quenching experiments

Steady-state fluorescence quenching experiments were performed on soluble and aggregated proteins. Aliquots of the stock quenching solutions (5M, freshly prepared) were added to the cuvette containing 10 µM proteins in PBS (pH 7.4). Quenching experiments were performed with excitation at 280 nm. Quenching data were fit to the Stern-Volmer equation, $F_0/F_c = 1 + K_{SV}[Q]$, where F_0 and F_c are the fluorescence intensity in the absence and in the presence of quencher [Q], respectively, K_{SV} is the Stern-Volmer quenching constant (Lakowicz, 1999).

2.6.3 GuHCl denaturation of PHFs

Equally important as the question of PHF aggregation is that of PHF stability and disaggregation. The stability can be probed by exposing pre-formed PHFs to denaturants such as guanidine hydrochloride (GuHCl) using tryptophan fluorescence as a reporter.

For inhibiting tau polymerization, 10 µM soluble tau proteins (which contained a tryptophan mutation) were incubated with GuHCl (concentration range between 0 and 4 M) overnight at 37°C. The tryptophan fluorescence was measured the next day.

For disaggregation of PHFs, pre-formed PHFs were centrifuged at 100 000 ×g for 30 min at room temperature (bench top-centrifuge TL-100, Beckman), the pellet was resuspended in PBS (pH 7.4), 10 µM of this PHFs solution was incubated with GuHCl (concentration range between 0 and 4 M) overnight at 37°C and tryptophan fluorescence was analyzed the next day.

2.6.4 Fluorescence resonance energy transfer

Fluorescence resonance energy transfer (FRET) is based on a transfer of the excited-state energy from the initially excited donor (D) to an acceptor (A). The most common application of FRET is to measure the distance between two sites on a macromolecule. The rate of energy transfer from a donor to an acceptor (k_T) is given by equation:

$$k_T = 1/\tau_D \, (R_0/r)^6$$

Where τ_D is the decay time of the donor in the abscence of acceptor, R_0 is the Förster distance (the distance at which FRET is 50% efficient), r is the donor-to-acceptor distance. The most commonly observed FRET in proteins is from tyrosine (as donor) to tryptophan (as acceptor), the typical Förster distance (R_0) for energy transfer between Tyr and Trp is 1 nm (Chiu and Bersohn, 1977; Eisinger, 1969). When the distance between Tyr and Trp is less than 1 nm, Tyr will transfer the energy to Trp. Human tau contains five tyrosine residues (Y18, Y29, Y197, Y310, Y394) and no tryptophan. Therefore when tryptophan scanning mutations are introduced, one can easily observe

the distance change between Tyr and Trp during the PHF aggregation using fluorescence spectroscopy.

III. Results

1. Interactions between hexapeptide motifs PHF6* and PHF6 during tau aggregation

Tau protein contains almost no secondary structure in solution (Cleveland et al., 1977; Schweers et al., 1994), but in the disease state, tau aggregates into fibers as straight (untwisted) or paired helical filaments (PHFs). In the frontotemporal dementias (FTDP-17), one of the deletion mutations – ΔK280 – has a strong tendency for β-sheet formation and one can achieve aggregation of the repeat domain *in vitro* within minutes. Furthermore, this mutation is able to polymerize even in the absence of polyanionic cofactors which are commonly used to promote aggregation (Barghorn et al., 2000; von Bergen et al., 2001). Previous work identified the minimal hexapeptide interaction motif of PHF6 (^{306}VQIVYK^{311}, at the beginning of the third repeat) as having the highest predicted β-structure potential in tau (von Bergen et al., 2000). Moreover, point mutations in this hexapeptide region by prolines disrupted a potential β-strand and inhibited aggregation into PHFs (von Bergen et al., 2000).

Regarding the different splicing of exon 10, the second repeat is of special interest because there is another hexapeptide motif PHF6* (^{275}VQIINK^{280}) at the beginning of second repeat. Now the question arises, whether 4R and 3R tau isoforms follow identical principles of aggregation? How can the two hexapeptide motifs PHF6* and PHF6 in 4R isoforms interact with each other? If two intact hexapeptides are necessary for PHF assembly in 4R isoforms, how can the ΔK280 mutation override a proline mutation in the other hexapeptide? Therefore in this part of the study, single or double proline mutations in the hexapeptide PHF6* (second repeat, Ile-277-Pro) or PHF6 (third repeat, Ile-308-Pro) based on the full-length isoform htau40 and short construct K18 were generated (Fig. 3). In addition proline mutations based on the FTDP-17 mutant of the full-length isoform htau40-ΔK280 and the construct K18-ΔK280 were created.

Fig. 3A shows htau40, the longest isoform of tau in the human brain, which contains 441 amino acids, with four repeats in the C-terminal half and two N-terminal inserts. Fig. 3B shows the K18 construct, which consists of only four repeats corresponding to the repeat domain of htau40, (residues 244-372, about 129 amino acids). The hexapeptide motifs PHF6* in the second repeat and PHF6 in the third repeat of the K18 construct are shown in dark grey colour, and the positions of the mutants I277P, I308P and the FTDP-17 mutant ΔK280 are also indicated.
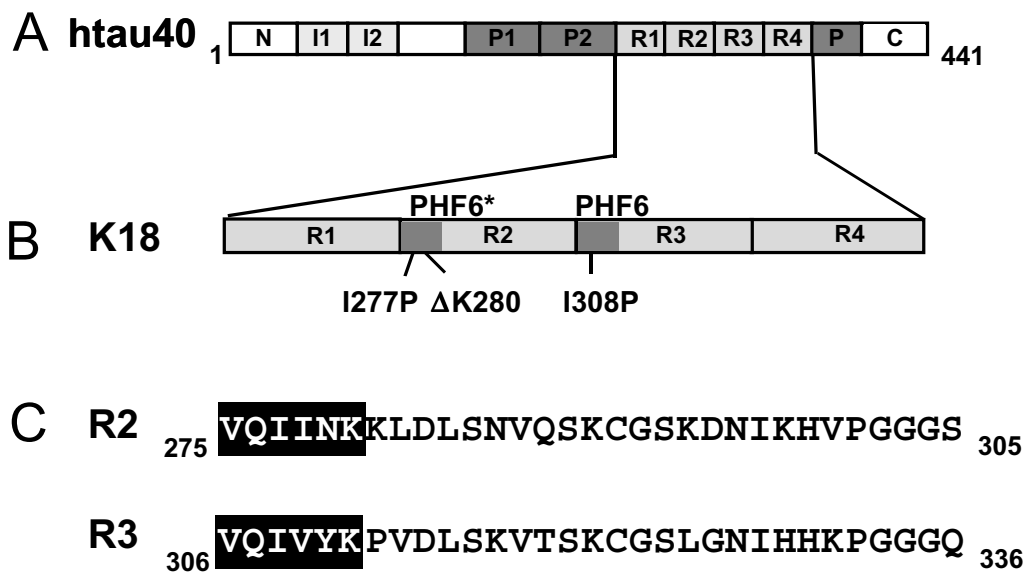

Fig. 3: Bar diagram of proline mutations in tau isoform htau40 and construct K18.

(A) Shows htau40, the longest isoform in the human brain (441 residues). The C-terminal half contains four repeats (~31 amino acids each, R1-R4, light grey), which together with their flanking regions (proline-rich region, dark grey) constitute the microtubule-binding domain. (B) Shows the location of hexapeptide motifs PHF6* and PHF6 in the second repeat R2 and the third repeat R3 of construct K18 (dark grey). The position of FTDP-17 mutant ΔK280, which lies in the second repeat, and the proline mutants I277P (in the PHF6* motif) and I308P (in the PHF6 motif), which intended to interrupt β-structure are also shown. (C) Shows the sequences of repeat R2 and R3, the PHF6* and PHF6 motifs in the R2 and R3 are marked in black boxes.

1.1 The kinetics of polymerization of tau protein into PHFs

Several polyanionic cofactors facilitate the aggregation of tau protein into PHFs *in vitro* (Goedert et al., 1996; Kampers et al., 1996; Perez et al., 1996). In this work, heparin

(MW ~3000 Da) was used to accelerate the protein polymerization. For quantifying the rate and extent of PHF aggregation *in vitro*, the Thioflavine S (ThS) assay was performed (Friedhoff et al., 1998b).

1.1.1 The kinetics of polymerization of tau and its proline mutants based on the construct K18 and K18-ΔK280

Fig. 4A shows the time course of the aggregation of construct K18 and its proline mutants in the absence of polyanions. Only the K18-ΔK280 mutant can polymerize without heparin with a half-time of ~3 h (red dashed line), confirming earlier observations (Barghorn et al., 2000; von Bergen et al., 2001). Protein with proline mutants in the second repeat I277P and in the third repeat I308P do not polymerize. This is true even when they are embedded in the 4R construct K18-ΔK280. These results show clearly that a proline within the hexapeptides PHF6 and PHF6* inhibits the aggregation of tau in the absence of polyanionic cofactors.

Fig. 4B shows the time course of the aggregation of construct K18 and its proline mutants in the presence of heparin. Construct K18 aggregates with a half-time of ~4 h (blue dashed line), but both the proline mutant I277P and I308P in the hexapeptide motifs suppress PHF formation (black solid lines, bottom). This was also confirmed by electron microscopy (Fig. 6) and FTIR data (Fig. 7). The K18-ΔK280 mutant aggregates rapidly and to a higher extent in the presence of heparin (ThS fluorescence intensity of ~6, half-time of ~1.5 h, red dashed curve). Disruption of the PHF6* motif by the I277P mutant just upstream of the ΔK280 mutant abrogates PHF formation. Surprisingly, however, the mutant I308P in the PHF6 motif reduces but does not suppress PHFs (green dashed curve, half-time of ~2.5 h). In other words, the PHF6* motif with the ΔK280 mutation is so potent that it can induce aggregation even when the PHF6 motif in R3 cannot participate in nucleating β-structure.
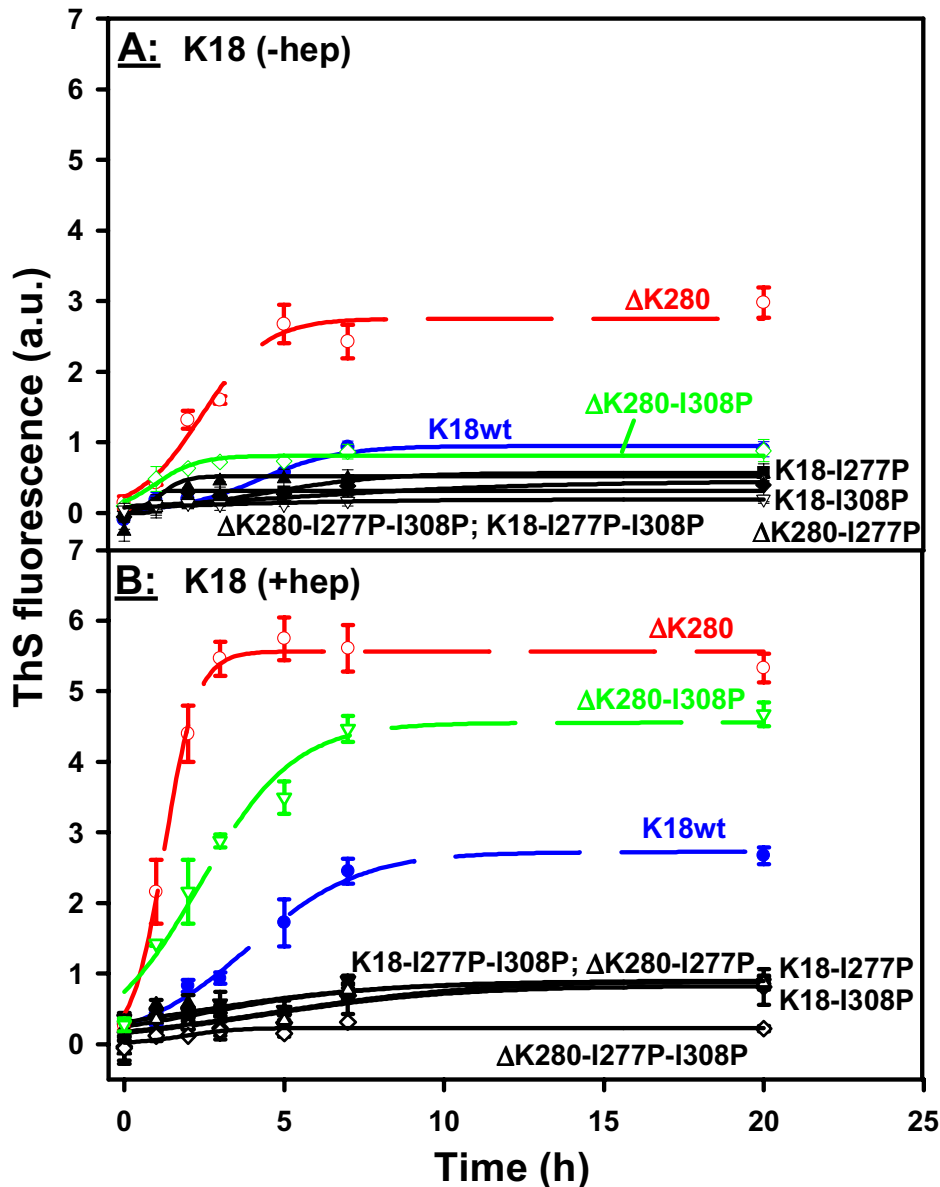
Fig. 4: Time course of the aggregation of construct K18 and its proline mutants.

(A) The kinetics of aggregation of mutated K18 constructs into PHFs in the absence of heparin was measured fluorometrically using the dye Thioflavine S (Friedhoff et al., 1998b). Tau protein concentrations were 40 µM in PBS (pH 7.4). Shown is the average value (n=3) with the standard deviation. The mutant K18-ΔK280 shows aggregation (red dashed line, top curve) with a half-time of ~3 h, construct K18wt (blue solid line) and the other mutants (solid lines) show little or no aggregation at all (note the ThS fluorescence signal of 1 is almost always the background signal).

(B) Time course of the aggregation of construct K18 and its proline mutations in the presence of heparin. Conditions were similar as in (A), except the heparin concentration was 10 µM. Construct K18 aggregates in the presence of heparin with a half-time of ~4 h (blue dashed line in the middle). The mutant K18-ΔK280 shows the fastest aggregation, with a half-time of ~1.5 h (red dashed line, top curve), the mutant K18-ΔK280-I308P also shows aggregation into PHFs (half-time of ~2.5 h, green dashed line). Note that the other proline mutants in the hexapeptide motifs abrogate the ability to polymerize (black solid lines at the bottom).

1.1.2 The kinetics of polymerization of tau and its proline mutants based on the full-length isoform htau40 and htau40-ΔK280

The question was whether the full-length tau isoforms exhibit the same features as short constructs. Therefore, proline mutants as in the case of construct K18 were created based on the longest isoform htau40 (see Fig. 3A). Because the full-length isoforms of tau aggregated slowly *in vitro*, heparin was used to accelerate the reaction. Fig. 5 shows the time course of the aggregation of the longest isoform htau40 and its proline mutants in the presence of heparin. All aggregations show lower efficiency compared to the short construct K18. Htau40 wild-type aggregates with a half-time of ~1 day (blue dashed line), htau40-ΔK280 aggregates faster than wild-type with a half-time of ~0.3 days and with higher efficiency (red dashed line). The htau40-ΔK280-I308P mutant shows a similar result as K18-ΔK280-I308P, with an aggregation half-time of ~0.5 days (green dashed line). The other proline mutants show no significant increase in the PHF specific signal (black solid lines, bottom).
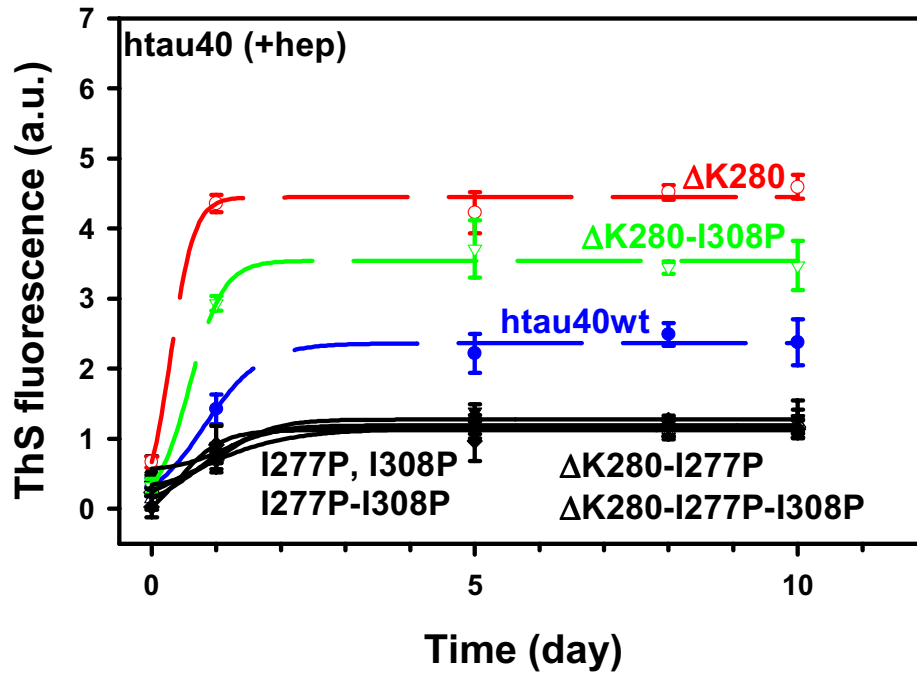
Fig. 5: Aggregation of the htau40 mutants into paired helical filaments.

The kinetics of aggregation of htau40 mutants into PHFs was measured by the ThS fluorescence assay. Tau protein concentrations were 50 µM and the heparin concentration was 12.5 µM in PBS (pH 7.4). In general, htau40 aggregated much more slowly than the short construct K18 and has a low efficiency to aggregate. The wild-type htau40 has an aggregation half-time of ~1 day (please note the time scale is in days, not hours, blue dashed line, in the middle), the mutant htau40-ΔK280 aggregates faster with a half-time of ~0.3 days (red dashed line, top curve) and the mutant htau40-ΔK280-I308P aggregates as well (half-time of ~0.5 days, green dashed line).

These results suggest that 4R forms of tau require both hexapeptide motifs to induce PHF formation. A proline mutant in one of the motifs is enough to disrupt the aggregation potential of the other. This behaviour of 4R tau is in contrast to 3R tau where the single PHF6 motif is sufficient for aggregation. An exception to this rule is the mutation ΔK280 in the PHF6* hexapeptide which is able to overrule an inhibiting proline within the hexapeptide motif PHF6 in the presence of heparin.

1.1.3   Electron microscopic analysis

To verify that the aggregation observed by the Thioflavine S fluorescence assay is caused by filaments resembling PHFs, they were analyzed by electron microscopy. Aliquots from the polymerization reaction were negatively stained with 2% uranyl acetate (see Materials and Methods), and examined by EM (Fig. 6).
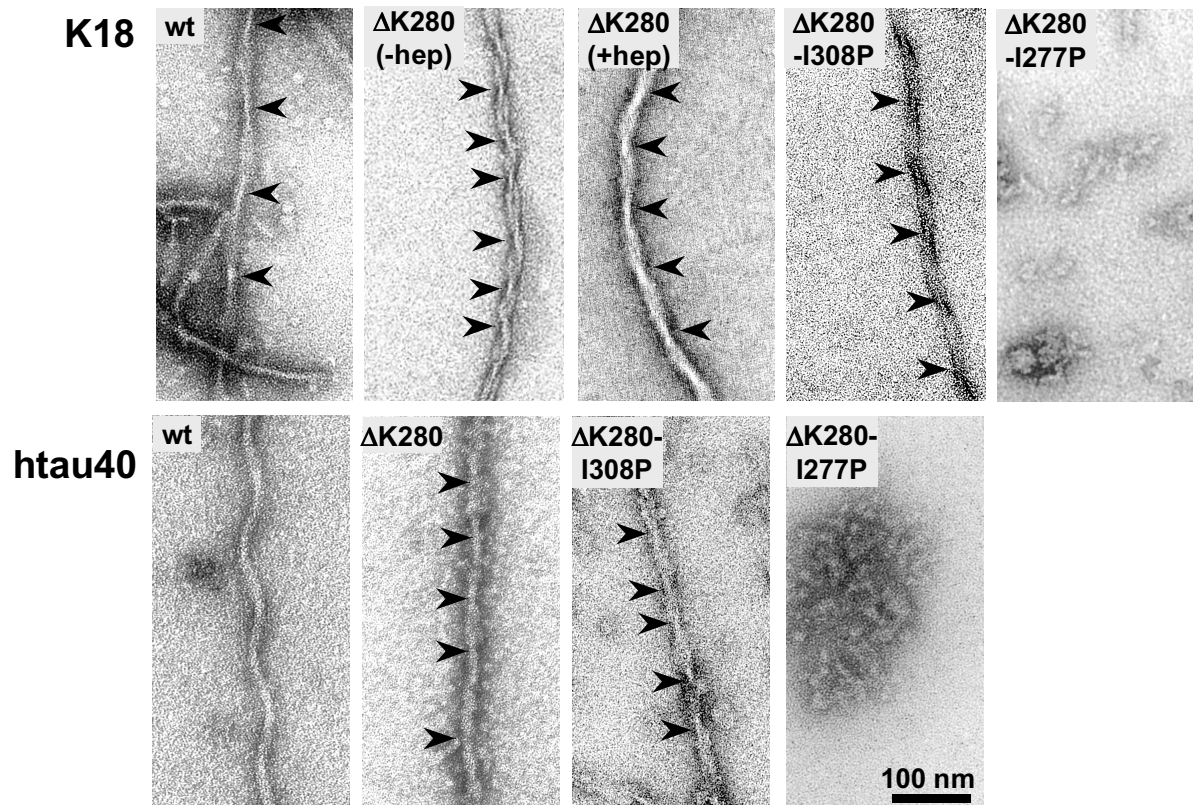

Fig. 6: Electron micrographs of PHFs.

The upper panels from left to right are K18wt, K18-ΔK280 in the absence of heparin (-hep), K18-ΔK280 in the presence of heparin (+hep). They show the typical twisted filament morphology. K18-ΔK280-I308P is still capable of forming typical PHFs in the presence of heparin. However, the other proline mutants cannot form any filaments (e. g. K18-ΔK280-I277P). The lower panels from left to right illustrate the longest tau isoform htau40wt, htau40-ΔK280, and proline mutant htau40-ΔK280-I308P (all in the presence of heparin). They showed filaments with a twisted structure as well as straight filaments, but htau40-ΔK280-I277P did not form filaments.

Electron microscopy of the assembly products revealed that the ΔK280 mutant formed regular filaments with the typical PHF structure. For constructs based on K18 this was true both in the absence and presence of heparin. ΔK280-I308P mutants with a proline

in the PHF6 motif are still capable of forming PHFs. In contrast, the other proline mutants didn't form any filaments.

1.2 Polymerization of tau and proline mutants into PHFs is accompanied by the formation of β-structure in the repeat domain

In the case of tau aggregation into PHFs, X-ray and CD studies show that the PHF6 (^{306}VQIVYK^{311}) motif at the beginning of the third repeat can adopt β-structure, and the same was shown for the hexapeptide PHF6* (^{275}VQIINK^{280}) motif at the beginning of the second repeat (von Bergen et al., 2001). A suitable technique for the detection of β-structure is Fourier transform infrared spectroscopy (FTIR) (Byler and Susi, 1986; Susi and Byler, 1983).

While CD is a reliable technique for distinguishing well the α-helical structure from β-structure and random coil, FTIR is more sensitive for β-structure. Furthermore, FTIR spectroscopy allows studies of proteins in a variety of environments, including optically turbid media. The analysis of secondary structure is based on the absorption of the amide I band in the region between 1600 to 1700 cm^{-1} (Surewicz et al., 1993).

In the FTIR spectrum soluble tau protein has a maximum main peak at 1650 cm^{-1} (illustrated for the K18 construct in Fig. 7, black lines), which constitute with mostly random coil structure and is typical for a low content of secondary structure. In the aggregated state, the maximum of the main peak has shifted to about 1620-1630 cm^{-1} (e.g. Fig. 7A, red line), which reveals an increase in β-sheet formation upon tau aggregation (Byler and Susi, 1986; Susi and Byler, 1983; von Bergen et al., 2001). The introduced proline mutants should act as an inhibitor of β-structure as described elsewhere (Wood et al., 1995) and therefore no β-sheet should be observable in the FTIR spectra of proline mutants (e.g. Fig. 7C, red line). The sensitivity for the detection

of β-sheet in the samples of polymerized protein was enhanced by pelleting pre-formed filaments. Pellet and supernatant were analyzed separately.

Fig. 7 shows the FTIR spectra of the 4R containing construct K18 and its proline mutants before (black lines) and after aggregation (red lines). The FTIR spectrum of the construct K18wt exhibits a peak of absorbance in the amide I band around 1650 cm^{-1} in the soluble state (Fig. 7A, black line), indicating mostly random coil structure. The spectrum of polymerized protein exhibits a maximum peak around 1630 cm^{-1} (Fig. 7A, red line) indicating an increased content of β-sheet. The same is true for the mutation K18-ΔK280 and K18-ΔK280-I308P (Fig. 7B and 7F) – the maximum shifts from 1650 to 1630 cm^{-1} upon polymerization. The other proline mutants show nearly no change during the PHF aggregation, indicating that both proline mutants in the PHF6 and PHF6* motifs diminished the β-structure propensity in the repeat domain. However, the inhibition by the I308P mutation in the PHF6 mutation can be overcome by turning PHF6* into a strong assembly promoter via the FTDP-17 mutation ΔK280 (Fig. 7F).
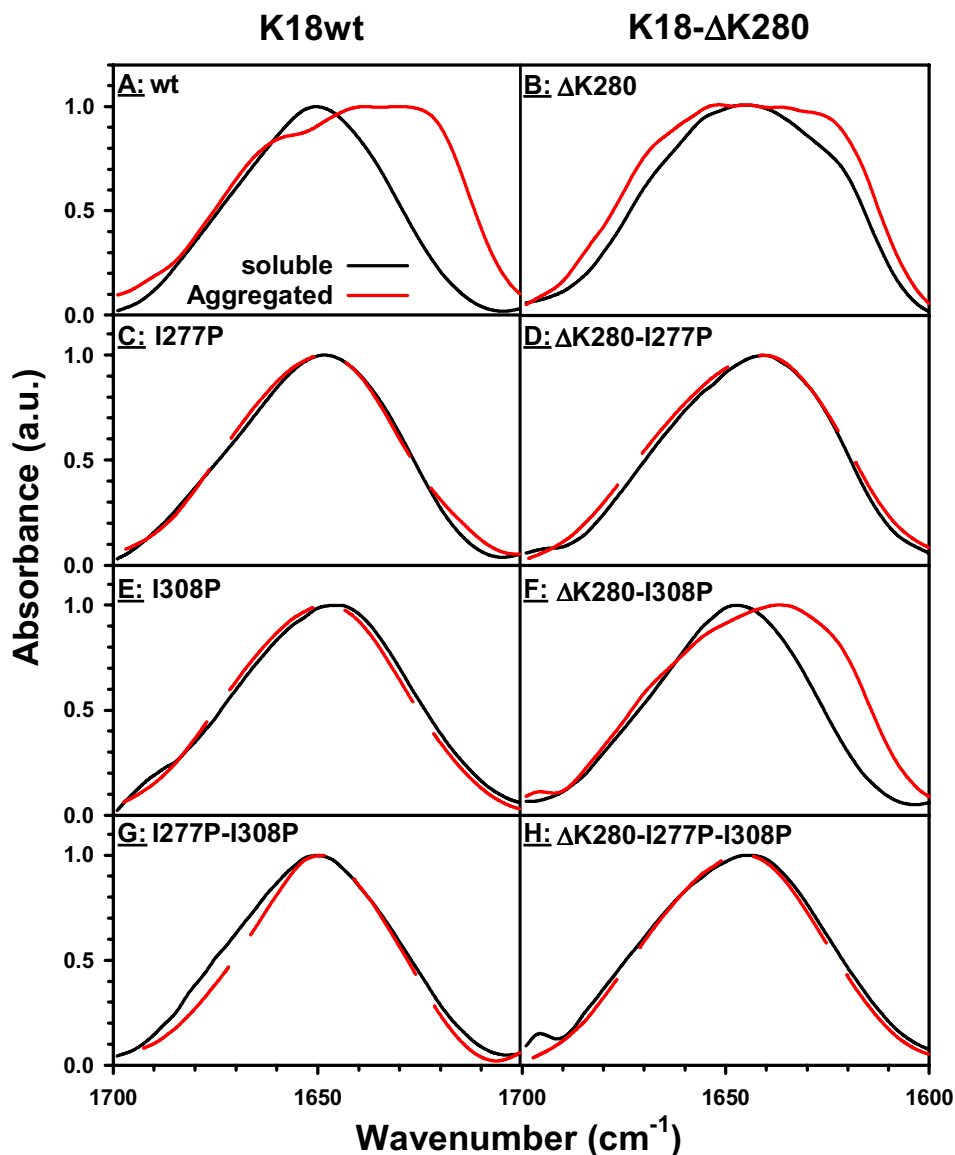
Fig. 7: FTIR spectra of the 4R construct K18 and its proline mutants in the soluble and aggregated states.

For getting high concentration of proteins, soluble tau proteins were precipitated with cold acetone and resuspended in D_2O. For aggregated proteins, pre-polymerized proteins were centrifuged and the pellet washed pellet two times with D_2O and resuspended in D_2O, the supernatants were precipitated with acetone and resuspended in D_2O. The concentrated pellet and supernatant were analyzed separately. The soluble protein spectra show similar amide I bands at about 1650 cm^{-1} (all black lines), while the aggregated K18wt, mutations ΔK280 and ΔK280-I308P (from pellets) spectra have a shift from 1650 to 1630 cm^{-1} (Fig. 7A, B, F, red solid lines). However, the other proline mutants show no spectra shift compared to the soluble and polymerized protein (Fig. 7C, D, E, G, H)(please note, K18-I277P, K18-I308P, K18-I277P-I308P, K18-ΔK280-I277P, K18-ΔK280-I277P-I308P cannot aggregate, therefore supernatant was used instead of pellet for the spectrum analysis).

1.3 Microtubule assembly promoted by full-length isoform htau40 and its proline mutants

Tau protein plays an important role in the assembly of tubulin monomers into microtubules. The repeat domain of tau and its adjacent regions are involved in the binding of tau to microtubules, and stabilize the microtubule network (Butner and Kirschner, 1991; Gustke et al., 1994). To determine the effect of the proline mutants on specific functions of tau, the ability of full-length tau to promote microtubule assembly was investigated by using the light scattering technique (Gaskin et al., 1974).

The results are shown in Fig. 8. Phosphocellulose-purified tubulin (30 µM) was used which was below the critical concentration of the protein so that almost no turbidity increase was observed without tau (Fig. 8, red filled squares, bottom line). By the addition of 5 µM htau40 wild-type, the scattering increased rapidly and reached maximum turbidity within 1.5 minutes, illustrating the strong assembly-promoting effect of tau (Fig. 8, blue filled circles). Typical half-times were ~40 s, and the lag time necessary for microtubule nucleation was very short (~10 s). When the proline mutants of htau40 were tested with the same procedure, they all showed a similar behaviour compared to htau40wt. Although some differences were observed, they were not significant. This was also true for the mutant htau40-ΔK280 that showed a strong tendency for aggregation into PHFs (see Fig. 5). These results confirm earlier results (Barghorn et al., 2000). In conclusion, these results indicate that the proline mutants in the PHF6 and PHF6* motifs have nearly no added effect on promoting the microtubule assembly by full-length tau.
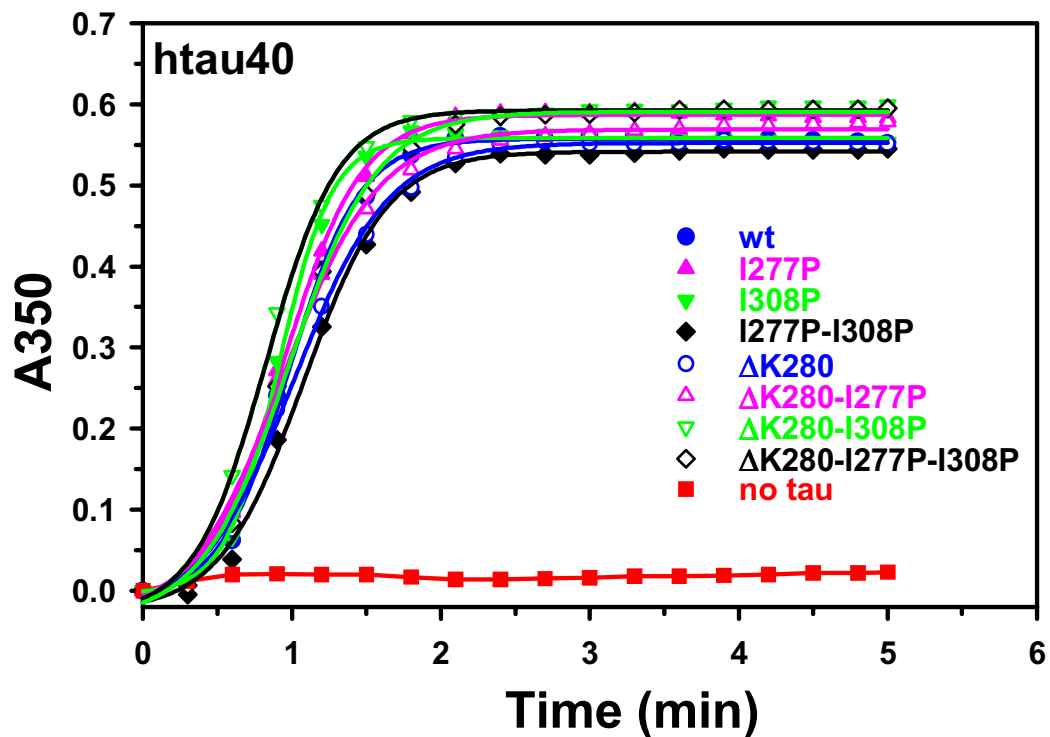
Fig. 8: Microtubule assembly promoted by htau40 and its proline mutants.

Assembly of microtubules was observed by the optical density at 350 nm (A_{350}). 30 µM tubulin (dimer concentration) was mixed with 5 µM htau40 at 4°C. The reaction was started by warming up the samples to 37°C. Tubulin alone is unable to polymerize because its concentration is below the critical concentration (bottom red curve). Htau40 wild-type induces assembly with a half-time of ~40 s and a lag time of ~10 s. All htau40 proline mutants show a similar ability to promote MT assembly.

Taken together, the following conclusions can be drawn from these results and are summarized in table 3 and 4.

1. Three-repeat forms of tau (3R), which have only one hexapeptide motif (PHF6 in the third repeat), loose their capacity to form PHFs by any β-breaking mutant in the PHF6 hexapeptide (such as I308P)(von Bergen et al., 2000).

2. In the case of four-repeat forms of tau (4R) which have two hexapeptide motifs (PHF6* in the second repeat and PHF6 in the third repeat), both single proline mutants in the PHF6* or PHF6 hexapeptide inhibit PHF formation completely. This means that 4R forms of tau require both hexapeptide motifs to adopt β-structure

upon polymerization. Conversely, a non-β-conformation in one of the motifs is enough to disrupt the aggregation potential of the other.

3. However, the inhibition by the I308P mutant in PHF6 can be overcome by turning PHF6* into a strong assembly promoter via the ΔK280 mutation (in the presence of heparin). In other words, the PHF6* motif with the ΔK280 mutant is so potent in terms of PHF assembly that it can induce aggregation even if the PHF6 motif in the third repeat cannot nucleate β-structure. This is reminiscent to the situation in 3R tau where a single competent hexapeptide motif is sufficient for aggregation. But for the ΔK280 mutant, the polymerization requires the presence of polyanions when the PHF6 motif is disabled.

Protein	Mutation in PHF6*	Mutation in PHF6	Polyanions (heparin)	Aggregation
K18wt	-	-	-	-
K18wt	-	-	+	+
K18-I277P	+	-	-	-
K18-I277P	+	-	+	-
K18-I308P	+	+	-	-
K18-I308P	+	+	+	-
K18-I277P-I308P	+	+	-	-
K18-I277P-I308P	+	+	+	-
K18-ΔK280	+	-	-	+
K18-ΔK280	+	-	+	+
K18-ΔK280-I277P	+	-	-	-
K18-ΔK280-I277P	+	-	+	-
K18-ΔK280-I308P	+	+	-	-
K18-ΔK280-I308P	+	+	+	+
K18-ΔK280-I277P-I308P	+	+	-	-
K18-ΔK280-I277P-I308P	+	+	+	-

Table 3: 4R construct K18 and its proline mutants in the PHF6* and PHF6 motifs prevent PHF aggregation.

Symbols mean: - = negative (e.g. K18wt has no mutations in PHF6* motif and PHF6 motif, it cannot aggregate in the absence of heparin), + = positive (e.g. K18wt can aggregate in the presence of heparin), + = unusual aggregation of tau protein (e.g. K18-ΔK280 mutant, it has a mutation in the PHF6* motif and can aggregate in the absence of heparin).

Protein	Mutation in PHF6*	Mutation in PHF6	Polyanions (heparin)	Aggregation
htau40wt	-	-	+	+
htau40-I277P	+	-	+	-
htau40-I308P	-	+	+	-
htau40-I277P-I308P	+	+	+	-
htau40-ΔK280	+	-	+	+
htau40-ΔK280-I277P	+	-	+	-
htau40-ΔK280-I308P	+	+	+	+
htau40-ΔK280-I277P-I308P	+	+	+	-

Table 4: Full-length isoform htau40 and its proline mutants in the PHF6* and PHF6 motifs prevent PHF aggregation (in the presence of heparin).

Symbols mean: - = negative (e.g. htau40wt has no mutations in PHF6* motif and PHF6 motif, it cannot aggregate in the absence of heparin), + = positive (e.g. htau40wt can aggregate in the presence of heparin), + = unusual aggregation of tau protein (e.g. htau40-ΔK280-I308P mutant, it has a mutation in the PHF6* and PHF6 motifs and can still aggregate).

2. Analysis of stability and intramolecular interaction of paired helical filaments from tau protein by intrinsic fluorescence

Several principles of the aggregation of tau protein have emerged over the past few years: The repeat domain is important for PHF aggregation (Wille et al., 1992); aggregation is strongly favoured by oxidation, which leads to tau dimerization by disulfide crosslinks at Cys322 (Schweers et al., 1995; Wille et al., 1992); aggregation is also strongly enhanced in the presence of polyanions such as heparin, ribonucleic acids, or acidic peptides such as poly-Glu (Goedert et al., 1996; Kampers et al., 1996; Perez et al., 1996). Based on these principles, an assay of PHF aggregation *in vitro* has been developed that can be used in solution and in real time (Friedhoff et al., 1998b). This assay was based on the fact that the fluorophore Thioflavine S (ThS) strongly increases its fluorescence yield when it binds to PHFs. Although the ThS assay works reproducibly, it was conceptually not ideal because it relies on an exogenous reagent that could possibly alter some features of the aggregation pathway. Therefore it is better to search for an aggregation assay based on signals that are intrinsic to tau protein. Recently some reports showed the intrinsic fluorescence approaches for β-amyloid (Fraser et al., 1994; Garzon-Rodriguez et al., 2000). Unfortunately tau contains very few aromatic amino acids. The longest isoform htau40 comprises three phenylalanines (F8, F346, F379), five tyrosines (Y18, Y29, Y197, Y310, Y394) and no tryptophan at all. None of these lie in alternatively spliced regions so that all tau isoforms have the same aromatic residues. Tyr310 lies within the PHF6 hexapeptide, which undergoes a conformational transition upon polymerization and is therefore prone to show a conformational dependent fluorescence. After initial experiments we decided to exchange the tyrosine by a tryptophan, considering the greater dependence of its fluorescence to environmental factors and its higher emission yield. Its fluorescence was used as a reporter to obtain new insights into the conformation of tau in the soluble state and after incorporation into PHFs. In this part of this work it was shown that Trp fluorescence can be used to determine the stability of PHFs, their solvent accessibility and the proximity of Trp and Tyr residues, as seen by fluorescence resonance energy

transfer (FRET), and this fluorescence assay also can be used to monitor the effects of compounds that act as PHF inhibitors.

A valuable feature of intrinsic protein fluorescence is the high sensitivity of tryptophan to its local environment (Gryczynski et al., 1988). One can observe changes in emission spectra of tryptophan in response to protein conformational transitions or subunit association or denaturation – all of these factors can affect the local environment surrounding the indole ring (Lakowicz, 1999). For tryptophan in a completely apolar environment, the emission spectrum shows a blue-shift. When tryptophan moves towards hydrogen-bonding groups or becomes exposed to water, the emission spectrum shifts to longer wavelengths (Shopova, 1983).

2.1 A tryptophan residue in the repeat domain of tau is a sensitive reporter of the stages of PHF aggregation

In order to monitor PHF formation by tryptophan fluorescence, tryptophans were introduced as single mutations in different sites within the repeat domain. First we exchanged Tyr310 to Trp310, because of the critical role of this part of the sequence for PHF assembly. In order to monitor the change of the local environment upon PHF assembly a tryptophan scanning strategy was set up. In most cases conservative exchanges were performed at aliphatic (L266W, I297W, I328W, I360W) or aromatic amino acids (Y310W, F346W), except for Q244W, with the aim of minimizing any perturbation in the protein structure. Because of the prominent role of the hexapeptide motifs PHF6 and PHF6* in PHF assembly we were especially interested in the impact of PHF formation on the fluorescence of tryptophan at these sites.

All constructs and isoforms, which were used in this part of work, are shown in Fig. 9. Tryptophan mutations were generated based on the 4R short construct K18 (Fig. 9C), 3R short construct K19 (Fig. 9D), full-length 4R tau isoforms htau40 (Fig. 9A) and 3R tau isoform htau39 (Fig. 9B).
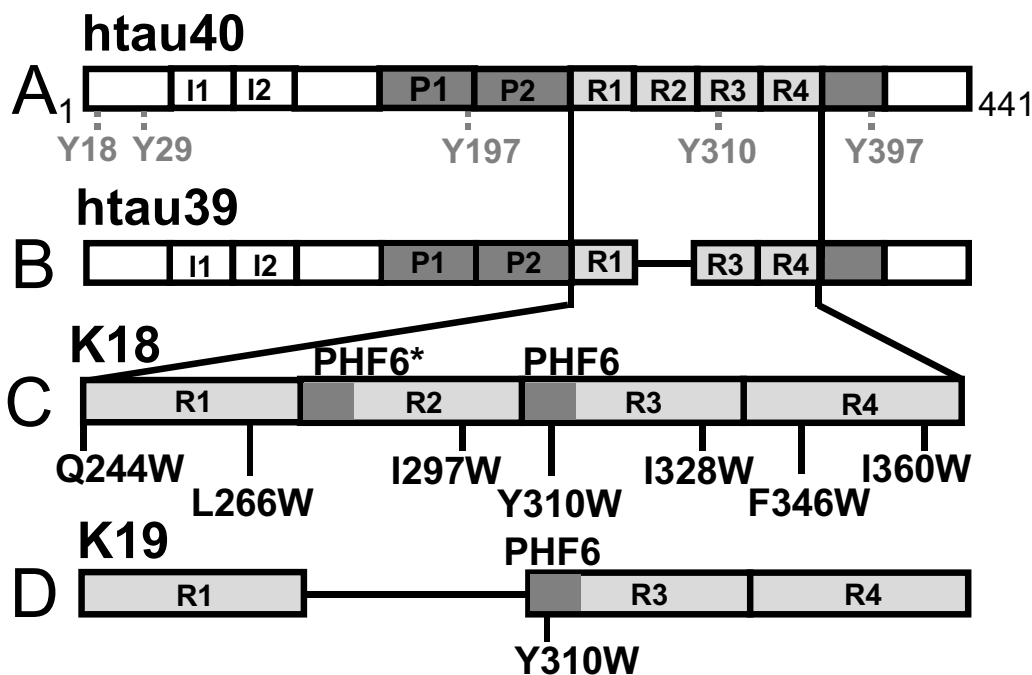
Fig. 9: Bar diagram of tau isoforms, constructs and tryptophan mutants.

(A) Full-length isoform htau40 (the largest isoform in human CNS, containing 2 alternatively spliced inserts near the N-terminus (I1, I2) and 4 repeats (R1-R4) in the C-terminal half; 441 residues. The protein contains 5 Tyr residues (no. 18, 29, 197, 310, 397, indicated in grey), but no Trp. Tyr310 is the only one in the repeat domain. The mutant Y310W generates intrinsic Trp fluorescence without inhibiting aggregation (see below). (B) Isoform htau39 (only 3 repeats due to alternative splicing of exon 10 so that R2 is removed). It contains the same 5 Tyr residues as htau40. (C) Enlarged view of repeat domain construct K18 (four repeats only, 129 residues, Q244-E372). (D) Repeat domain construct K19 (three repeats only, 98 residues, Q244-K274, V306-E372). The numbering is according to htau40, the longest isoform in human CNS containing 441 residues. The dark grey areas flanking the repeats shown for htau40 and htau39 represent the basic and proline-rich domains that contribute strongly to microtubule binding ("jaws", (Gustke et al., 1994)). The dark grey boxes in K18 and K19 show the hexapeptide motifs PHF6* (^{275}VQIINK^{280}) and PHF6 (^{306}VQIVYK^{311}) whose conversion to β-structure is an early step in PHF assembly (von Bergen et al., 2001; von Bergen et al., 2000). The mutation Y310W (in repeat R3) was introduced in all isoforms and constructs. Mutations Q244W, L266W, I297W, I328W, F346W, and I360W covering positions along the whole sequence of the repeat domain are indicated for K18.

2.1.1 Comparison of Tyr and Trp fluorescence of construct K18 and mutant K18-Y310W upon aggregation

The fluorescence spectra of the repeat domain construct K18 wild-type (containing the single tyrosine Y310 within the PHF6 hexapeptide motif, but no tryptophan), and the spectra of mutated K18-Y310W are shown in Fig. 10. The tyrosine containing K18 exhibits only a small change in the fluorescence spectrum during PHF assembly. Fig. 10A and B show the excitation and emission spectra of K18wt in the soluble state

(black curves) and after PHF assembly (red curves). The fluorescence wavelength shows a slight red-shift of ~2-3 nm after aggregation (Fig. 10A, B). In contrast, the mutant K18-Y310W shows a clear shift upon PHF assembly, equivalent to a blue-shift of ~15 nm from 354 nm in the soluble state to 339 nm in the polymerized state (Fig. 10D). The positions of the excitation and emission maxima, 288 nm and 354 nm (Fig. 10C, D), indicate that the tryptophan residue is almost fully exposed to the solvent in the soluble state and not buried in the interior of the protein. The blue-shift following PHF aggregation can be explained by an increased hydrophobicity in the local environment (Gasymov et al., 2001; Ropson and Dalessio, 1997) and suggests that W310 becomes embedded in a hydrophobic pocket within the PHFs.
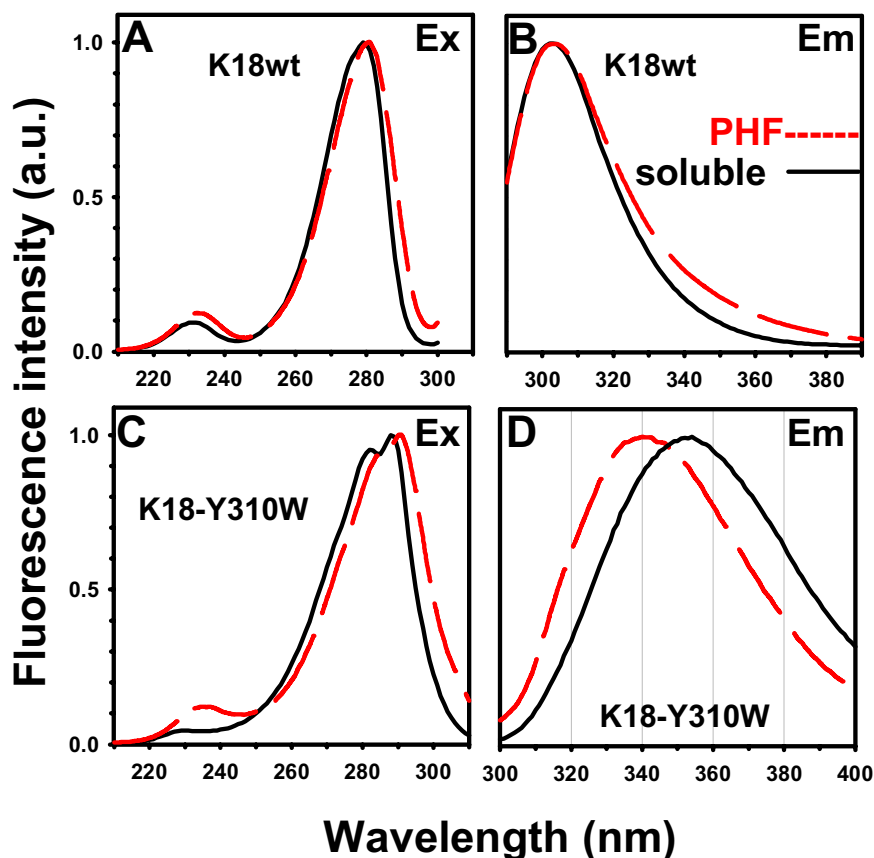

Fig. 10: Tyrosine and tryptophan fluorescence spectra of the 4R constructs K18wt and K18-Y310W.

(A) and (B) show the excitation and emission spectra of construct K18wt in the soluble state (black curves) and after PHF assembly (red curves), normalized to the same height (peaks at ~280 nm and ~305 nm, respectively). The fluorescence is entirely due to the single Y310, which shows a slight red-shift upon aggregation. (C) and (D) show the equivalent excitation and emission spectra for the mutant K18-Y310W. (C) Shows an excitation scan with emission fixed at 350 nm which peaks at 290 nm. (D) Shows the emission scan with excitation at 280 nm. The spectra exhibit a maximum at 354 nm for the soluble (black curve) and 339 nm for the aggregated (red curve) protein. Note the significant blue-shift of the emission maximum in (D) following PHF assembly (~15 nm, from 354 nm to 339 nm).

2.1.2   Tryptophan fluorescence spectra of full-length isoforms htau39-Y310W and htau40-Y310W before and after PHF assembly

Similar results as described for the repeat domain K18 were obtained with the full-length isoforms htau40 and htau39 (lacking R2)(Fig. 11). The unmodified proteins contain five tyrosine residues (Y18, Y29, Y197, Y310, Y394) whose fluorescence spectra are essentially the same as in K18wt. However, when a tryptophan is introduced at residue 310 it dominates the spectrum in the tryptophan specific region. In the soluble state, the maxima of the emission scan is ~352 nm (Fig. 11, black curve), indicating almost full solvent exposure. This means that W310 does not become embedded in other domains of the protein in the soluble state, even in the full-length protein. When htau40 is aggregated into PHFs, a blue-shift down to 334 nm is observed (Fig. 11A, red line). This shift is even more extensive than that of K18 and suggests effective burial of the tryptophan in a hydrophobic pocket inside the PHFs. A similar, although less extensive, blue-shift is observed with the Y310W mutant of htau39 (emission wavelength from 352 nm in the soluble to 342 nm in the polymerized state, Fig. 11B).
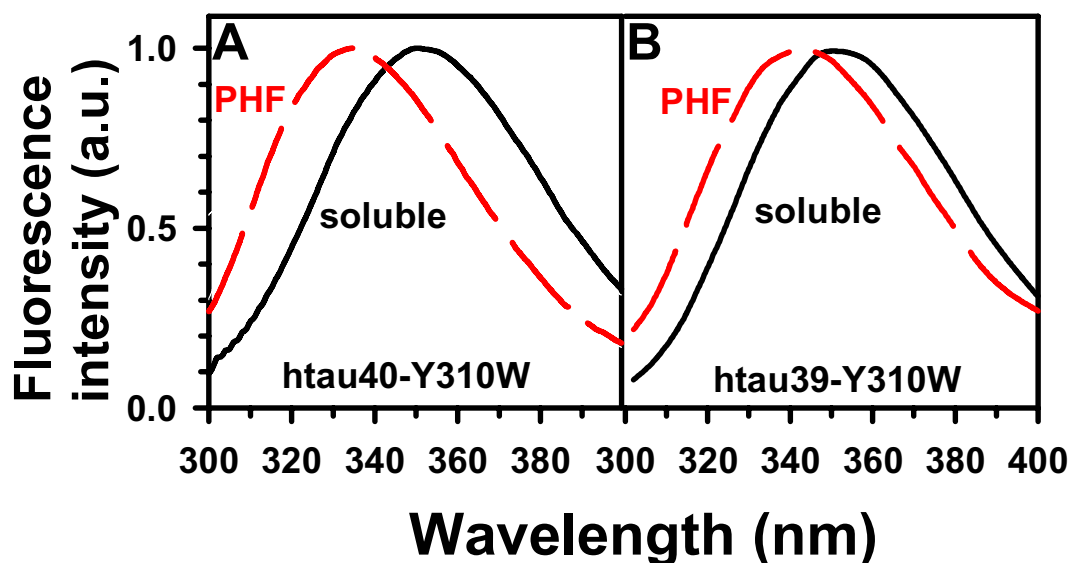
Fig. 11: Tryptophan fluorescence spectra of the full-length isoforms htau39-Y310W and htau40-Y310W before and after PHF assembly.

(A) Shows the emission spectra of the isoform mutants htau40-Y310W (excitation at 290 nm), the spectra exhibit a maximum at 352 nm in the soluble state (black curve) and 334 nm in the aggregated state (red curve), there is a pronounced blue-shift upon PHF assembly (~18 nm). (B) Shows the emission spectra of the isoform mutants htau39-Y310W before (black curve) and after (red curve) PHF assembly (excitation at 290 nm), which shows a similar blue-shift as htau40-Y310W.

In summary, these results are consistent with an open unfolded structure of the repeat domain in the soluble state, and with its burial inside the PHFs during aggregation. All other tryptophan single mutations lead to blue-shifts from the soluble to the aggregated state whose magnitude depends on the site of mutation (see below).

2.2 Comparison of the kinetics of aggregation, conformational transitions and microtubule interactions of tryptophan mutants and wild-type tau protein

Introducing mutants into the structural analysis of tau and PHFs requires evidence that the mutation does not alter the specific activities of the protein. This is illustrated by

data on PHF assembly, PHF morphology, analysis of the conformation of soluble and polymerized protein and analysis of tau promoted microtubule assembly.

2.2.1 The kinetics of PHF aggregation from Y310W mutants based on the short construct K18 and the FTDP-17 mutation K18-ΔK280 followed by Thioflavine S

In the earlier studies of PHF aggregation the accelerating effect of polyanions was used and the assembly was monitored by the fluorescence of Thioflavine S (Friedhoff et al., 1998b). For the tryptophan fluorescence study it was checked whether the tryptophan mutants behave similarly by the same criteria.

Fig. 12 illustrates that this is the case for PHF assembly, with only minor modifications. The repeat domain K18wt aggregates with roughly similar kinetics, with or without the Y310W mutation; in both cases polyanions (heparin in this case) are needed to achieve efficient aggregation within an aggregation half-time of ~5 h (Fig. 12A). The result is noteworthy because residue 310 is part of the hexapeptide motif PHF6 (^{306}VQIVYK^{311}) involved in the generation of β-structure during aggregation. Apparently the exchange of Tyr to Trp does not destroy the motif's capacity to support aggregation, in contrast to proline mutations (Wallon et al., 2000)(see Fig. 4).

The K18-ΔK280 mutant was also checked. This mutant was discovered in a search for FTDP-17 mutations (Rizzu et al., 1999); it is particularly interesting for *in vitro* studies because this mutation is highly efficient for PHF assembly (Barghorn et al., 2000) even without polyanions (von Bergen et al., 2001). Here, too, the Y310W mutation has little influence on the behaviour of the protein: In both cases it is able to aggregate into PHFs with similar kinetics without heparin, although heparin still has an accelerating effect (Fig. 12B).
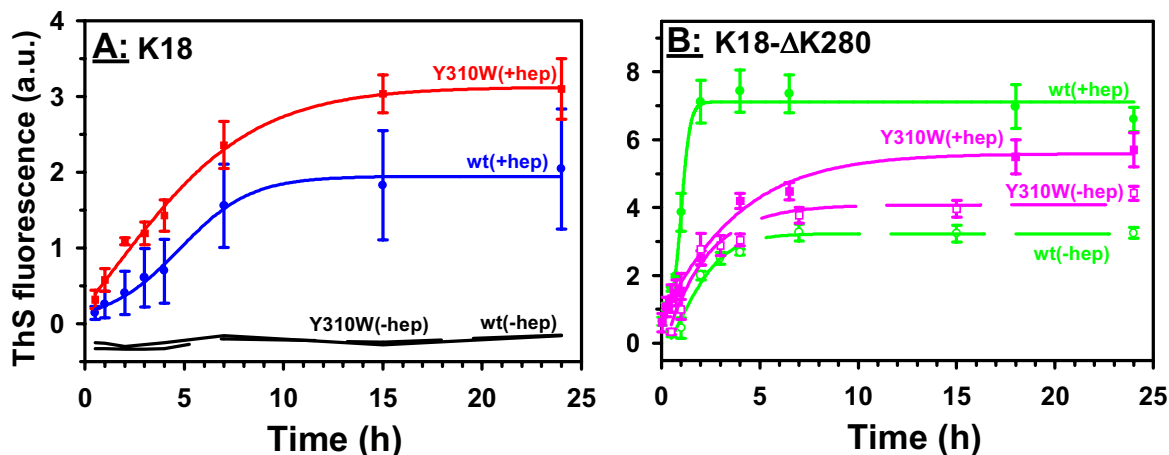
Fig. 12: Time course of PHF assembly from K18 and tryptophan mutants followed by ThS assay.

(A) Kinetics of PHF formation of K18wt in the presence of heparin (blue solid line) or without heparin (dashed curve, bottom); and kinetics of K18-Y310W in the presence of heparin (red solid line) or without heparin (solid line, bottom) measured by ThS. Note that both the wild-type and the Trp mutant require polyanions (heparin) for efficient polymerization and that the time course of assembly is similar, even though the extent differs. (B) Kinetics of PHF assembly of construct K18-ΔK280 with or without heparin (green solid line, top curve, and green dashed line, bottom curve), and kinetics of K18-ΔK280-Y310W with or without heparin (pink solid and dashed lines, middle curves). The ΔK280 mutant allows both proteins to polymerize even without heparin, but heparin accelerates the process.

2.2.2   The time course of PHF assembly from the constructs K18, K19 and K18-ΔK280 followed by tryptophan fluorescence

After having shown that the Y310W mutation leaves the capacity for PHF formation intact, it was tested whether the fluorescence of W310 could serve as an intrinsic reporter of aggregation. In Fig. 13 the wavelength of the emission maximum was plotted versus time of aggregation. Soluble K18-Y310W and K19-Y310W begin at values of ~354-356 nm and change gradually towards final values of ~340-346 nm (filled circles and squares). The half times of ~10 hours are of comparable magnitude but longer than the values obtained with ThS fluorescence (~5 h, see Fig. 12A), indicating that these two fluorophores emphasize different aspects in the aggregation process.
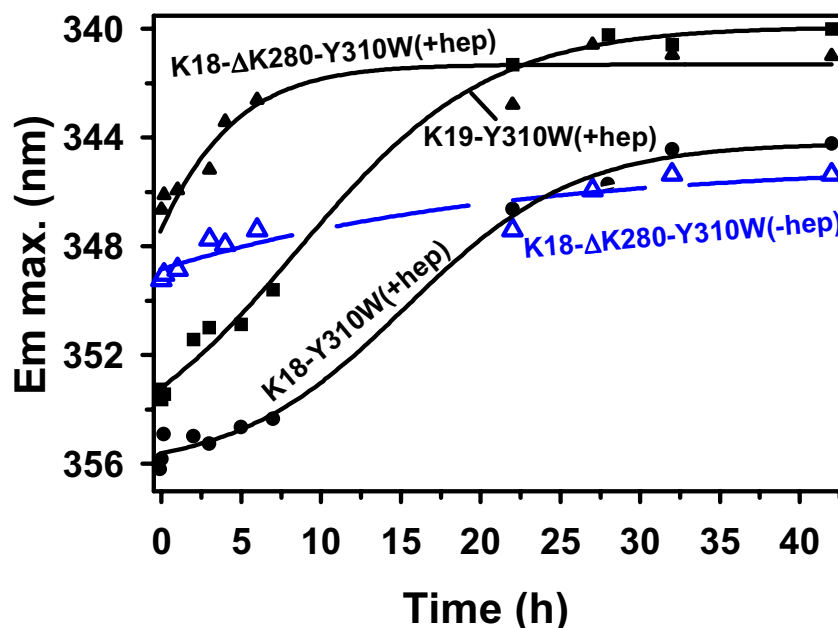
Fig. 13: Time course of PHF assembly from constructs K18 and K19 followed by tryptophan fluorescence.

Kinetics of PHF formation observed by tryptophan fluorescence in Y310W mutants of K18 and K19 (excitation at 290 nm, emission scan 300-420 nm, wavelength of emission maximum is plotted versus time). The proteins containing the ΔK280 mutations (K18-ΔK280-Y310W, filled and open triangles) aggregate rapidly and start from a lower maximum wavelength (~348 nm) than K18-Y310W and K19-Y310W (start at 355 and 353 nm, respectively).

A likely interpretation is that the fluorescence of W310 and ThS responds differently to intermediate steps in PHF formation (e.g. dimerization, nucleation, annealing). In addition, the weighting of the assembly states is different: In the case of W310, all molecules contribute, resulting in an overlap of spectra with different emission maxima. In the case of ThS, the spectrum is dominated by molecules attached to aggregates, whereas the contribution of monomers, dimers, and low oligomers is thought to be negligible. Thus, it is possible that incipient aggregation is highlighted by ThS, but not by the intrinsic fluorescence of tryptophan. The mixture of aggregation states is well illustrated by the curves of the K18-ΔK280-Y310W mutants (Fig. 13, open and filled triangles), which start already midway on the y-axis, around 348 nm. This is due to the high tendency of this mutant to aggregate, so that oligomers and small aggregates become noticeable even at the earliest time points. Note that K19-Y310W (Fig. 13, filled squares) reaches the same extent of polymerization as K18-ΔK280-Y310W (Fig. 13, filled triangles) in the presence of heparin regarding the emission maximum, whereas K18-Y310W (Fig. 13, filled circles) in the presence of heparin behaves similar

to K18-ΔK280-Y310W in the absence of heparin (Fig. 13, opened triangles). This shows one advantage of tryptophan fluorescence in comparison to the ThS assay because the extent of the shift is defined as the ratio of the soluble to the aggregated protein (the exact values for the aggregated protein are taken from table 5, for which PHFs were pelleted and measured without contamination of soluble protein). The extent of polymerization for the proteins was calculated from the relative shift in the emission maximum: K19-Y310W 93%, K18-Y310W 54%, K18-ΔK280-Y310W 56% in the absence of heparin, and 89% in the presence of heparin. Note that with the tryptophan fluorescence assay no centrifugation step is needed to determine the efficiency of polymerization.

**Table 5:** Parameters of intrinsic Trp fluorescence of different tau derivatives

Mutants	Emission max. in soluble state (Ex at 290nm)	emission max. in PHF state (Ex at 290nm)	midpoint of denaturation GuHCl [M]	slope (K) of quenching by acrylamide, soluble state	slope (K) of quenching by acrylamide, PHF state
K19-Y310W	353	340	1.2		
K18-Y310W	355	339	1.1	13.8	4.2
K18-ΔK280-Y310W	348	339	1.8	9.0	3.7
K18-Q244W	354	342	1.5	11.3	7.1
K18-L266W	353	341	1.3	13.6	8.0
K18-I297W	352	332	1.8	13.5	3.6
K18-I328W	352	340	1.6	11.0	5.0
K18-F346W	352	349	1.0	13.6	9.2
K18-I360W	354	352	1.0	12.0	11.2
htau40-Y310W	352	334	1.0	13.0	3.7
htau39-Y310W	350	342	0.5	16.5	8.1

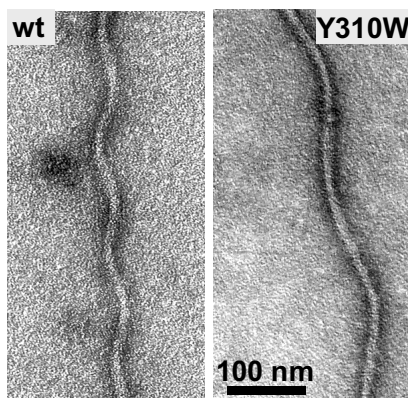### 2.2.3 *Electron micrographs of PHFs from the tryptophan mutants*

Since proteins can often aggregate into different forms, we ascertained that all aggregation products were indeed PHFs or related structures. Fig. 14 shows panels of fibers assembled from different K18 mutants and isoforms of tau. They show the morphology and variability of PHFs assembled *in vitro*, i.e. widths between 10 and 20 nm, a twist which can be variable (between 50 and 200 nm), or even 'straight fibers' similar to those which are also observed in Alzheimer's disease. In addition there are frequent short fiber stubs (100-200 nm), which may be breakdown products during

specimen preparation. All of these features are also present in PHFs preparations obtained from Alzheimer brain or reassembled from wild-type tau, indicating that the tryptophan mutations do not alter the building plan of the assembly reaction.
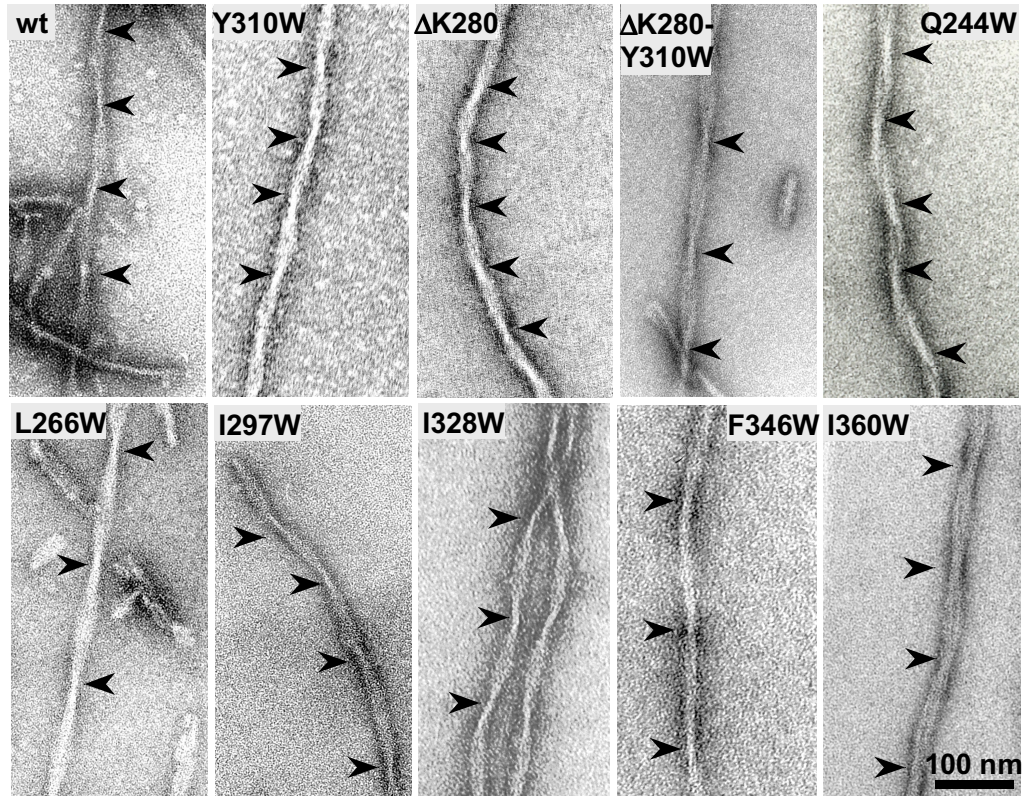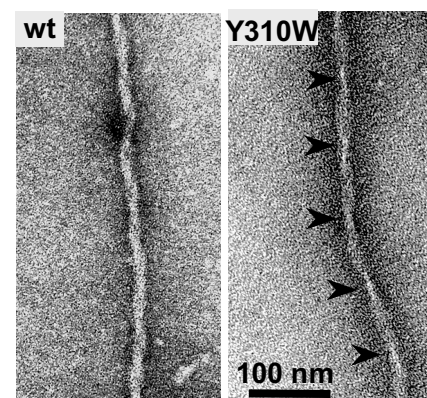

Fig. 14: Tryptophan mutants show similar morphology and variability of PHFs as wild-type isoforms and short constructs.

Panels from left to right show negatively stained electron micrographs of K18wt, K18-Y310W, K18-ΔK280, K18-ΔK280-Y310W, K18-Q244W, K18-L266W K18-I297W, K18-I328W, K18-F346W, and K18-I360W. Isoforms htau40wt, htau40-Y310W, htau39wt, htau39-Y310W. The images show that all mutants aggregate into similar paired helical filament structures as well as straight filaments. There is some variation in the degree of twisting, but this is not correlated with the type of mutant.

2.2.4   FTIR spectra of PHF and soluble 4R construct K18 and tryptophan mutants

The aggregation of tau into PHFs is accompanied by the formation of local β-structure around the hexapeptide motifs PHF6* ([275]VQIINK[280]) and PHF6 ([306]VQIVYK[311]). Mutations in these regions can have a strong influence on PHF aggregation, either favourable (e.g. ΔK280, P301L, both found in frontotemporal dementias)(Barghorn et al., 2000) or unfavourable (any proline mutation, (von Bergen et al., 2000), see Results 1). It was therefore important to ascertain whether the Y310W mutation or any of the other tryptophan mutations had an influence on β-structure formation. This was investigated by FTIR spectroscopy. The spectrum of the soluble wild type K18 protein exhibits a maximum at ~1652 wavenumbers (Fig. 15A, black line) indicating mostly random coil structure (Byler and Susi, 1986; Susi and Byler, 1983). During aggregation it is shifted to lower values, at ~1630 cm^{-1} (Fig. 15A, red line) – a typical behaviour for an increased content of β-structure. The tryptophan mutant K18-Y310W shows a comparable shift (although not as prominent, with only a shoulder at 1625 cm^{-1}, Fig. 15B), and indeed all of the Trp mutants of K18 gave similar results (Fig.15C-H). This argues that all mutants show an increase of β-sheet content during their aggregation into PHFs. Note that the change in conformation is nearly invisible for full-length tau since the fraction of β-structure is too low (von Bergen et al., 2000).
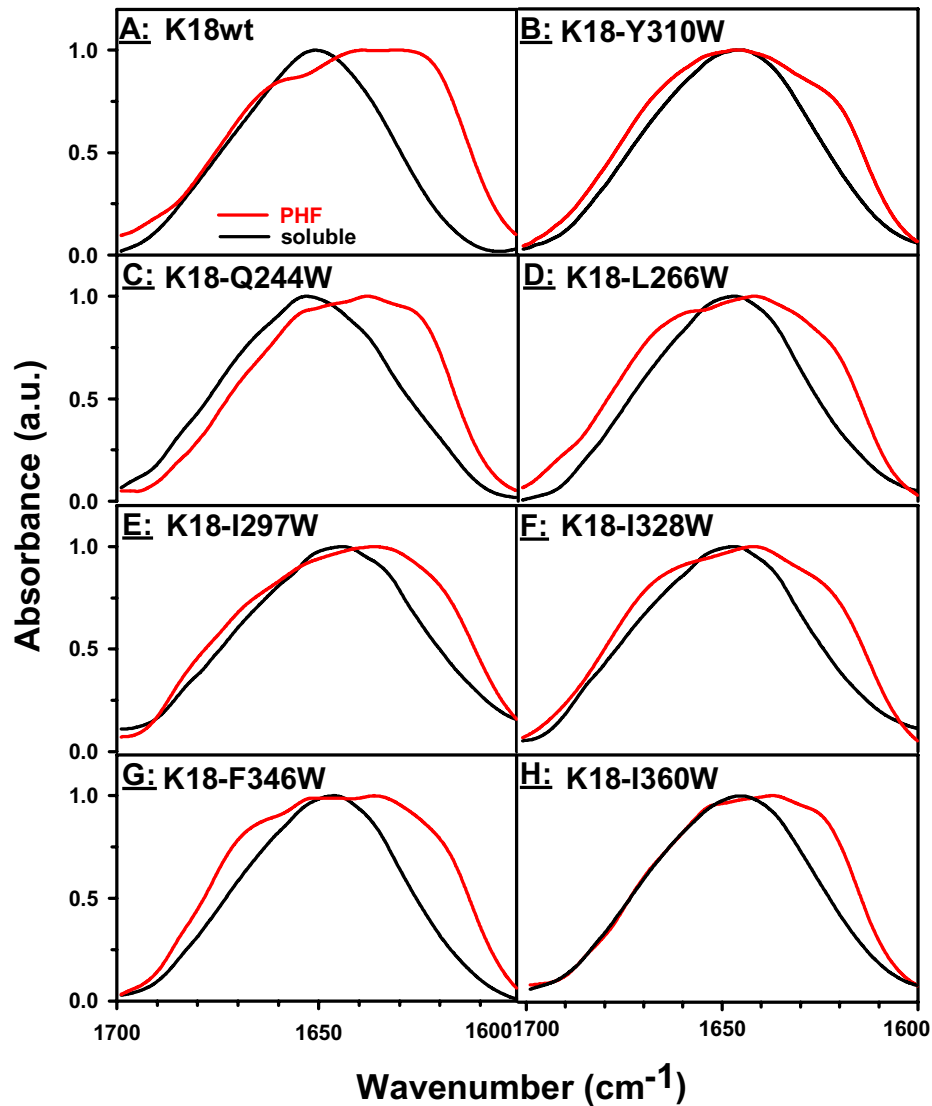
Fig. 15: FTIR spectra of PHF and soluble tau protein of tryptophan mutants.

(A-H) K18wt, K18-Y310W, K18-Q244W, K18-L266W, K18-I297W, K18-I328W, K18-F346W, K18-I360W. The soluble proteins (black curves) have maxima around 1652 cm^{-1}; polymerization (red curves) shifts the curves to the right (lower wavenumbers), indicating an increase in β-structure.

2.2.5 Microtubule assembly induced by full-length isoforms htau39, htau40 and Y310W mutants

The physiological role of tau is to stabilize neuronal microtubules. This function involves the repeat domain (Butner and Kirschner, 1991; Goode and Feinstein, 1994; Gustke et al., 1994) and can be observed *in vitro* by UV light scattering from assembling microtubule solutions. We therefore asked whether the tryptophan

mutations in the repeat domain would impair tau's assembly promoting function. Fig. 16 illustrates for the tau isoforms containing the exchange Y310 to W that these proteins do not differ from the wild-type proteins. Tubulin alone does not self-assemble in these conditions (filled circles, bottom line), but assembly is strongly enhanced by htau40 or its Y310W mutant (half time of ~0.5 min, open triangles and squares). A similar result is obtained with htau39 and its Y310W mutant, except that the assembly stimulation is less pronounced, consistent with the absence of one repeat, R2 (half time of ~1.2 min, filled triangles and squares). Note that these experiments cannot be carried out with the repeat domain alone (K18 or its mutants) since its binding to microtubules and its capacity of inducing microtubules is too weak at the concentrations used here while the flanking domains of tau are absent (Gustke et al., 1994).
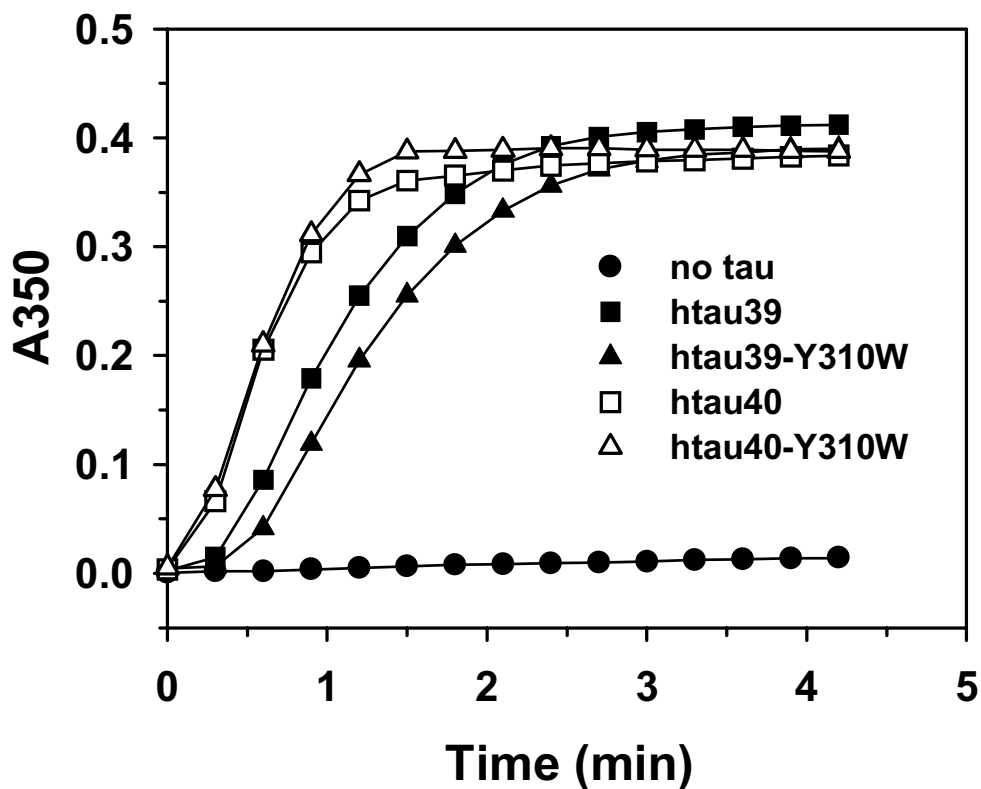

Fig. 16: Microtubule assembly induced by tau isoforms or Y310W mutants.

Assembly of microtubules from tubulin was induced by a temperature shift to 37°C and measured by light scattering (absorption at 350 nm). Without tau, tubulin does not self-assemble at the chosen concentration (30 µM tubulin heterodimer, filled circles, bottom curve). Both tau isoforms htau40 and htau39 (5 µM) are competent to induce microtubule assembly (open and filled squares), and the Y310W mutation does not affect the efficiency in either case (htau40-Y310W open triangles and htau39-Y310W filled triangles).

Taken together, the results show that the tryptophan mutations introduced into the repeats of tau have little effect on the structure and functions of tau that matter for PHF aggregation or microtubule assembly. Therefore, these mutations can be regarded as valid reporters on conformations and assembly states of tau.

2.3 Solvent accessibility of tryptophan in the repeat domain of tau

Fluorescence quenching refers to any process which decreases the fluorescence intensity of a sample. Collisional quenching of proteins has been extensively utilized to determine the extent of tryptophan exposure to the aqueous phase (Eftink and Ghiron, 1977; Eftink and Ghiron, 1976). The basic idea is that collisional quenching is essentially a contact phenomenon, so that the fluorophore and quencher need to be in molecular contact to enable quenching. If the tryptophan residue is buried inside the protein, no or less quenching is expected to occur. If the tryptophan residue is on the protein surface, then quenching is expected.

2.3.1   The Stern-Volmer plot of fluorescence quenching by acrylamide of K18 and the tryptophan mutants

Since the repeat domain forms the core of PHFs, one may expect that its residues become buried within the PHF structure. The degree of solvent exposure before and after aggregation can be monitored by means of a fluorescence quenching agent, e.g. acrylamide. Seven tryptophan mutants were generated based on the construct of K18 where the tryptophans are distributed over the molecule (see Fig. 9) and their accessibility to the quenching reagent was analyzed. In this type of experiment the data are plotted in a Stern-Volmer plot which displays the ratio of F_0 to F_c (without/with quencher at concentration c) as a function of the quencher concentration. In the plots, the larger slopes indicate stronger quenching effects. Fig. 17A shows the Stern-Volmer plot of soluble proteins, which exhibit nearly the same slopes of ~11-14 (solid lines, for

overview, see table 5), indicating that almost all of the tryptophan residues show maximal accessibility for the quenching reagent. In contrast, Fig. 17B shows the Stern-Volmer plots for the aggregated proteins. The slopes of the polymerized proteins are much lower, they vary from 3-10 (solid lines). Interestingly, the tryptophan mutants in the second repeat (I297W) and the third repeat (Y310W, I328W) show lower slopes than the tryptophan mutants in the first repeat (Q244W, L266W) and the fourth repeat (F346, I360W), indicating that the tryptophan mutants in R2 and R3 are more buried in the PHF structure (for overview, see table 5).
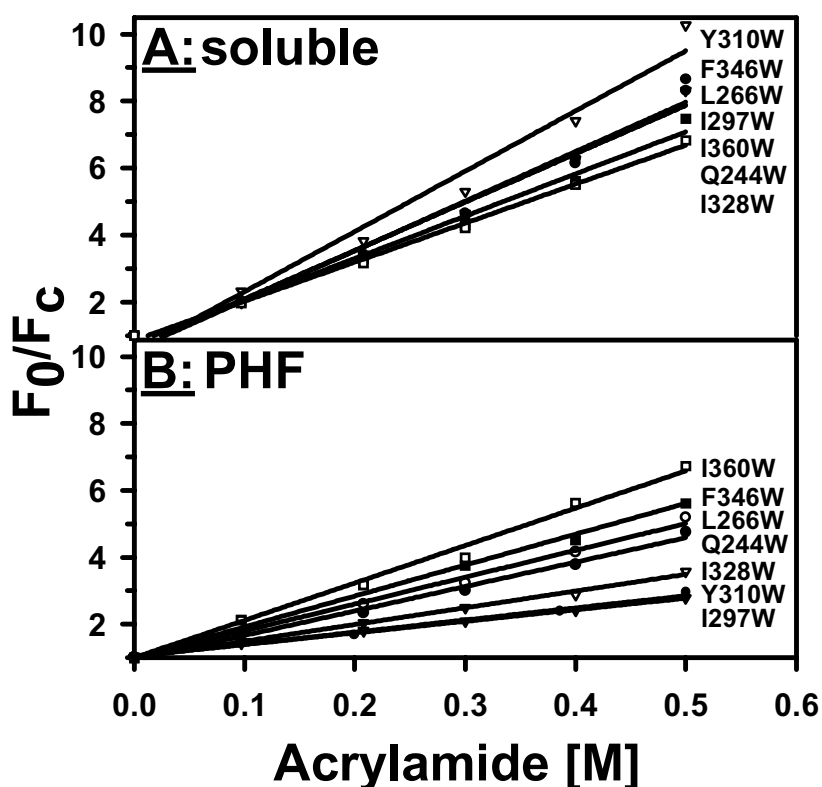

Fig. 17: Fluorescence quenching by acrylamide of K18 Trp mutants.

Seven residues, distributed over the repeat domain (construct K18) were mutated into tryptophans and probed for their exposure to the solvent (Q244, L266, I297, Y310, I328, F346, I360) before and after aggregation. Excitation at 290 nm, emission scan 300-420 nm, with maxima around 350 nm. (A) is fluorescence quenching by acrylamide of soluble proteins, represented as Stern-Volmer plot $F_0/F_c = 1 + Kc$ (c = acrylamide concentration). They exhibit similar slopes (11-14). (B) shows fluorescence quenching by acrylamide of PHFs formed from K18 mutants. A high slope K indicates high solvent accessibility. The solid curves represent seven mutants of K18 in the polymerized states, with significantly lower slopes depending on the position of the Trp residue (slopes between 4-10, see Fig. 18), indicating reduced solvent exposure.

2.3.2 *Dependence of solvent accessibly of the tryptophan mutants on position along sequence*

For a better understanding of the relationship between solvent accessibility of the tryptophan mutants and the sequence position, the plot of slopes vs. sequence position is illustrated in Fig. 18. The smoothed curve for aggregated proteins is shown roughly U-shaped (dashed line), with minimal values in repeats R2 and R3 (mutations I297W, Y310W and I328W, slopes 4-5) and higher values towards the two ends, R1 and R4 (Q244W, L266W, F346W and I360W). More specifically, the two mutants with the tryptophan within the first repeat show a lower slope than those in the fourth repeat, and the slope for the I360W mutant near the C-terminal end of the repeats is almost maximal, indicating full solvent accessibility even after PHF assembly. Thus the quenching experiments emphasize the importance of the second and third repeat for building the PHF core.
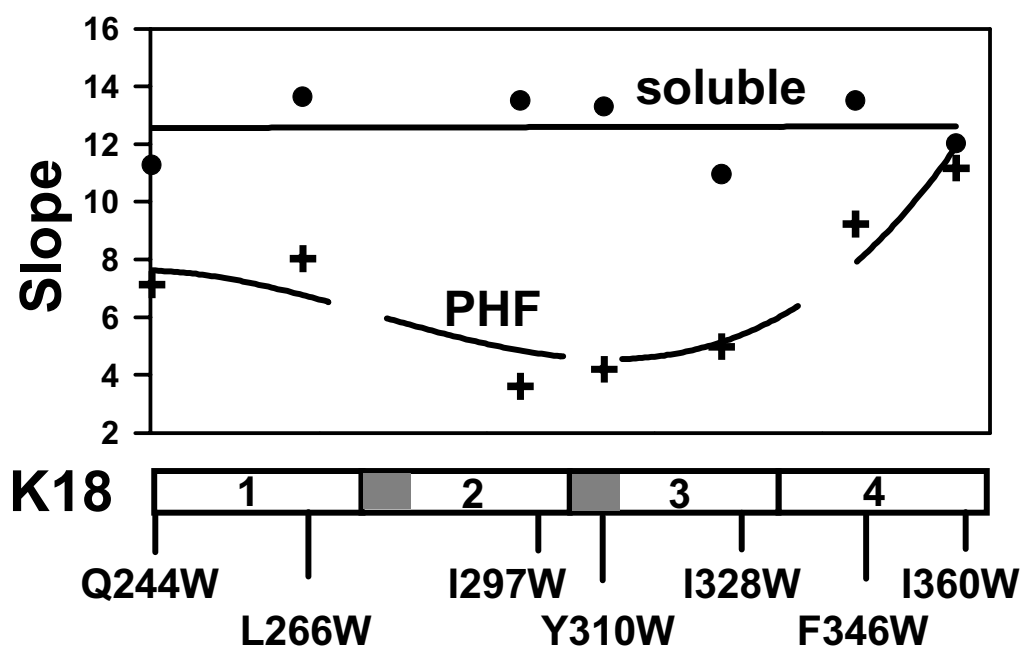

Fig. 18: Dependence of solvent accessibility on sequence position of Trp residues.

The slopes of the soluble proteins show no systematic dependence on the sequence (filled circles, solid line on top), showing that no shielded pockets are detectable. After PHF assembly (+ symbols, dashed line), a U-shaped curve emerges, illustrating that the residues near the ends of the sequence (in R1, R4) are more exposed than those in the middle (in R2, R3). Most of the residues are more buried in the PHF state than in the unpolymerized state (except I360W).

2.3.3   Dependence of the emission maximum wavelength of the tryptophan mutants on positions along the sequence

The conclusions mentioned above were confirmed independently by analyzing the wavelength shift of the different tryptophan mutants before and after PHF aggregation (Fig. 19, for overview, see table 5). Fig. 19 shows the plot of the maximum wavelengths vs. sequence position. The soluble proteins (filled circles, top line) exhibit emission maxima of ~352 nm with very little variation. In contrast the emission maxima of the polymerized proteins show a strong dependence on sequence position, with the largest blue-shift (to 332 nm) for the mutant I297W and the smallest shift (to 350 nm) for I360W. Remarkably, the curve of wavelength shift vs. sequence has almost the same U-shape as the quenching slopes in Fig. 18. This demonstrates that the emission maximum is a reliable sensor of the local environment, and that repeats R2 and R3 (notably residue 297) become buried in the PHF structure whereas the tail (residues 346, 360) is nearly exposed to the solvent.
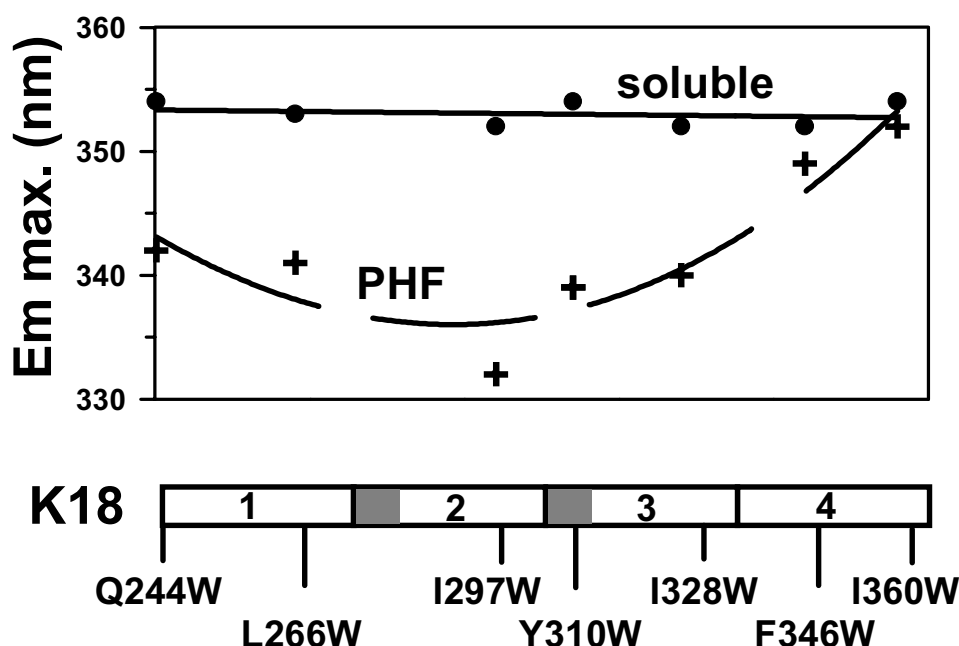

Fig. 19: Dependence of emission maximum wavelength on the position of the Trp residues along sequence.

For the soluble proteins (filled circles, solid line on top) the maxima are around 350-355 nm, indicating full solvent accessibility. After PHF assembly (+ symbols, dashed line) the emission maximum shows a pronounced blue-shift. As in Fig.18 there is a U-shaped dependence on the position of Trp in the sequence, arguing that the residues in the middle are more shielded than those at the edges of the repeat domain.

2.4 Interaction of hexapeptides analyzed by fluorescence resonance energy transfer between tyrosine and tryptophan

Fluorescence resonance energy transfer (FRET) means transfer of the excited-state energy from the initially excited donor to an acceptor. The donor molecules typically emit at shorter wavelengths with an overlap of the emission spectrum with the absorption spectrum of the acceptor. The most commonly observed FRET in proteins occurs from tyrosine to tryptophan (Eisinger, 1969). The full-length tau contains five tyrosines (Y18, Y29, Y197, Y310, Y394), after replacement of Y310 four tyrosine residues remain, most of them are located in the N-terminal half. Since the Y310 was replaced by tryptophan (Y310W) in the repeat domain, it is possible to observe the interaction of different domains by FRET analysis.

2.4.1   FRET analysis of htau40-Y310W, htau39-Y310W and htau39-Y310W dimer

Fig. 20A shows that there is a difference between soluble and aggregated htau40-Y310W (solid and dashed lines). The soluble protein shows an emission maximum at 352 nm (excitation at 275 nm), as expected from the fluorescence of W310, and an additional shoulder around 305 nm representing the fluorescence of the combined tyrosines. In principle, tryptophan could take up the fluorescence from nearby tyrosine residues closer than the Förster distance (1 nm for Tyr/Trp as the donor/acceptor pair, (Chiu and Bersohn, 1977; Eisinger, 1969)). Conversely, the existence of a pronounced shoulder implies that the distance of most tyrosine residues to W310 is larger than the Förster distance and so FRET is prevented. A different result is obtained for the polymerized protein: The emission maximum shows the blue-shift described above, but in addition the tyrosine shoulder disappears (dashed line). This implies that the tyrosine residues are now close enough to W310 to allow energy transfer by FRET. At present it is not possible to distinguish whether the transfer occurs within a molecule or between neighbouring molecules (this can be investigated by generating more donor/acceptor pairs), but the results emphasize the close approach of

tau's outer regions (N- and C-terminal tails) to the PHF core formed by the repeat domain. A similar behaviour is found for htau39-Y310W (Fig. 20B), i.e. no or little FRET in the soluble state (solid line) and therefore a shoulder at 305 nm, which becomes deleted by FRET in the aggregated state (dashed line).

PHF assembly is greatly enhanced by tau dimers, which can act as building blocks (Schweers et al., 1995; Wille et al., 1992). Therefore we asked whether spatial relationships could be detected by FRET that distinguishes monomers and dimers. A homogeneous solution of dimers can be obtained by oxidation from 3R tau isoforms since they contain only the single cysteine 322. Fig. 20C shows the emission spectrum (excitation at 275 nm) for tryptophan of monomeric (solid line) and dimeric (dashed line) htau39-Y310W. Both spectra show a clear shoulder for tyrosine fluorescence at 305 nm, with some reduction in the dimeric state. This means that in the monomeric and dimeric state the tyrosines outside the repeat domain are mostly too far from the tryptophan at position 310 to enable FRET. Moreover, there is no blue-shift of the maximum, indicating that residue 310 remains in a hydrophilic environment, in contrast to the fully aggregated PHF state (compare dashed curves in Fig. 20A, B).
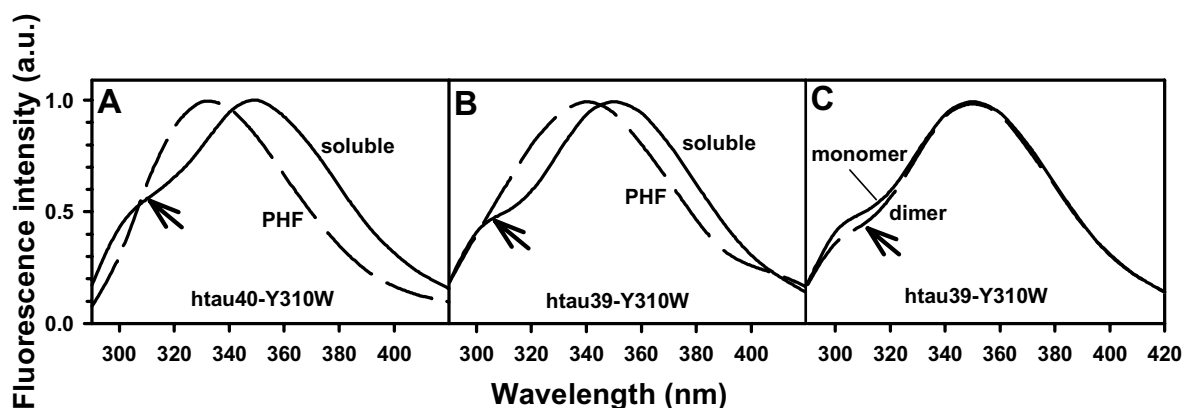

Fig. 20: Fluorescence resonance energy transfer (FRET) analysis between tyrosine and tryptophan of tau isoforms.

Tau proteins containing the Y310W mutation were irradiated at 275 nm, which excites both the Tyr and Trp fluorescence. (A) In the soluble state of htau40-Y310W (solid line), the combined fluorescence of Y18, Y29, Y197, Y397 is visible as a shoulder at ~305 nm (arrow) on the dominant fluorescence of W310 peaking at 350 nm. Upon PHF aggregation (dashed line), the W310 spectrum shows the characteristic blue-shift due to the burial of the residue, and the shoulder at 305 nm disappears because the tyrosines are now within the Förster distance and transfer their energy to the tryptophan. (B) Fluorescence spectra of htau39-Y310W in the soluble (solid line) and PHF state (dashed line), showing similar behaviour as htau40-Y310W. (C) The emission spectra of the monomeric and the dimeric mutant of htau39-Y310W (separated by gelfiltration) are shown (monomer solid line, dimer dashed line). Note that there is no significant difference, indicating that dimerization alone does not bring Tyr residues into proximity of Trp.

2.4.2 FRET analysis of the tryptophan mutants based on the 4R construct K18

A different situation applies to the tryptophan mutants of K18 (Fig. 21). In this case there is only one tyrosine, Y310, which acts as the donor, and tryptophan introduced at other positions can serve as the acceptor (at residues 244, 266, 297, 328, 346, or 360, for overview see Fig. 9C). In all cases (all excitation at 275 nm), the shoulder at 305 nm (arrows) is weak or absent since the single tyrosine is dominated by the tryptophan fluorescence. A weak shoulder can be discerned with the Q244W mutant in the soluble state (Fig. 21A, solid line) which disappears after aggregation (Fig. 21A, dashed line). This argues that residue 244 at the beginning of the repeats is far from residue Y310 within any given molecule (since FRET is absent in the soluble state) and approaches Y310, probably of neighbouring molecules, during PHF aggregation. In contrast, W360 (Fig. 21F) shows a shoulder at 305 nm both in the soluble and in the aggregated state, indicating that the C-terminal end of the repeats stays far from Y310 in both states. Finally, in the cases of the more centrally located tryptophan residues (266, 297, 328, 346, Fig. 21B-E) FRET occurs both in the soluble and aggregated state, likely because these residues are near Y310 in all conditions. Together, the data argue that (a) residues at the edges of the repeat domain (266, 360) are far from the center (Y310) in individual molecules, (b) residue 244 approaches the PHF core during aggregation but residue 360 remains far and (c) the more internal residues are spatially near the center of PHF. Since the Förster distance of 1 nm is equivalent to the spacing of 2-3 residues, the results also suggest that the repeat domain must be folded rather than being extended.
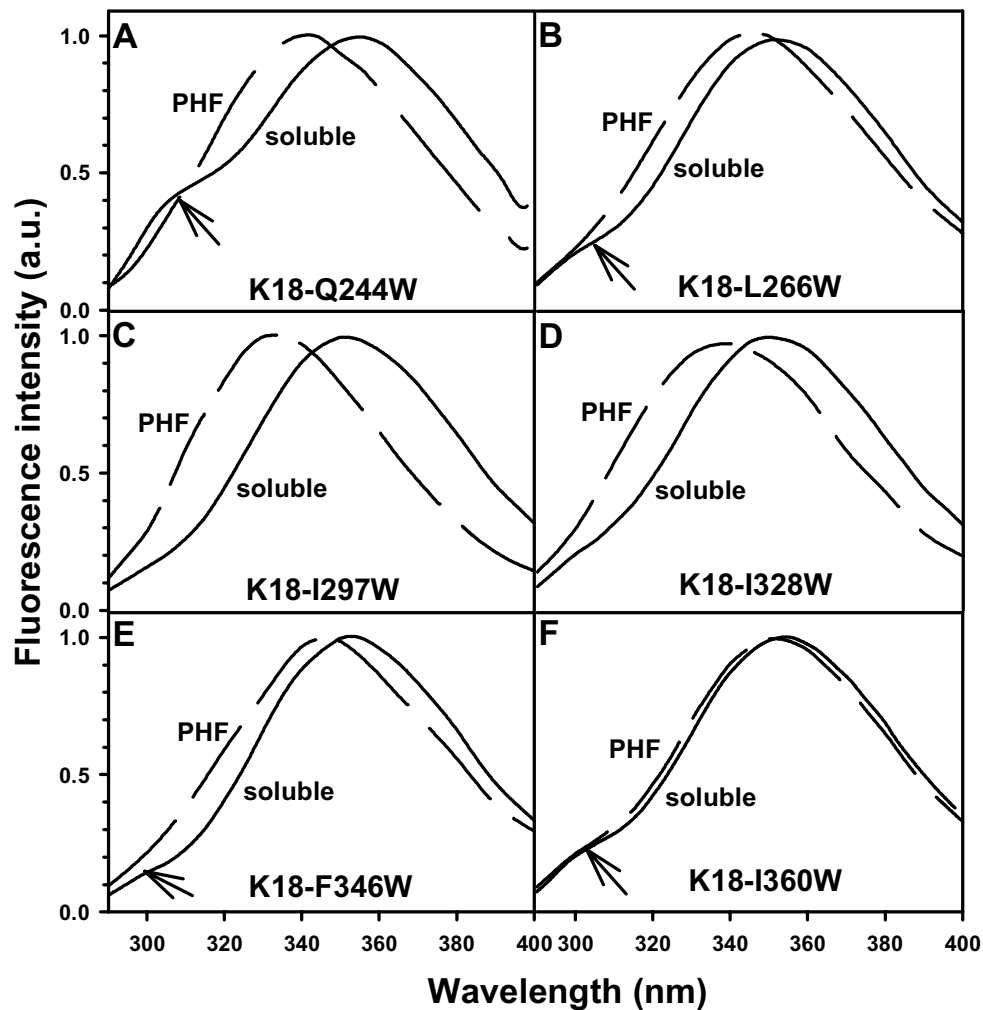
Fig. 21: FRET analysis between tyrosine and tryptophan of the K18 construct.

In the aggregated state (all dashed curves), all Trp mutants show FRET except I360W, indicating that Trp and Tyr are within the Förster distance, and Tyr transfers energy to Trp. In the soluble state (all solid curves), Q244W, L266W, F346W and I360W have a small Tyr shoulder at 305 nm, while I297W and I328W have no shoulder at all, indicating that although in the soluble state, I297W and I328W have FRET between Y310 and W.

2.5 Stability of PHFs against denaturation by guanidine hydrochloride

It is well accepted that the proper folding of proteins is an important prerequisite for functional integrity for most of the proteins. Partial unfolding appears to play a critical role in amyloid fibril formation in human amyloid diseases, which was the motivation to look more carefully at the kinetics and thermodynamics of the denaturation pathway

(Lai et al., 1997; Peretz et al., 1997). The most widely used denaturant is guanidine hydrochloride (GuHCl), which induces lower protein stability in proportion to the concentration (Dill and Shortle, 1991; Shortle et al., 1989). GuHCl is thought to interact preferentially with the hydrophobic groups in the denatured state; however, the binding is very weak, which may explain the high concentration required (Dill and Shortle, 1991).

2.5.1   *GuHCl induced denaturation of PHFs monitored by tryptophan fluorescence*

The pathway of PHF aggregation from soluble tau *in vitro* has been studied by several authors; however, it has been difficult to address the question of PHF stability. This issue becomes accessible to investigation by using the intrinsic tryptophan fluorescence. The core of Alzheimer PHFs consists mainly of the repeat domain (Jakes et al., 1991; Novak et al., 1993; Wischik et al., 1988b), and one may ask how the composition of the repeats affects PHF stability. Therefore the thermodynamic stability of PHFs assembled from the short constructs K19 or K18 (3 or 4 repeats) containing the Y310W mutation was analyzed in the presence of increasing concentrations of GuHCl (Fig. 22). With pre-formed PHFs, the emission maximum is 340 nm in the absence of GuHCl (excitation at 290 nm); at higher GuHCl concentrations it rises to 354 nm (the value typical of soluble tau) as the PHFs become denatured and disintegrate (this was also checked by electron microscopy, see Fig. 23). K19-Y310W and K18-Y310W show half maximal denaturation at similar GuHCl concentrations – around 1.1 M (Fig. 22A, filled circles and triangles). This means that the loss of one repeat in 3R tau does not influence the stability of PHFs made from the repeat domain, even though 3R constructs and isoforms assemble more readily (presumably a kinetic effect, because dimerization and nucleation is faster (Friedhoff et al., 1998a)). In contrast, PHFs made from K18 lacking residue K280 (one of the FTDP-17 mutations) show a significantly higher stability with half maximal denaturation at 1.8 M GuHCl (Fig. 22A, opened square, for overview, see table 5). This emphasizes the importance of the β-structure around the hexapeptide motifs, which is stabilized by the ΔK280 mutation (von Bergen et al., 2001).

To verify these results for full-length tau, the isoforms htau39-Y310W and htau40-Y310W were also tested (Fig. 22B). Surprisingly, here the second repeat has a significant impact on stability. PHFs made from htau39-Y310W (3R) started with an emission maximum of 342 nm and were red-shifted to 352 nm with a midpoint of ~0.5 M GuHCl. In other words, this isoform has only about half the stability of the repeat domain alone. On the other hand, PHFs made from htau40-Y310W shift from an initial 331 nm emission maximum to final 350 nm with a midpoint of ~1.0 M GuHCl, comparable to that of the repeat constructs alone. Thus there are two interesting differences between htau39 and htau40; first the absolute emission maximum in the PHF state, suggesting a more hydrophobic surrounding in the case of htau40, and secondly an increased stability of a 4R isoform versus a 3R isoform. It appears as if 4R PHFs active additional stability by factors outside the repeat domain, possibly because the flanking domains cannot be packed tightly enough into the PHF structure or perhaps there might be an interaction of flanks with R2.
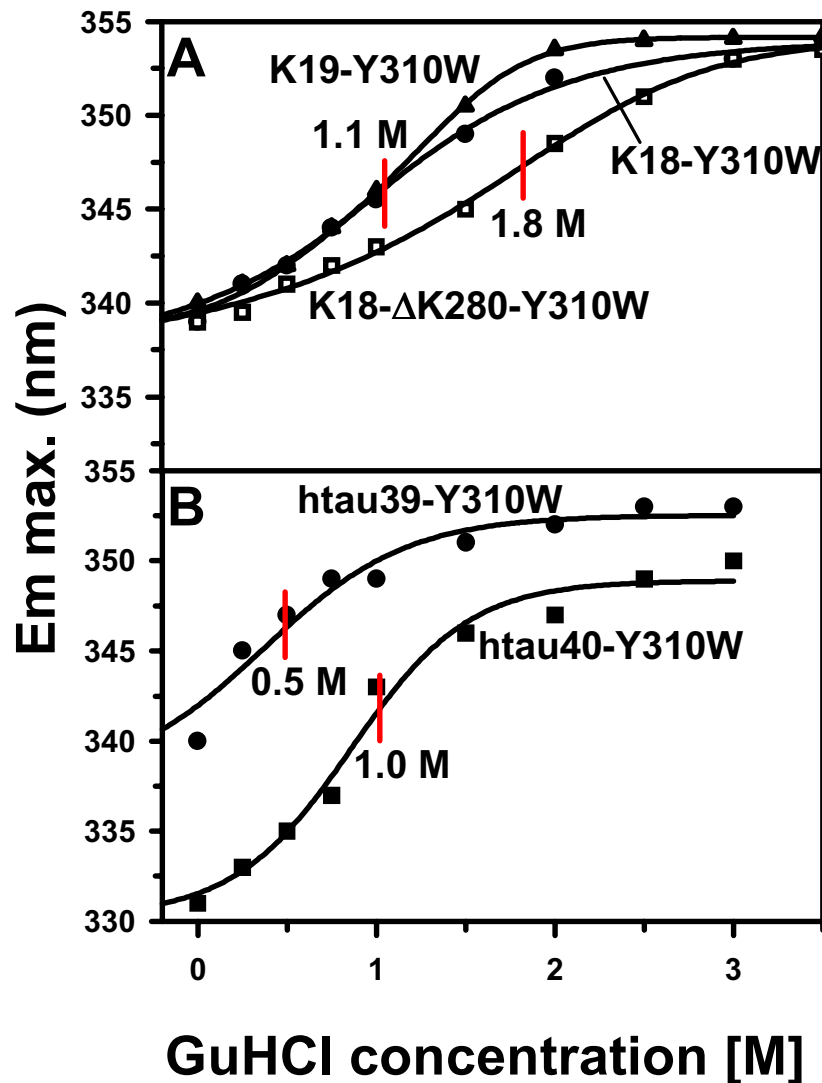
Fig. 22: Stability of PHFs against denaturation by GuHCl.

(A) PHFs were first assembled from K19, K18, or K18-ΔK280, each carrying the Y310W mutation as a reporter residue. The emission maximum is plotted versus increasing concentrations of GuHCl. All of them start with emission maxima of ~338 nm and were shifted to ~353 nm. K19 and K18 show nearly identical stabilities (half point of denaturation at ~1.1 M GuHCl, upper curves, filled symbols), indicating that PHFs made from the repeat domain gain no additional stability from the extra repeat in K18. In contrast, PHFs made from the mutant K18-ΔK280 (carrying one of the FTDP-17 mutations) are much more stable (half point at ~1.8 M GuHCl, lower curve, open symbols), consistent with the higher propensity for β-structure. (B) Disintegration of PHFs made from htau40-Y310W and htau39-Y310W. PHFs made from htau40-Y310W exhibit an initial emission maximum of about 331nm (lower curve, filled squares), in contrast to htau39-Y310W (upper curve) and K19 or K18 (see A). The half point of denaturation is ~0.5 M GuHCl for htau39-Y310W and ~1.0 M GuHCl for htau40-Y310W. This indicates that the stability of PHFs made from full-length isoforms is higher when 4R are present (as in htau40), and that PHFs from 3R isoforms (e.g. htau39) are particularly labile.

2.5.2 PHF denaturation analyzed by electron microscopy

To confirm the results from fluorescence spectroscopy studies, electron microscopy was performed. Fig. 23 shows the electron micrographs of pre-formed PHFs from K18-Y310W mutants in the absence or presence of GuHCl with concentrations of 1.0 M, 1.5 M or 3.0 M. Without GuHCl (Fig. 23, 0 M), K18-Y310W shows the typical PHF morphology. In the presence of increasing concentrations of GuHCl, PHFs become shorter (Fig. 23, 1.5 M), and eventually disappear (Fig. 23, 3.0 M). These changes are associated with the denaturation of PHFs, and confirm the fluorescence results above.
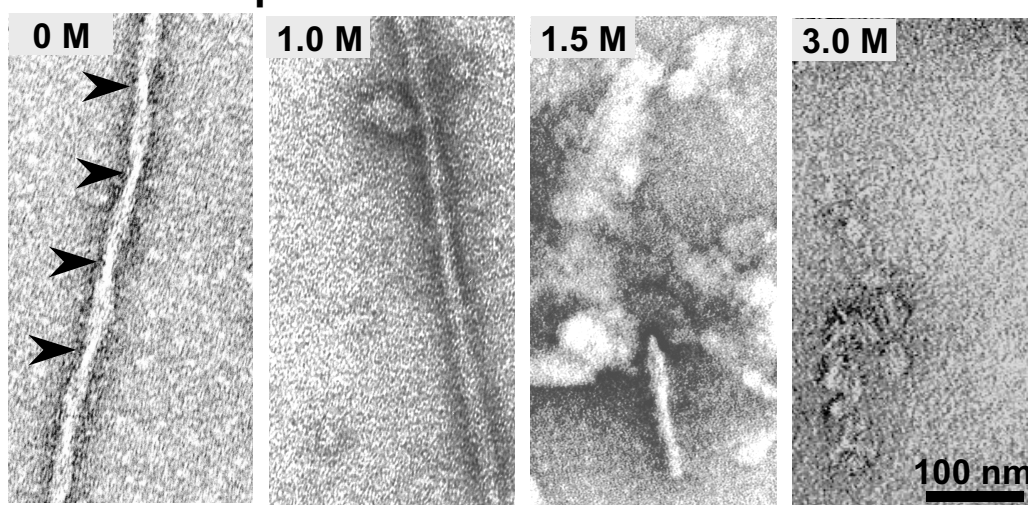
K18-Y310W plus GuHCl

Fig. 23: Electron micrographs of K18-Y310W incubated with GuHCl.

PHFs are visualized by negatively stained (2% uranyl acetate). With increasing concentrations of GuHCl, PHFs swell, become shorter and eventually disappear. The concentrations of GuHCl are indicated on the electron micrographs.

2.6 The tryptophan fluorescence can be used to monitor the efficiency of small molecules to inhibit PHF formation

The principle of measuring PHF stabilities by the intrinsic Trp fluorescence is not restricted to denaturants such as GuHCl, but can also be applied to other PHF destabilizing factors and can be extended to inhibitors of PHF formation. As an example, Fig. 24 shows a dose response curve of PHFs in the presence of a compound

tested for its ability to destabilize PHFs. This method was used because the self-fluorescence of the compound prohibited the use of the ThS assay for monitoring the state of assembly. The emission scans in the presence of increasing concentrations of the compound are increasingly red-shifted, concomitant with decreasing PHF concentrations (Fig. 24A). Fig. 24B shows difference spectra (before and after incubation with compound) of the normalized spectra of PHFs pre-assembled from K19-Y310W in the presence of inhibitor concentrations from 6 to 60 µM. The difference maxima at 325 nm (positive) and 370 nm (negative) increase with rising compound concentrations. The isosbestic point for all spectra is at about 350 nm, this indicates that Trp310 exists in two main states (exposed and buried). The example shows that the tryptophan fluorescence can be used to monitor the disassembly of PHFs where other techniques like ThS fluorescence cannot be applied.
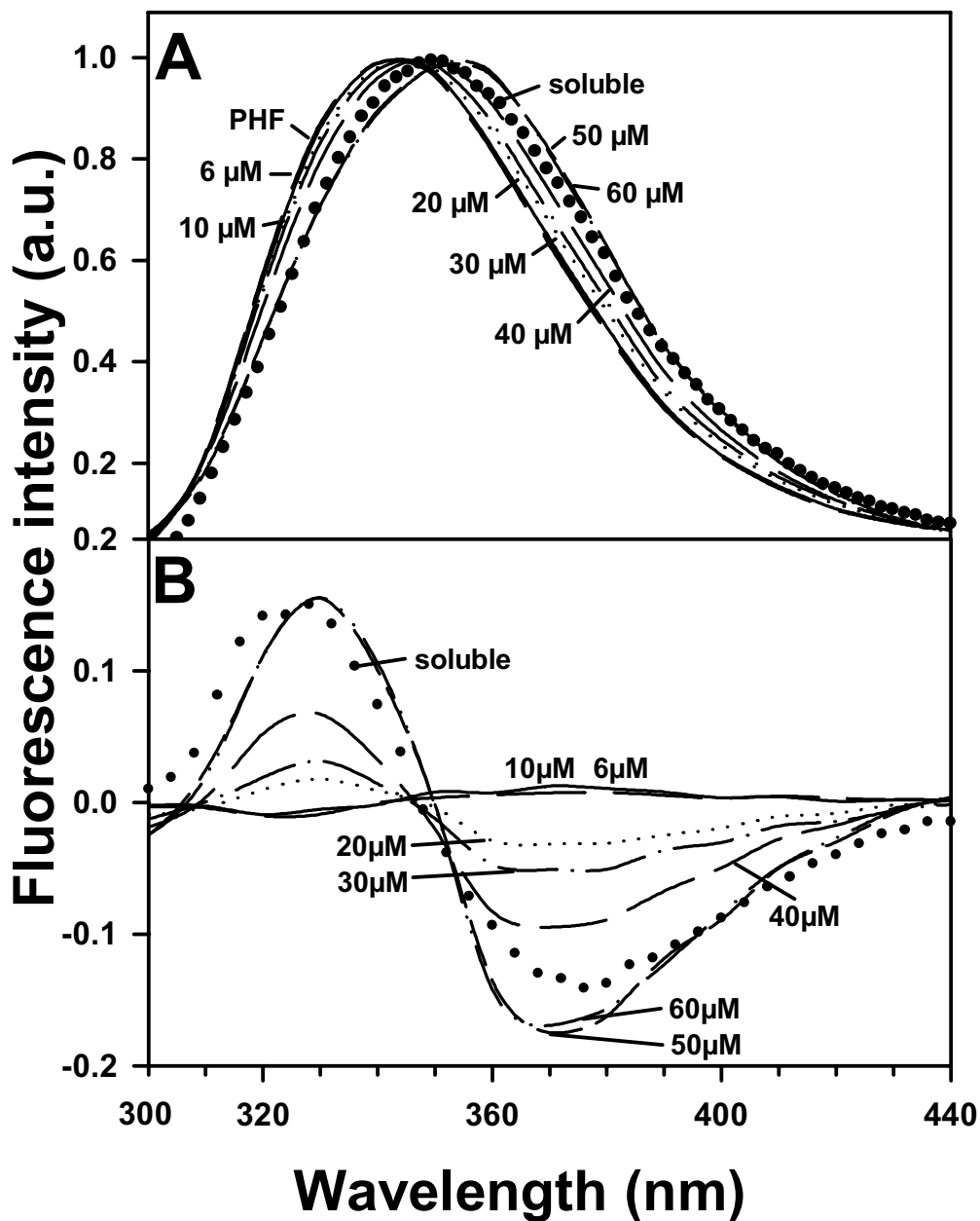
Fig. 24: Tryptophan fluorescence can be used to monitor the efficiency of small molecules to inhibit PHF formation.

PHFs were first formed from K19-Y310W and then exposed to inhibitor substance to disaggregate the PHFs, using the tryptophan fluorescence as a monitor. The emission spectra are normalized to the same maximum. (A) Emission spectra before PHF assembly (circles, emission maximum of 352 nm, excitation at 290 nm), after PHF assembly (solid line, emission maximum of 340 nm), and after exposing the PHFs to the inhibitor compound in different concentrations for 15 min (6 µM long-dashed line, 10 µM solid line, 20 µM dotted line, 30 µM dash-dot line, 40 µM medium-dashed line, 50 µM short-dashed line, 60 µM dash-dot-dot line). The blue-shift from 352 to 340 nm, induced by the initial PHF assembly, is reversed by exposing the PHFs to the inhibitor compound. (B) Difference spectra of the spectra given in Fig. 24A. All spectra measured in the presence of compound are substracted from the spectrum of intact PHFs. The resulting difference curves have a positive maximum around 325 nm and a negative maximum around 370 nm, with an isosbestic point around 350 nm. The example shows that the tryptophan fluorescence can be used to monitor the disassembly of PHFs where other techniques such as ThS fluorescence are not applicable.

For further confirmation, electron microscopy and SDS-PAGE were performed. Fig. 25 shows the electron micrographs of pre-formed PHFs from the 3R construct K19-Y310W, which was incubated with the inhibitor compound overnight. In the absence of inhibitor compound, the fibers exhibit the typical paired helical appearance (width ~10-20 nm). With increasing concentrations of the inhibitor (60 µM), the fibers became indistinct and shorter, indicating that the PHFs were disaggregated by the inhibitor compound.
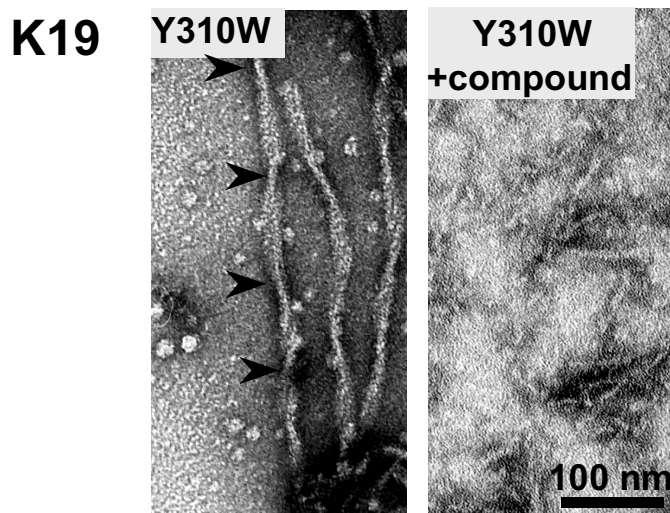

Fig. 25: Electron micrographs of PHFs from K19-Y310W in the absence and presence of the chemical compound.

K19-Y310W mutant shows typical PHF structure (left). When 10 µM pre-formed K19-Y310W filaments incubated with 60 µM compound at 37°C overnight, the filaments are seen indistinct and shorter (right).

Fig. 26 shows the SDS-PAGE confirming the disaggregation of PHFs by the inhibitor compound. PHF assembly of K19-Y310W was performed overnight, after ultracentrifugation supernatant and pellet of the reaction mixtures were applied to a 17% SDS-PAGE and stained with Coomassie blue. In the absence of compound (left side, 0 µM), all of the protein was present in the pellet, while increasing the concentration of the compound (6 µM, 10 µM, 20 µM, 30 µM, 40 µM, 50 µM, 60 µM), PHFs became dissolved and the protein was increased in the supernatant. These data confirm the fluorescence results and point to the potential of open the view on small compounds which might be used for dissolving PHFs in a therapy of AD.
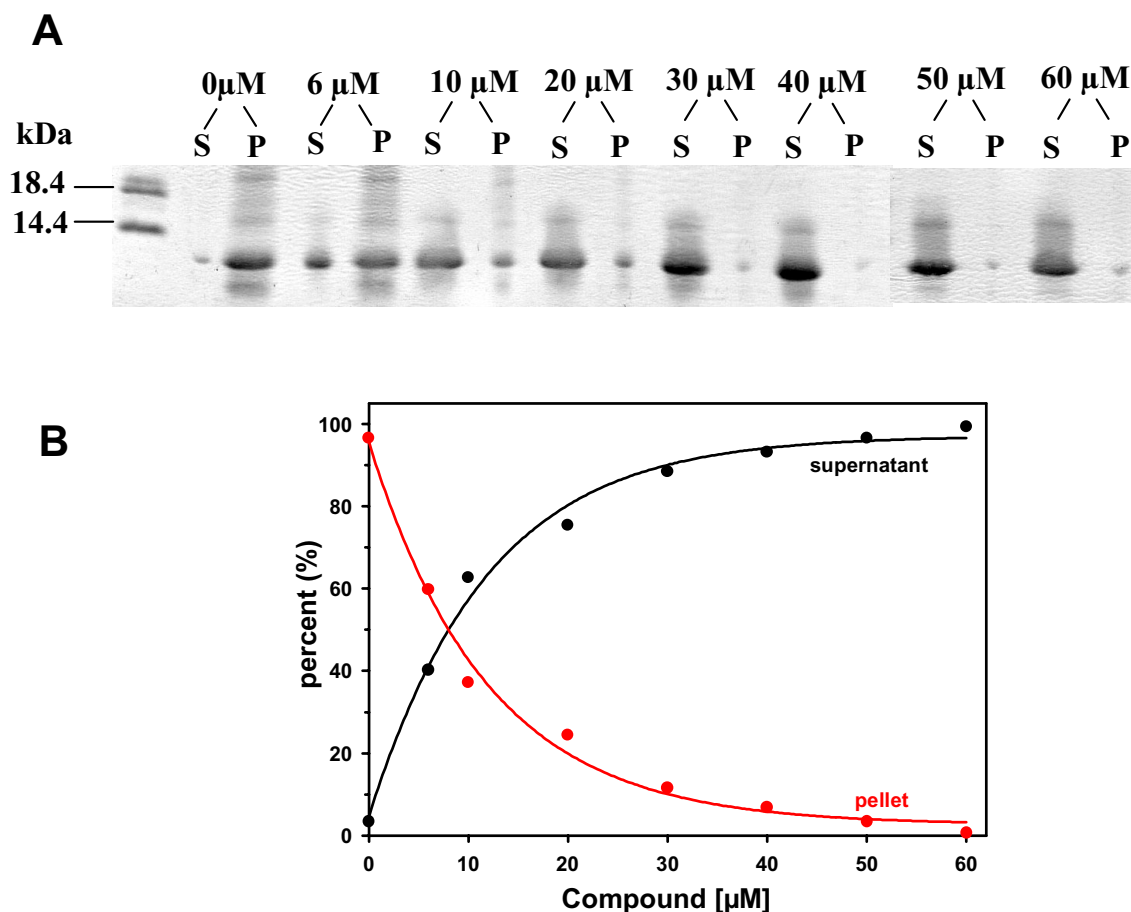
A

B

Fig. 26: SDS-PAGE analysis of soluble and insoluble fractions of PHFs from K19-Y310W after chemical compound treatment.

(A) Pre-formed PHFs from K19-Y310W were incubated at 37°C overnight with different concentration of compound, after ultracentrifugation, the supernatants and pellets were subjected to a 17% SDS-PAGE and stained by coomassie blue. The compound concentration was 6 µM, 10 µM, 20 µM, 30 µM, 40 µM, 50 µM and 60 µM respectively. (B) shows the plot of compound concentration vs. the percentage of supernatants and pellets which obtained from scanned SDS-PAGE of (A).

In summary, a new method of tryptophan fluorescence was explored that can be used to monitor the process of tau aggregation into PHFs. Its fluorescence can be used as a reporter to obtain new insights into the conformation of tau in the soluble state and after incorporation into PHFs. The tryptophan fluorescence can be used to determine the stability of PHFs, their solvent accessibility, and the proximity of tryptophan and tyrosine residues, as seen by fluorescence resonance energy transfer (FRET). Finally this tryptophan fluorescence can be used to monitor the effects of compounds that act as PHF inhibitors.

IV. Discussion

Pathological protein aggregation is increasingly recognized as a common denominator underlying a variety of diseases, especially in diseases of the brain where the disposal of non-functional components and the regeneration of cells is slow or absent. This applies to inappropriately processed amyloid protein or hyperphosphorylated tau protein in Alzheimer's disease, huntingtin with extended polyglutamine tracts in Huntington's disease, prion protein with altered conformations in Creutzfeld-Jacob's disease, accumulated α-synuclein in Parkinson's disease, or mutated tau protein in certain frontotemporal dementias (Goedert, 1998; Lansbury and Kosik, 2000; Prusiner, 1998; Rochet and Lansbury, 2000; Wanker, 2000).

Despite the diversity of proteins involved in the diseases, the process of aggregation appears to rest on a remarkably uniform principle, the formation of intermolecular β-sheets by locally unfolded segments of the polypeptide chain. The proteins tend to aggregate into fibers such that the β-strands runs roughly perpendicular to the fiber axis. This 'cross-β' structure can be recognized by fiber x-ray diffraction (Harada et al., 1971; Kirschner et al., 1986; Serpell et al., 1999; von Bergen et al., 2000).

In the case of tau aggregation in Alzheimer's disease, the recognition of the principle of aggregation was a complex process. Tau is an unusually hydrophilic protein, containing many polar and charged residues, and remains in solution even after heat and acid treatment (Cleveland et al., 1977; Lindwall and Cole, 1984); this would appear to make tau unlikely candidate for pathological aggregation. Contrary to other amyloids, PHFs from Alzheimer brains show little or no evidence of β-structure by x-ray diffraction (Kirschner et al., 1986; Schweers et al., 1994), consistent with the results from CD spectroscopy. However, in fibers assembled from shorter constructs, such as the repeat domain, the fraction of β-structure is correspondingly larger and becomes visible (von Bergen et al., 2001). On the other hand, the induction of β-structure by the hexapeptide motifs PHF6 and PHF6* alone is not sufficient to generate fibers with PHF appearance, since a PHF-like appearance requires at least 3 or 4 repeats. Thus, elements

outside the hexapeptide motifs are needed for building and shaping the PHF structure. It is therefore of major interest to understand the pathway of abnormal protein aggregation in the brain and to find methods to prevent it or at least to slow it down.

1. Interplay between the two hexapeptide motifs of 4R tau during PHF aggregation

3R forms of tau have only one hexapeptide motif (PHF6), which lies in the third repeat (^{306}VQIVYK^{311}) and is capable of initiating β-structure and PHF aggregation, whereas 4R forms have two hexapeptide motifs PHF6* in the second repeat (^{275}VQIINK^{280}) and PHF6 in the third repeat (^{306}VQIVYK^{311}). Initially, this would suggest that 4R tau should polymerize more readily than 3R tau, but this is not supported by experimental evidence. To test the relationship between the two hexapeptide motifs, two tools were used in this thesis: 1) Assembly-promoting mutants (ΔK280, one of the FTDP-17 mutants which shows enhanced aggregation, (Barghorn et al. 2000)) and 2) assembly-inhibiting mutants (I277P and I308P; Fig. 4). Fig. 27 illustrates that when only one hexapeptide motif is present (e.g. in the 3R construct K19), a simple model describes the situation (Fig. 27B). The motif PHF6 promotes aggregation; any β-breaking mutant in PHF6 disrupts it (such as I308P). When two hexapeptide motifs are present (e.g. in the 4R construct K18) their contributions to aggregation can be analyzed by single and double proline mutations (Fig. 27C). Interestingly, both proline mutations in the PHF6 or PHF6* motifs inhibit PHF formation. Thus, one assembly-promoting hexapeptide is not enough to induce aggregation when the other is 'poisoned' by mutation. However, the inhibition by the I308P in PHF6 mutation can be overcome by turning PHF6* into a strong assembly promoter via the ΔK280 mutation (Fig. 27D, the ΔK280-proline PHF6 mutant still can aggregate, while ΔK280-proline PHF6* which proline mutant in the R2 cannot form any filaments).
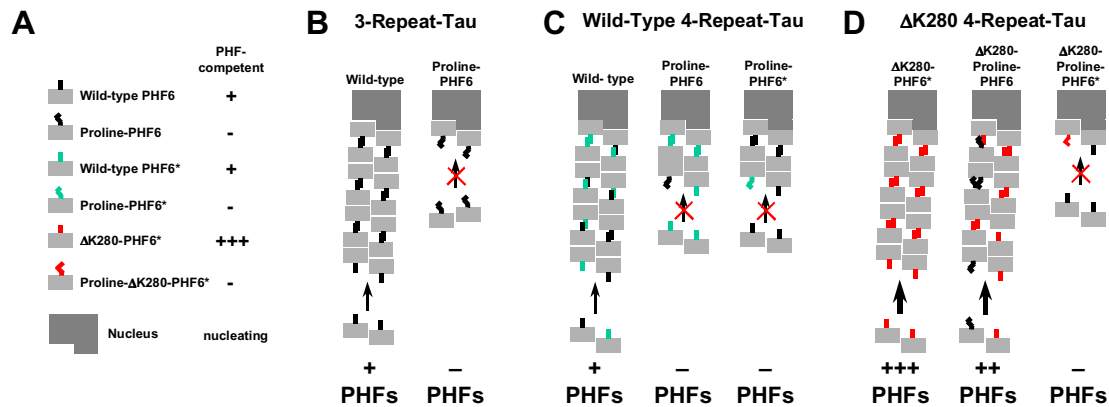
Fig. 27: Model of the effects of proline mutants in the hexapeptide motifs PHF6 and PHF6* on tau aggregation.

(A) Elements of PHFs: Grey boxes = tau molecules (dark grey = initial nucleus of assembly). Black line = PHF6 motif in R3, capable of interacting with another PHF6 or PHF6* motif during aggregation. Black wiggle = PHF6 motif 'poisoned' by Pro mutation and therefore incompetent to promote aggregation. Green line = PHF6* motif in R2. Green wiggle = PHF6* motif disabled by Pro mutation. Red line = PHF6* motif with ΔK280 mutation, highly competent for aggregation. Red wiggle = PHF6*-ΔK280 motif disabled by Pro mutation. (B) In 3R tau, only the PHF6 motif is present, and promotes tau aggregation (left). A proline mutant in the PHF6 motif prevents PHF formation (right). (C) In 4R tau, two hexapeptide motifs PHF6 and PHF6* are present. Both can interact to promote aggregation (left). Disabling by a Pro mutant either in PHF6 (middle) or in PHF6* (right) inhibits aggregation. (D) The ΔK280 mutant of 4R tau greatly promotes tau aggregation (left). Disabling PHF6 by a proline mutation still allows aggregation because the inhibition is overcome by the ΔK280 mutation in PHF6* (middle). However, disabling the PHF6* motif by an additional proline mutation inhibits aggregation (right)(diagram courtesy of S. Barghorn).

Several scenarios can be envisaged to explain this. One is that the two hexapeptide motifs interact with each other and thus change their overall capacity for aggregation. In this case, disrupting one motif by a proline mutation would inactivate both of them with regard to aggregation. The possibility of direct interference is consistent with earlier observations from fluorescence transfer experiments that cysteines 291 and 322, downstream of the PHF6* and PHF6 motifs, are in close proximity in solution (Schweers et al., 1995). Strengthening the β-propensity in PHF6* (by the ΔK280 mutation) might keep the whole molecule assembly-competent, even when PHF6 is poisoned by a proline mutation. A second model is that the hexapeptide motifs interact for a critical sub-step of aggregation, such as dimerization, which is known to be an important prerequisite (Friedhoff et al., 1998b; Schweers et al., 1995; Wille et al., 1992). For example, poisoning the hexapeptide motifs by a proline mutation might still

allow dimer formation but prevent the subsequent conformational change required for filament elongation. A similar model was postulated for the aggregation of Aβ peptides (Esler et al., 1996). A third model is that the two hexapeptide motifs contribute independently of each other to PHF growth. Each aggregation-competent β-strand could attach to a growth point and present an attachment site for the next molecule. In this scheme, poisoned motifs (containing a proline mutation) could become incorporated by 'piggy-backing' on competent motifs, but accumulation of too many poisoned sites would slow down or stop aggregation eventually. This is reminiscent of the limited incorporation of tubulin subunits poisoned by colchicine into microtubules (Jordan and Wilson, 1998).

2. Insights into the structure of paired helical filaments by intrinsic fluorescence of tau

2.1 Tryptophan fluorescence as an assay for PHF assembly

Since abnormally aggregated tau represents one of the hallmarks of Alzheimer's disease and other dementias it is of obvious importance to study the aggregation mechanism, both from the viewpoint of basic science and for developing methods of intervention. Efforts to study tau aggregation have been hampered mainly by the fact that tau is an unusually hydrophilic and soluble protein, and therefore it aggregates very slowly and inefficiently, if at all, in physiological buffer conditions. Over the past decade several findings have helped to overcome this barrier:

(i)   Certain domains such as the repeat domain aggregate faster than the intact protein (Wille et al., 1992), presumably because the repeats form the core of Alzheimer PHFs (Jakes et al., 1991).

(ii)   Dimerization of tau accelerates aggregation, presumably because dimers have a conformation conducive for tau-tau interactions (Schweers et al., 1995; Wille et al., 1992).

(iii)   Cofactors such as polyanions or fatty acid micelles promote aggregation, apparently by compensating tau's numerous positive charges (Goedert et al., 1996; Kampers et al., 1996; Perez et al., 1996; Wilson and Binder, 1997).

(iv)   Mutations of tau found in FTDP-17 dementias favour aggregation (Barghorn et al., 2000; Gamblin et al., 2000; Goedert et al., 1999a). The reasons for this may be heterogeneous, depending on the type of mutation, but at least in the cases of ΔK280 and P301L they can be traced back to an enhanced propensity for β-structure, a feature common to many pathological amyloids (Fraser et al., 1994; Kirschner et al., 1987; Lansbury, 1997; Pike et al., 1995).

With these developments it is now possible to form tau aggregates rapidly from recombinant protein and to analyze the structure, kinetics and biochemistry of the process.

Another hurdle in the investigations was the paucity of assay methods of tau aggregation. Electron microscopy is slow, difficult to quantify, and limited in resolution, and therefore not well suited for kinetic and structural analysis, although it is important for distinguishing fibers with 'paired helical' appearance from other types of aggregates. Spectroscopic methods (CD, FTIR) are applicable to solutions but are also of limited value since tau does not exhibit pronounced changes between the soluble and aggregated state, due to its mostly random coil structure (Cleveland et al., 1977; Schweers et al., 1994). Two methods which have come into routine use for kinetic studies, together with faster aggregation conditions, are Thioflavine S fluorescence and light scattering (Friedhoff et al., 1998b; Gamblin et al., 2000; Wilson and Binder, 1997), although here, too, certain limitations apply, for example low sensitivity to initial states of aggregation. We have therefore searched for alternative methods which would reveal structural aspects of tau and PHFs, and here we report results obtained with the use of the intrinsic fluorescence of tryptophan. The advantages of this approach can be summarized as follows:

- Trp does not occur in normal tau protein, and therefore it can be used as a direct reporter on the local environment when it is inserted by a point mutation. Tau contains very few aromatic amino acids, the longest isoform htau40 comprises three phenylalanines (F8, F346, F379), five tyrosines (Y18, Y29, Y197, Y310, Y394) and no tryptophan at all. None of these lie in alternatively spliced regions so that all tau isoforms have the same composition of aromatic residues, and only Y310 lies within the third repeat domain.

- Trp reports to the local environment by a change in emission maximum and/or fluorescence intensity. The blue-shift which occurs especially in the tryptophan at 310 underlines an increase in hydrophobicity during PHF aggregation. The emission maximum of 339 nm (in the case of aggregated K18-Y310W) is similar to that of proteins in which the tryptophan is buried within defined secondary structures and partially shielded from solution (Eftink, 1991).

- The spectral change can be used to monitor solvent accessibility and thus protein folding and packing during aggregation, as well as protein stability, denaturation, or disassembly. Tryptophan fluorescence is widely used in the literature as an intrinsic monitor of conformational changes and for analysis of conformational stability (Garzon-Rodriguez et al., 2000; Gasymov et al., 2001).

- Since Trp can be inserted anywhere it allows analysis of the protein from many local 'points of view'. It was shown that the mutation of Tyr310 does not alter the specific activity of tau in any means, neither of the physiological nor the pathological function or in terms of secondary structure, therefore the biggest advantage of the tryptophan fluorescence based assay lies in the independence of external dyes and its simplicity.

- The transfer of fluorescence energy from Tyr to Trp residues serves as a rough marker for distances within a protein.

- Since Trp is an intrinsic component of the protein it reports on the entire population of protein molecules, including monomers, oligomers, and aggregates.

- Trp allows screening of aggregation modifiers (e.g. inhibitors or enhancers) independently of other additives (such as Thioflavine S whose fluorescence may overlap with that of inhibitor compounds).

2.2 Tryptophan mutations do not alter tau's physiological and pathological functions

In the case of tau the five naturally occurring Tyr residues show only small responses to the state of aggregation and are thus not very useful probes of aggregation (Fig. 10A, B). In contrast, Trp inserted into the repeat domain displays a strong signal of aggregation in the form of a blue-shift of the emission maximum; the intensity increase (~ 10%) is relatively small and was not exploited here. The repeat domain is a natural target of Trp insertion since it forms the backbone for PHF aggregation and contains the hexapeptide motifs, which play an important role in the local conversion to β-structure when tau aggregates into PHFs (Fig. 10C, D, Fig. 11). The replacement of Y310 by Trp is particularly interesting since this lies at the center of the repeat domain and within the PHF6 hexapeptide motif; with Trp at position 310, the aggregation process results in bona fide PHFs without interference (Fig. 12), and without obstructing the formation of β-structure (as seen by FTIR, Fig. 15). In this regard the insertion of Trp is neutral with regard to aggregation, in contrast to the insertion of prolines into the hexapeptide motifs, which prevent aggregation because they are breakers of β-structure (Fig. 4) (von Bergen et al., 2000). As a control, this insertion is also neutral with regard to tau's ability to promote microtubule assembly (Fig. 16).

2.3 Solvent accessibility of tau

Previous studies suggested that dimerization was the initial event in tau aggregation and that the dimer represents an important building block for further fibril assembly

(Schweers et al., 1995; Wille et al., 1992)(note that this depends on assembly conditions, see Barghorn et al., 2002). However, much remains to be elucidated regarding the structure of the PHF and the mechanism of the tau dimer-fibril transition. Determining which parts of tau (particularly the repeat domain) are accessible to the solvent and how these environments change during polymerization will be important to understand the conformational change during the aggregation. All these factors can be measured by the quenching of tryptophan fluorescence.

Trp inserted into other sites in the repeat domain respond in a qualitatively similar fashion, but with notable variations, as shown by the solvent accessibility studies (Fig. 17, 18). Monomeric tau shows almost complete accessibility (judged by the slope of the Stern-Volmer plot). This confirms the previous conclusions from X-ray scattering that tau has a 'natively unfolded' structure (Schweers et al., 1994). When Trp residues are inserted in different positions along the repeat domain, most of them become less accessible upon PHF aggregation. This is consistent with the view that the repeat domain becomes packed when tau aggregates into PHFs. Interestingly, the tightest packing occurs in R2 and R3, in the region around residue 300-310 where the hexapeptide motif PHF6 is located, while the edges are less tightly packed. In fact residue 360 (end of R4) remains almost as accessible as the monomeric protein. This conclusion is reached by two independent criteria (Fig. 18, 19) and fits well with the concept that the repeat domain forms the protease-resistant core of PHFs, whereas the regions outside the repeats contribute to the protease-sensitive 'fuzzy coat' (Jakes et al., 1991; Wischik et al., 1988a). Refining this concept, the beginning of R1 and the end of R4 are already less tightly packed in PHFs and may represent transition regions to the 'fuzzy coat', whereas R2 and R3 form the more central part of the PHF core.

2.4 Fluorescence resonance energy transfer of tau

Fluorescence resonance energy transfer (FRET) is a useful method to study the assembly or folding of a protein. The most common application of FRET is to measure the distance between two sites on a macromolecule. One of the advantages of introducing tryptophan fluorescence into tau is the possibility to use it for FRET

analysis between tyrosine and tryptophan. In the case of the short construct K18, where the natural Tyr310 was still present and the position of the tryptophan varies the distances could be analyzed by FRET. In the case of the isoforms of tau, Tyr310 was replaced by Trp, and there were still four natural tyrosines left.

One of the challenges in understanding tau's role is the postulated transition to a 'pathological conformation'. Indications for this come from antibodies that recognize early stages of Alzheimer degeneration and are suggested to respond to folded conformations where discontinuous parts of the sequence cooperate to generate the antibody epitope. Examples are antibodies Alz50 (the epitope is aa's 5-15, 312-322 of tau protein), MC-1 (the epitope is aa's 5-15, 312-322 of tau protein), TG-3 (the epitope is phosphothreonine 231 of tau protein), SMI34 (conformational antibody, the epitope is in or near the repeat region)(Abraha et al., 2000; Carmel et al., 1996; Jicha et al., 1997; Lichtenberg-Kraag et al., 1992). Therefore it was asked if proximities between residues or folded states would be detectable by FRET (Fig. 20, 21). With Trp in position 310 at the center of the repeats, one can ask whether the intrinsic Tyr residues (which are mostly near the N and C termini) are capable of transferring resonance energy to Trp, i.e. whether they are located within the Förster distance of ~1 nm for this donor/acceptor pair (Chiu and Bersohn, 1977; Eisinger, 1969). For monomeric tau the answer is negative, as seen from the independent Tyr fluorescence shoulder around 305 nm. However, upon PHF aggregation the distance becomes smaller than the critical value, and the Tyr shoulder disappears due to the FRET effect. Two interpretations are possible: Either tau adopts a more compact folding before aggregation (leading to intra-molecular FRET), or the tails of the molecule are constrained to lie near Trp acceptors in neighbouring tau molecules in the PHF structure. The results favour the second interpretation because of the experiment shown in Fig. 20C: Tau monomers and covalent dimers display a similar Tyr fluorescence shoulder, indicating in both cases a large distance (>1 nm) between the central Trp at position 310 and the Tyr residues in the tails, even though the dimer is already much more assembly-competent than the monomer. Thus, the change from monomer to dimer is not accompanied by a gross change in folding (nor in solvent accessibility), as judged by the Tyr/Trp fluorescence properties. Conversely, the packing is more likely to occur at a later step, e.g. PHF

nucleation or elongation (Friedhoff et al., 1998a). These structural changes during PHF aggregation can be summarized in Fig. 28.
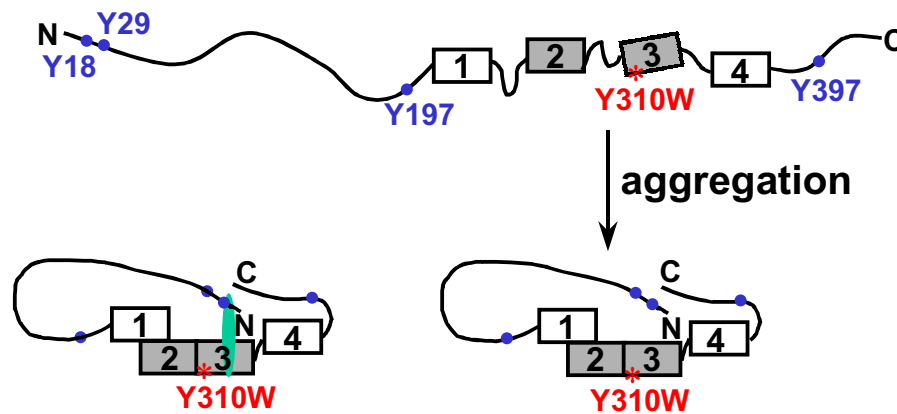

Fig. 28: Diagram of structural changes during PHF aggregation (from Trp fluorescence measurements)

The Trp mutant Y310W (red) based on the 4R tau isoform contains in addition four Tyr residues (Y18, Y29, Y197 in the N-terminal region, and Y397 in the C-terminal region, blue points).
In the soluble state (top), tau has almost no secondary structure and no FRET is observed between Y and W, indicating a loose extended structure. After PHF assembly (bottom), all Y residues come close to 310W (as judged by FRET, see Fig. 20). This indicates that in the aggregated state, the N-terminal part of tau folds back onto the core of PHFs (R2 and R3), and the C-terminal part also has an interaction with the repeat domain. These changes are compatible with the epitopes of Alz50 and MC-1 antibodies (left at the bottom, green area) which was assumed a folded structure during tau aggregation (Abraha et al., 2000; Carmel et al., 1996; Jicha et al., 1997).

2.5 Thermodynamic stability of tau

Perhaps equally important as the question of PHF aggregation is that of PHF stability and disaggregation since the net load of PHFs in a cell is the result of both opposing processes, and since one may expect a high degree of turnover, at least in the initial stages of the disease (as shown recently for the analogous case of amyloid aggregates (Hyman et al., 2001)). The stability can be probed by exposing preformed PHFs to denaturants such as GuHCl (Fig. 22), with Trp in position 310 as a reporter. One

surprising result is that PHF aggregation is readily reversible. A second surprise is that PHF disassembly is achieved by relatively mild denaturation conditions, ~1 M GuHCl, compared with ~ 4 M for compact globular proteins such as lysozyme (Takano et al., 2001). In other words, the initial assembly of PHFs appears rather reversible, and their buildup in cells could probably be prevented if one could avoid stabilization by covalent crosslinking reactions such as glycation (Ledesma et al., 1994; Perry et al., 1991) or transglutaminase (Appelt et al., 1997). The repeat domain by itself has the same stability with either 3 or 4 repeats, arguing that the extra repeat R2 (exon 10), when present, offers no additional protection for the PHF core per se (but see below). As expected, the ΔK280 mutation makes the aggregate almost twice as stable, due to its promotion of β-structure. A somewhat different picture emerges with full-length tau isoforms. PHFs from the 4R isoform htau40 have the same stability as PHFs made from the repeat domain alone, but PHFs from the 3R isoform htau39 are much less stable (~0.5 M GuHCl). This points to a possible interaction between the tails of tau and the PHF core (note that the N-terminal region of tau, including the inserts of exons 2 and 3, is rather acidic and thus might affect the packing of the basic PHF core). In the context of FTDP-17 dementias the higher stability of 4R PHFs is potentially important since many of these mutations (including the intronic mutations that do not affect protein sequence) lead to an overproduction of 4R tau isoforms (D'Souza and Schellenberg, 2000; Hong et al., 1998), this might therefore increase the level of stable PHFs.

2.6 Summary of structural properties of tau deduced from tryptophan mutants

The structural properties of tau, which could be deduced by tryptophan fluorescence, are summarized below. Judging from fluorescence quenching and emission spectrum, in soluble tau most of the sequence is solvent accessible; in PHFs the repeat domain becomes buried, especially R2 and R3 which appear to form the center of the PHF core. Analyzed by FRET and blue-shift, residues in R2 and R3 are close to the inner core (marked by Y310 in the central hexapeptide motif), those in R1 and R4 are further apart but may approach the inner core upon PHF aggregation. Residues near the N- and C-terminal tails of full-length tau are far from the center of the repeat domain but appear to fold back during PHF aggregation. Although the aggregation is triggered by the

β-inducing hexapeptide motifs the stability of PHFs is intrinsically weak, but they can be stabilized by more repeats (i.e. 4R-PHFs are more stable than 3R-PHFs) and FTDP-17 mutations.
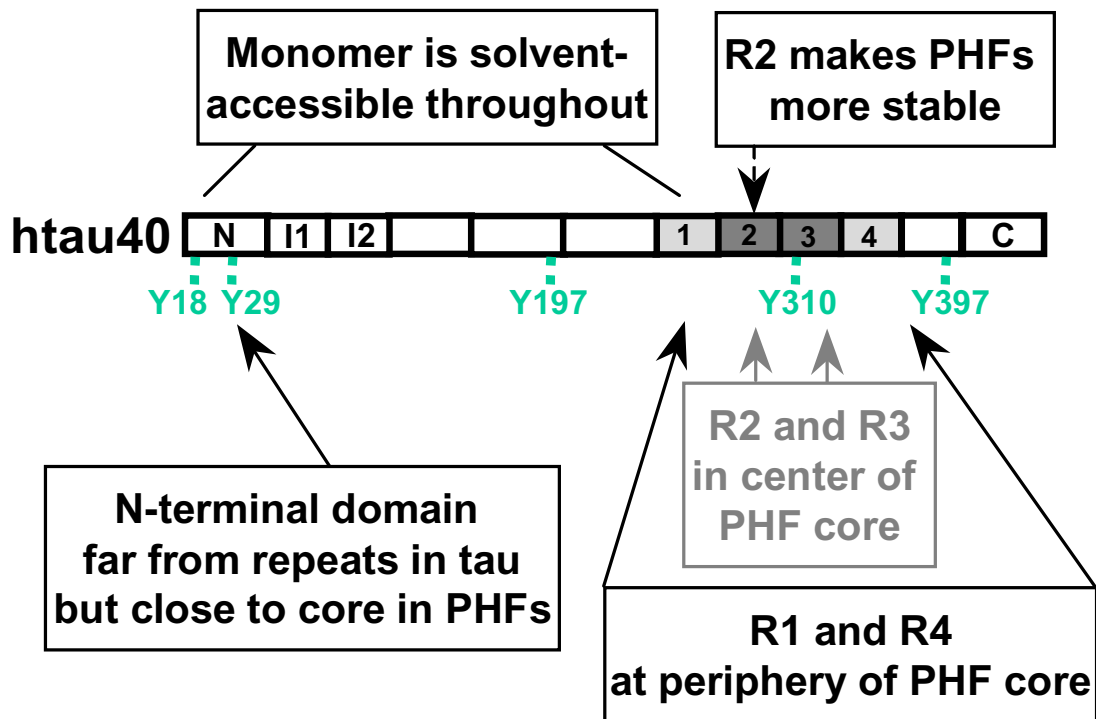
2.7 Disaggregation of PHFs by chemical compounds

Finally it is noteworthy that Trp reporter constructs might be ideally suited for screening substances capable of inhibiting or reversing the formation of PHFs. One reason is that exogenous reporter molecules (like ThS), which might interfere with the test substance, are not required. Moreover, test substances are frequently fluorescent by themselves, so that the ThS assay would no longer be applicable. In automated screens this problem could be avoided by intrinsic probes such as Trp (Fig. 24).

Every attempt to treat tau pathology at an advanced state would aim at the destabilization of PHFs, and therefore more should be known about it. First the conditions and mechanism and furthermore the structure and character of the intermediates and end products have to be analyzed. The disaggregation of β-amyloid plaques was shown by a vaccination approach of transgenic mice (Nicolau et al., 2002;

Schenk et al., 1999; Vehmas et al., 2001). The antibody based approach is possible due to the extracellular location of β-amyloid deposits. For intracellular proteinaceous deposits the antibody based approach might not be suitable but chemical compounds capable of crossing the cell membrane might be useful. A recent publication suggests that not the filamentous components but intermediates of partially dissolved synuclein fibers are the toxic components (Lansbury and Kosik, 2000). A similar effect was recently shown for β-amyloid aggregates (Walsh et al., 2002). This suggests that merely dissolving the PHFs might not be sufficient, but perhaps chemical compounds will be able to dissolve the PHFs readily enough to enable proteases to digest them.

For tau it is still unknown which process drives the deposition of filaments within the cells. It might be caused by increased levels of soluble protein not bound to MTs (perhaps due to increased phosphorylation of critical epitopes in the microtubule binding domain). This could represent a (toxic) gain of function. Alternatively, there could be a loss of function of the normal proteolytic activities in the aged cell. In this case an attenuation of filament formation or even the disaggregation by chemical compounds might be helpful even if the change in rate constants is small. In Alzheimer's disease and other neurodegenerative diseases based on protein aggregation (Prion disease, Parkinson's disease, Huntington's disease), which develop over years, even small changes in aggregation rates, could cause large differences, in the disease process.

V. Abstract

Alzheimer's disease is accompanied by a number of structural and metabolic alterations in the brain. Two characteristic hallmarks are the protein aggregates in amyloid plaques (made up mostly of Aβ peptide) and in the neurofibrillary tangles (consisting largely of the microtubule-associated protein tau).

Tau protein is a natively unfolded protein in the solution, yet it is able to polymerize into the ordered paired helical filaments (PHF) which bundled into neurofibrillary tangles. Recently it was shown that a small fraction of tau, the hexapeptide motif PHF6 (^{306}VQIVYK^{311}) in the third repeat is capable of inducing tau aggregation via formation of a β-structure (von Bergen et al., 2000). In the present study, we performed scanning mutagenesis (proline mutants and tryptophan mutants) to investigate the *in vitro* structural requirements for PHF polymerization of tau protein containing four repeats. We show that there is a cross-talk between the two hexapeptide motifs PHF6* (^{275}VQIINK^{280}) in the second repeat and PHF6 (^{306}VQIVYK^{311}) in the third repeat during PHF aggregation. A single proline mutant in the hexapeptide motif PHF6* or PHF6 inhibits PHF formation completely, however, the inhibition by the I308P mutant in PHF6 can be overcome by turning PHF6* into a strong assembly promoter via one of the FTDP-17 mutants, ΔK280 (in the presence of heparin).

Using tryptophan scanning mutagenesis we observed the kinetics and structure of tau's polymerization into PHFs independently of exogenous reporter dyes. The fluorescence exhibits pronounced blue-shifts due to burial of the residue inside PHFs, depending on Trp position. The effect is greatest near the center of the repeat domain, showing that the packing is tightest near the β-structure inducing hexapeptide motifs. The tryptophan response allows measurement of PHF stability made by different tau isoforms and mutants. Unexpectedly the stability of PHFs is quite low (denaturation half points ~1.0 M GuHCl), implying that incipient aggregation should be reversible, and that the observed high stability of Alzheimer PHFs is due to other factors. The stability increases with the number of repeats and with tau mutants promoting β-structure,

arguing for a gain of toxic function in frontotemporal dementias. Fluorescence resonance energy transfer (FRET) was used to analyze the distances of Tyr310 to tryptophans in different positions. The degree of FRET in the soluble protein was position dependent, with highest signals within the second and third repeats but low or no signals further away. In PHFs most mutants showed FRET, indicating that tight packing results from assembly of tau into PHFs.

VI. References

Abraha, A., Ghoshal, N., Gamblin, T. C., Cryns, V., Berry, R. W., Kuret, J., and Binder, L. I. (2000). "C-terminal inhibition of tau assembly in vitro and in Alzheimer's disease." J Cell Sci *113 Pt 21*: 3737-45.

Ackmann, M., Wiech, H., and Mandelkow, E. (2000). "Nonsaturable binding indicates clustering of tau on the microtubule surface in a paired helical filament-like conformation." J Biol Chem *275*(39): 30335-43.

Alzheimer, A. (1907). "Über eine eigenartige Erkrankung der Hirnrinde." Allg. Z. Psychiatrie *64*: 146-148.

Anderton, B. H., Brion, J. P., Couck, A. M., Davis, D. R., Gallo, J. M., Hanger, D. P., Ladhani, K., Latimer, D. A., Lewis, C., Lovestone, S. (1995). "Modulation of PHF-like tau phosphorylation in cultured neurones and transfected cells." Neurobiol Aging *16*(3): 389-97; discussion 398-402.

Andreadis, A., Brown, W. M., and Kosik, K. S. (1992). "Structure and novel exons of the human tau gene." Biochemistry *31*: 10626-10633.

Appelt, D. M., Balin, B. J. (1997). "The association of tissue transglutaminase with human recombinant tau results in the formation of insoluble filamentous structures." Brain Res *745*(1-2): 21-31.

Bancher, C., and Jellinger, K. A. (1994). "Neurofibrillary tangle predominant form of senile dementia of Alzheimer type: a rare subtype in very old subjects." Acta Neuropathol *88*(6): 565-70.

Barghorn, S., Zheng-Fischhofer, Q., Ackmann, M., Biernat, J., von Bergen, M., and Mandelkow, E. (2000). "Structure, Microtubule Interactions, and Paired Helical Filament Aggregation by Tau Mutants of Frontotemporal Dementias." Biochemistry *39*(38): 11714-11721.

Barghorn, S., Mandelkow, E. (2002). "Towards a unified scheme for the aggregation of tau into Alzheimer paired helical filaments." Biochemistry in Press.

Baumann, K., Mandelkow, E. M., Biernat, J., Piwnica-Worms, H., and Mandelkow, E. (1993). "Abnormal Alzheimer-like phosphorylation of tau-protein by cyclin- dependent kinases cdk2 and cdk5." FEBS Lett *336*(3): 417-24.

Bennett, B. D., Babu-Khan, S., Loeloff, R., Louis, J. C., Curran, E., Citron, M., and Vassar, R. (2000). "Expression analysis of BACE2 in brain and peripheral tissues." J Biol Chem *275*(27): 20647-51.

Berr, C., Hauw, J. J., Delaere, P., Duyckaerts, C., and Amouyel, P. (1994). "Apolipoprotein E allele epsilon 4 is linked to increased deposition of the amyloid beta-peptide (A-beta) in cases with or without Alzheimer's disease." Neurosci Lett *178*(2): 221-4.

Biernat, J., Gustke, N., Drewes, G., Mandelkow, E. M., and Mandelkow, E. (1993). "Phosphorylation of serine 262 strongly reduces the binding of tau protein to microtubules: Distinction between PHF-like immunoreactivity and microtubule binding." Neuron *11*: 153-163.

Biernat, J., and Mandelkow, E. M. (1999). "The development of cell processes induced by tau protein requires phosphorylation of serine 262 and 356 in the repeat domain and is inhibited by phosphorylation in the proline-rich domains." Mol Biol Cell *10*(3): 727-740.

Braak, H., and Braak, E. (1991). "Neuropathological staging of Alzheimer-related changes." Acta Neuropath. *82*: 239-259.

Braak, E., Braak, H., and Mandelkow, E. M. (1994). "A sequence of cytoskeleton changes related to the formation of neurofibrillary tangles and neuropil threads." Acta Neuropathol *87*(6): 554-67.

Braak, H., and Braak, E. (1997). "Frequency of stages of Alzheimer-related lesions in different age categories." Neurobiol Aging *18*(4): 351-7.

Bramblett, G. T., Goedert, M., Jakes, R., Merrick, S. E., Trojanowski, J. Q., and Lee, V. M. Y. (1993). "Abnormal tau phosphorylation at Ser(396) in Alzheimer's disease recapitulates development and contributes to reduced microtubule binding." Neuron *10*: 1089-1099.

Brandt, R., and Lee, G. (1993). "The balance between tau protein's microtubule growth and nucleation activities: implications for the formation of axonal microtubules." J Neurochem *61*(3): 997-1005.

Brandt, R., Leger, J., and Lee, G. (1995). "Interaction of tau with the neural plasma-membrane mediated by tau amino-terminal projection domain." J. Cell Biol. *131*: 1327-1340.

Brion, J. P., Tremp, G., and Octave, J. N. (1999). "Transgenic expression of the shortest human tau affects its compartmentalization and its phosphorylation as in the pretangle stage of Alzheimer's disease." Am J Pathol *154*(1): 255-270.

Brookmeyer, R., Gray, S., and Kawas, C. (1998). "Projections of Alzheimer's disease in the United States and the public health impact of delaying disease onset." Am J Public Health *88*(9): 1337-42.

Buee, L., and Delacourte, A. (1999). "Comparative biochemistry of tau in progressive supranuclear palsy, corticobasal degeneration, FTDP-17 and Pick's disease." Brain Pathol *9*(4): 681-93.

Buee, L., Bussiere, T., Buee-Scherrer, V., Delacourte, A., and Hof, P. R. (2000). "Tau protein isoforms, phosphorylation and role in neurodegenerative disorders." Brain Res Brain Res Rev *33*(1): 95-130.

Bullock, W. O., Fernandez, J.M., Short, J.M. (1987). "XL1-Blue-A high-efficiency plasmid transforming recA eschericha-coli strain with beta-Galactosidase selection." Biotechniques *5*: 376-379.

Butner, K. A., and Kirschner, M. W. (1991). "Tau protein binds to microtubules through a flexible array of distributed weak sites." J Cell Biol *115*(3): 717-30.

Byler, D. M., and Susi, H. (1986). "Examination of the secondary structure of proteins by deconvolved FTIR spectra." Biopolymers *25*(3): 469-87.

Carmel, G., Mager, E. M., Binder, L. I., and Kuret, J. (1996). "The structural basis of monoclonal-antibody Alz50s selectivity for Alzheimer's-disease pathology." Journal of Biological Chemistry *271*(51): 32789-32795.

Castillo, G. M., Lukito, W., Wight, T. N., and Snow, A. D. (1999). "The sulfate moieties of glycosaminoglycans are critical for the enhancement of beta-amyloid protein fibril formation." J Neurochem *72*(4): 1681-7.

Chin, S. S., and Goldman, J. E. (1996). "Glial inclusions in CNS degenerative diseases." J Neuropathol Exp Neurol *55*(5): 499-508.

Chiu, H. C., and Bersohn, R. (1977). "Electronic energy transfer between tyrosine and tryptophan in the peptides Trp-(Pro)n-Tyr." Biopolymers *16*(2): 277-88.

Cleveland, D. W., Hwo, S. Y., and Kirschner, M. W. (1977). "Physical and chemical properties of purified tau factor and the role of tau in microtubule assembly." J Mol Biol *116*(2): 227-47.

Couchie, D., Mavilia, C., Georgieff, I., Liem, R., Shelanski, M., and J., N. (1992). "Primary structure of high molecular weight tau present in the peripheral nervous system." Proc. Natl. Acad. Sci. U.S.A. *89*: 4378-4381.

Crowther, R. A., and Wischik, C. M. (1985). "Image reconstruction of the Alzheimer paired helical filament." EMBO J. *4*: 3661-3665.

Crowther, R. A. (1991). "Straight and paired helical filaments in Alzheimer disease have a common structural unit." Proc. Natl. Acad. Sci. U.S.A. *88*: 2288-2292.

Cunningham, C. C., Leclerc, N., Flanagan, L. A., Lu, M., Janmey, P. A., and Kosik, K. S. (1997). "Microtubule-associated protein 2c reorganizes both microtubules and microfilaments into distinct cytological structures in an actin-binding protein-280-deficient melanoma cell line." J Cell Biol *136*(4): 845-857.

Dayanandan, R., Van Slegtenhorst, M., Mack, T. G., Ko, L., Yen, S. H., Leroy, K., Brion, J. P., Anderton, B. H., Hutton, M., and Lovestone, S. (1999). "Mutations in tau reduce its microtubule binding properties in intact cells and affect its phosphorylation." FEBS Lett *446*(2-3): 228-32.

Delacourte, A., Robitaille, Y., Sergeant, N., Buee, L., Hof, P. R., Wattez, A., Laroche-Cholette, A., Mathieu, J., Chagnon, P., and Gauvreau, D. (1996). "Specific pathological Tau protein variants characterize Pick's disease." Journal of Neuropathology and Experimental Neurology *55*(2): 159-168.

Delacourte, A. (1998). "Diagnosis of Alzheimer's disease." Ann Biol Clin (Paris) *56*(2): 133-42.

Dickson, D., Crystal, H., Bevona, C., Honer, W., Vincent, I., and Davies, P. (1995). "Correlations of synaptic and pathological markers with cognitive of the elderly." Neurobiol. Aging *16*: 285-304.

Dill, K. A., and Shortle, D. (1991). "Denatured states of proteins." Annu Rev Biochem *60*: 795-825.

Drechsel, D. N., Hyman, A. A., Cobb, M. H., and Kirschner, M. W. (1992). "Modulation of the dynamic instability of tubulin assembly by the microtubule-associated protein tau." Mol. Biol. Cell *3*: 1141-1154.

Drewes, G., Lichtenberg-Kraag, B., Doring, F., Mandelkow, E. M., Biernat, J., Goris, J., Doree, M., and Mandelkow, E. (1992). "Mitogen activated protein (MAP) kinase transforms tau protein into an Alzheimer-like state." Embo J *11*(6): 2131-8.

Drewes, G., Trinczek, B., Illenberger, S., Biernat, J., Schmitt-Ulms, G., Meyer, H. E., Mandelkow, E. M., and Mandelkow, E. (1995). "Microtubule-associated protein/microtubule affinity-regulating kinase (p110mark). A novel protein kinase that regulates tau-microtubule interactions and dynamic instability by phosphorylation at the Alzheimer-specific site serine 262." J Biol Chem *270*(13): 7679-88.

Drewes, G., Ebneth, A., Preuss, U., Mandelkow, E. M., and Mandelkow, E. (1997). "MARK, a novel family of protein kinases that phosphorylate microtubule- associated proteins and trigger microtubule disruption." Cell *89*(2): 297-308.

Drubin, D., and Kirschner, M. (1986). "Tau protein function in living cells." J. Cell Biol. *103*: 2739-2746.

D'Souza, I., Poorkaj, P., Hong, M., Nochlin, D., Lee, V. M., Bird, T. D., and Schellenberg, G. D. (1999). "Missense and silent tau gene mutations cause frontotemporal dementia with parkinsonism-chromosome 17 type, by affecting multiple alternative RNA splicing regulatory elements." Proc Natl Acad Sci U S A *96*(10): 5598-603.

D'Souza, I., and Schellenberg, G. D. (2000). "Determinants of 4-repeat tau expression. Coordination between enhancing and inhibitory splicing sequences for exon 10 inclusion." J Biol Chem *275*(23): 17700-9.

D'Souza, I., and Schellenberg, G. D. (2002). "tau Exon 10 expression involves a bipartite intron 10 regulatory sequence and weak 5' and 3' splice sites." J Biol Chem *277*(29): 26587-99.

Ebneth, A., Godemann, R., Stamer, K., Illenberger, S., Trinczek, B., and Mandelkow, E. (1998). "Overexpression of tau protein inhibits kinesin-dependent trafficking of vesicles, mitochondria, and endoplasmic reticulum: implications for Alzheimer's disease." J Cell Biol *143*(3): 777-794.

Eftink, M. R., and Ghiron, C. A. (1976). "Exposure of tryptophanyl residues in proteins. Quantitative determination by fluorescence quenching studies." Biochemistry *15*(3): 672-80.

Eftink, M. R., and Ghiron, C. A. (1977). "Exposure of tryptophanyl residues and protein dynamics." Biochemistry *16*(25): 5546-51.

Eftink, M. R. (1991). "Fluorescence techniques for studying protein structure." Methods Biochem Anal *35*: 127-205.

Eisinger, J. (1969). "Intramolecular energy transfer in adrenocorticotropin." Biochemistry *8*(10): 3902-8.

Esler, W. P., Stimson, E. R., Ghilardi, J. R., Lu, Y. A., Felix, A. M., Vinters, H. V., Mantyh, P. W., Lee, J. P., and Maggio, J. E. (1996). "Point substitution in the central hydrophobic cluster of a human beta- amyloid congener disrupts peptide folding and abolishes plaque competence." Biochemistry *35*(44): 13914-21.

Esmaeli-Azad, B., McCarty, J. H., and Feinstein, S. C. (1994). "Sense and antisense transfection analysis of tau function: tau influences net microtubule assembly, neurite outgrowth and neuritic stability." J Cell Sci *107*(Pt 4): 869-79.

Farzan, M., Schnitzler, C. E., Vasilieva, N., Leung, D., and Choe, H. (2000). "BACE2, a beta -secretase homolog, cleaves at the beta site and within the amyloid-beta region of the amyloid-beta precursor protein." Proc Natl Acad Sci U S A *97*(17): 9712-7.

Flanagan, L. A., Cunningham, C. C., Chen, J., Prestwich, G. D., Kosik, K. S., and Janmey, P. A. (1997). "The structure of divalent cation-induced aggregates of PIP2 and their alteration by gelsolin and tau." Biophys J *73*(3): 1440-1447.

Foster, N. L., Wilhelmsen, K., Sima, A. A., Jones, M. Z., D'Amato, C. J., and Gilman, S. (1997). "Frontotemporal dementia and parkinsonism linked to chromosome 17: a consensus conference." Ann Neurol *41*(6): 706-15.

Fraser, P. E., McLachlan, D. R., Surewicz, W. K., Mizzen, C. A., Snow, A. D., Nguyen, J. T., and Kirschner, D. A. (1994). "Conformation and fibrillogenesis of Alzheimer A beta peptides with selected substitution of charged residues." J Mol Biol *244*(1): 64-73.

Friedhoff, P., von Bergen, M., Mandelkow, E. M., Davies, P., and Mandelkow, E. (1998a). "A nucleated assembly mechanism of Alzheimer paired helical filaments." Proc Natl Acad Sci U S A *95*(26): 15712-15717.

Friedhoff, P., Schneider, A., Mandelkow, E. M., and Mandelkow, E. (1998b). "Rapid assembly of Alzheimer-like paired helical filaments from microtubule-associated protein tau monitored by fluorescence in solution." Biochemistry *37*(28): 10223-30.

Friedhoff, P., and Mandelkow, E. (1999). Tau Protein. In "Guidebooks to the Cytoskeletal," T. Kreis and R. Vale, eds. (Oxford: Oxford University Press).

Gamblin, T. C., King, M. E., Dawson, H., Vitek, M. P., Kuret, J., Berry, R. W., and Binder, L. I. (2000). "In vitro polymerization of tau protein monitored by laser light scattering: method and application to the study of FTDP-17 mutants." Biochemistry *39*(20): 6136-44.

Garzon-Rodriguez, W., Vega, A., Sepulveda-Becerra, M., Milton, S., Johnson, D. A., Yatsimirsky, A. K., and Glabe, C. G. (2000). "A conformation change in the carboxyl terminus of Alzheimer's Abeta (1- 40) accompanies the transition from dimer to fibril as revealed by fluorescence quenching analysis." J Biol Chem *275*(30): 22645-9.

Gaskin, F., Cantor, C. R., and Shelanski, M. L. (1974). "Turbidimetric studies of the in vitro assembly and disassembly of porcine neurotubules." J Mol Biol *89*(4): 737-55.

Gasymov, O. K., Abduragimov, A. R., Yusifov, T. N., and Glasgow, B. J. (2001). "Site-directed tryptophan fluorescence reveals the solution structure of tear lipocalin: evidence for features that confer promiscuity in ligand binding." Biochemistry *40*(49): 14754-62.

Ginsberg, S. D., Crino, P. B., Lee, V. M., Eberwine, J. H., and Trojanowski, J. Q. (1997). "Sequestration of RNA in Alzheimer's disease neurofibrillary tangles and senile plaques." Ann Neurol *41*(2): 200-9.

Ginsberg, S. D., Galvin, J. E., Chiu, T. S., Lee, V. M., Masliah, E., and Trojanowski, J. Q. (1998). "RNA sequestration to pathological lesions of neurodegenerative diseases." Acta Neuropathol (Berl) *96*(5): 487-494.

Goedert, M., Spillantini, M. G., Jakes, R., Rutherford, D., and Crowther, R. A. (1989a). "Multiple isoforms of human microtubule-associated protein tau: sequences and localization in neurofibrillary tangles of Alzheimer's disease." Neuron *3*(4): 519-26.

Goedert, M., Spillantini, M. G., Potier, M. C., Ulrich, J., and Crowther, R. A. (1989b). "Cloning and sequencing of the cDNA encoding an isoform of microtubule- associated protein tau containing four tandem repeats: differential expression of tau protein mRNAs in human brain." EMBO J *8*(2): 393-9.

Goedert, M., and Spillantini, M. G. (1990). "Molecular neuropathology of Alzheimer's disease: in situ hybridization studies." Cell Mol Neurobiol *10*(1): 159-74.

Goedert, M., Spillantini, M. G., and Crowther, R. A. (1992). "Cloning of a big tau microtubule-associated protein characteristic of the peripheral nervous-system." Proc. Nat. Acad. Sci. U.S.A. *89*: 1983-1987.

Goedert, M., Jakes, R., Spillantini, M. G., Hasegawa, M., Smith, M. J., and Crowther, R. A. (1996). "Assembly of microtubule-associated protein tau into Alzheimer-like filaments induced by sulfated glycosaminoglycans." Nature *383*: 550-553.

Goedert, M., Hasegawa, M., Jakes, R., Lawler, S., Cuenda, A., and Cohen, P. (1997). "Phosphorylation of microtubule-associated protein tau by stress- activated protein kinases." FEBS Lett *409*(1): 57-62.

Goedert, M. (1998). "Neurofibrillary pathology of Alzheimer's disease and other tauopathies." Prog Brain Res *117*: 287-306.

Goedert, M., Jakes, R., and Crowther, R. A. (1999a). "Effects of frontotemporal dementia FTDP-17 mutations on heparin-induced assembly of tau filaments." FEBS Lett *450*(3): 306-311.

Goedert, M., Spillantini, M. G., Crowther, R. A., Chen, S. G., Parchi, P., Tabaton, M., Lanska, D. J., Markesbery, W. R., Wilhelmsen, K. C., Dickson, D. W., Petersen, R. B., and Gambetti, P. (1999b). "Tau gene mutation in familial progressive subcortical gliosis." Nat Med *5*(4): 454-7.

Goode, B. L., and Feinstein, S. C. (1994). "Identification of a novel microtubule binding and assembly domain in the developmentally regulated inter-repeat region of tau." J Cell Biol *124*(5): 769-82.

Goode, B. L., Denis, P. E., Panda, D., Radeke, M. J., Miller, H. P., Wilson, L., and Feinstein, S. C. (1997). "Functional interactions between the proline-rich and repeat regions of tau enhance microtubule binding and assembly." Mol Biol Cell *8*(2): 353-65.

Gray, E. G., Paula-Barbosa, M., and Roher, A. (1987). "Alzheimer's disease: paired helical filaments and cytomembranes." Neuropathol Appl Neurobiol *13*(2): 91-110.

Greenfield, J. P., Gross, R. S., Gouras, G. K., and Xu, H. (2000). "Cellular and molecular basis of beta-amyloid precursor protein metabolism." Front Biosci *5*: D72-83.

Greenwood, J. A., Scott, C. W., Spreen, R. C., Caputo, C. B., and Johnson, G. V. (1994). "Casein kinase II preferentially phosphorylates human tau isoforms containing an amino-terminal insert. Identification of threonine 39 as the primary phosphate acceptor." J Biol Chem *269*(6): 4373-80.

Growdon, J. H. (1999). "Biomarkers of Alzheimer disease." Arch Neurol *56*(3): 281-3.

Gryczynski, I., Wiczk, W., Johnson, M. L., and Lakowicz, J. R. (1988). "Lifetime distributions and anisotropy decays of indole fluorescence in cyclohexane/ethanol mixtures by frequency-domain fluorometry." Biophys Chem *32*(2-3): 173-85.

Gu, Y., Oyama, F., and Ihara, Y. (1996). "Tau is widely expressed in rat tissues." J Neurochem *67*(3): 1235-44.

Gustke, N., Trinczek, B., Biernat, J., Mandelkow, E. M., and Mandelkow, E. (1994). "Domains of Tau protein and interactions with microtubules." Biochemistry *33*: 9511-9522.

Hanger, D. P., Hughes, K., Woodgett, J. R., Brion, J. P., and Anderton, B. H. (1992). "Glycogen synthase kinase-3 induces Alzheimer's disease-like phosphorylation of tau: generation of paired helical filament epitopes and neuronal localisation of the kinase." Neurosci Lett *147*(1): 58-62.

Haniu, M., Denis, P., Young, Y., Mendiaz, E. A., Fuller, J., Hui, J. O., Bennett, B. D., Kahn, S., Ross, S., Burgess, T., Katta, V., Rogers, G., Vassar, R., and Citron, M. (2000). "Characterization of Alzheimer's beta -secretase protein BACE. A pepsin family member with unusual properties." J Biol Chem *275*(28): 21099-106.

Harada, M., Isersky, C., Cuatrecasas, P., Page, D., Bladen, H. A., Eanes, E. D., Keiser, H. R., and Glenner, G. G. (1971). "Human amyloid protein: chemical variability and homogeneity." J Histochem Cytochem *19*(1): 1-15.

Hauw, J. J., Seilhean, D., Piette, F., Uchihara, T., and Duyckaerts, C. (1996). "Alzheimer's disease lesions: from morphology to cell biology." Bull Acad Natl Med *180*(7): 1687-700; discussion 1700-1.

Herzog, W., and Weber, K. (1978). "Fractionation of brain microtubule-associated proteins. Isolation of two different proteins which stimulate tubulin polymerization in vitro." Eur J Biochem *92*(1): 1-8.

Himmler, A., Drechsel, D., Kirschner, M., and Martin, D. (1989a). "Tau consists of a set of proteins with repeated C-terminal microtubule-binding domains and variable N-terminal domains." Molec. Cell. Biol. *9*: 1381-1388.

Himmler, A. (1989b). "Structure of the bovine tau gene: alternatively spliced transcripts generate a protein family." Mol Cell Biol *9*(4): 1389-96.

Hirokawa, N., Shiomura, Y., and Okabe, S. (1988). "Tau proteins: the molecular structure and mode of binding on microtubules." J Cell Biol *107*(4): 1449-59.

Hong, M., Zhukareva, V., Vogelsberg-Ragaglia, V., Wszolek, Z., Reed, L., Miller, B. I., Geschwind, D. H., Bird, T. D., McKeel, D., Goate, A., Morris, J. C., Wilhelmsen, K. C., Schellenberg, G. D., Trojanowski, J. Q., and Lee, V. M. (1998). "Mutation-specific functional impairments in distinct tau isoforms of hereditary FTDP-17." Science *282*(5395): 1914-7.

Hutton, M., Lendon, C. L., Rizzu, P., Baker, M., Froelich, S., Houlden, H., Pickering-Brown, S., Chakraverty, S., Isaacs, A., Grover, A., Hackett, J., Adamson, J., Lincoln, S., Dickson, D., Davies, P., Petersen, R. C., Stevens, M., de Graaff, E., Wauters, E., van Baren, J., Hillebrand, M., Joosse, M., Kwon, J. M., Nowotny, P., Heutink, P. (1998). "Association of missense and 5'-splice-site mutations in tau with the inherited dementia FTDP-17." Nature *393*(6686): 702-5.

Hyman, B. T., and Trojanowski, J. Q. (1997). "Consensus recommendations for the postmortem diagnosis of Alzheimer disease from the National Institute on Aging and the Reagan Institute Working Group on diagnostic criteria for the neuropathological assessment of Alzheimer disease." J Neuropathol Exp Neurol *56*(10): 1095-7.

Hyman, B. T. (1998). "New neuropathological criteria for Alzheimer disease." Arch Neurol *55*(9): 1174-6.

Hyman, B. T., Smith, C., Buldyrev, I., Whelan, C., Brown, H., Tang, M. X., and Mayeux, R. (2001). "Autoantibodies to amyloid-beta and Alzheimer's disease." Ann Neurol *49*(6): 808-10.

Ingelson, M., Vanmechelen, E., and Lannfelt, L. (1996). "Microtubule-associated protein tau in human fibroblasts with the Swedish Alzheimer mutation." Neurosci Lett *220*(1): 9-12.

Jakes, R., Novak, M., Davison, M., and Wischik, C. M. (1991). "Identification of 3- and 4-repeat tau isoforms within the PHF in Alzheimer's disease." EMBO J. *10*: 2725-2729.

Jenkins, S. M., and Johnson, G. V. (1998). "Tau complexes with phospholipase C-gamma in situ." Neuroreport *9*(1): 67-71.

Jicha, G. A., Bowser, R., Kazam, I. G., and Davies, P. (1997). "Alz-50 and MC-1, a new monoclonal antibody raised to paired helical filaments, recognize conformational epitopes on recombinant tau." J Neurosci Res *48*(2): 128-32.

Jicha, G. A., O'Donnell, A., Weaver, C., Angeletti, R., and Davies, P. (1999). "Hierarchical phosphorylation of recombinant tau by the paired-helical filament-associated protein kinase is dependent on cyclic AMP-dependent protein kinase." J Neurochem *72*(1): 214-224.

Johnson, G. V. (1992). "Differential phosphorylation of tau by cyclic AMP-dependent protein kinase and Ca2+/calmodulin-dependent protein kinase II: metabolic and functional consequences." J Neurochem *59*(6): 2056-62.

Johnson, G. V. W., and Hartigan, J. A. (1998). "Tau protein in normal and Alzheimer's disease brain: An update." Alzheimer's Dis. Rev. *3*: 125-141.

Jordan, M. A., and Wilson, L. (1998). "Microtubules and actin filaments: dynamic targets for cancer chemotherapy." Curr Opin Cell Biol *10*(1): 123-30.

Kampers, T., Friedhoff, P., Biernat, J., and Mandelkow, E. M. (1996). "RNA stimulates aggregation of microtubule-associated protein-tau into Alzheimer-like paired helical filaments." FEBS Letters *399*(3)): 344-349.

Kirschner, D. A., Abraham, C., and Selkoe, D. J. (1986). "X-ray diffraction from intraneural paired helical filaments and extraneural amyloid fibers in Alzheimer disease indicates cross-β conformation." Proc. Natl. Acad. Sci. U.S.A. *83*: 503-507.

Kirschner, D. A., Inouye, H., Duffy, L. K., Sinclair, A., Lind, M., and Selkoe, D. J. (1987). "Synthetic peptide homologous to beta protein from Alzheimer disease forms amyloid-like fibrils in vitro." Proc Natl Acad Sci U S A *84*(19): 6953-7.

Kosik, K., Orecchio, L., Binder, L., Trojanowski, J., Lee, V., and Lee, G. (1988). "Epitopes that span the tau molecule are shared with paired helical filaments." Neuron *1*: 817-825.

Ksiezak-Reding, H., Morgan, K., Mattiace, L. A., Davies, P., Liu, W. K., Yen, S. H., Weidenheim, K., and Dickson, D. W. (1994). "Ultrastructure and biochemical composition of paired helical filaments in corticobasal degeneration." American Journal of Pathology *145*(6): 1496-508.

Laemmli, U. K. (1970). "Cleavage of structural proteins during the assembly of the head of bacteriophage T4." Nature *227*(259): 680-5.

Lai, Z., McCulloch, J., Lashuel, H. A., and Kelly, J. W. (1997). "Guanidine hydrochloride-induced denaturation and refolding of transthyretin exhibits a marked hysteresis: equilibria with high kinetic barriers." Biochemistry *36*(33): 10230-9.

Lakowicz, J. R. (1999). "Principles of Fluorescence Spectroscopy, second edition." (Kluwer Academic/Plenum Publishers): 445-86.

Lansbury, P. J. (1997). "Structural neurology: are seeds at the root of neuronal degeneration?" Neuron *19*(6): 1151-1154.

Lansbury, P. T., Jr., and Kosik, K. S. (2000). "Neurodegeneration: new clues on inclusions." Chem Biol *7*(1): R9-R12.

Ledesma, M. D., Bonay, P., Colaco, C., and Avila, J. (1994). "Analysis of microtubule-associated protein tau glycation in paired helical filaments." J Biol Chem *269*(34): 21614-9.

Lee, G., Cowan, N., and Kirschner, M. (1988). "The primary structure and heterogeneity of tau protein from mouse brain." Science *239*: 285-288.

Lee, G., Newman, S. T., Gard, D. L., Band, H., and Panchamoorthy, G. (1998). "Tau interacts with src-family non-receptor tyrosine kinases." J Cell Sci *111*(Pt 21): 3167-77.

Liao, H., Li, Y., Brautigan, D. L., and Gundersen, G. G. (1998). "Protein phosphatase 1 is targeted to microtubules by the microtubule- associated protein Tau." J Biol Chem *273*(34): 21901-8.

Lichtenberg-Kraag, B., Mandelkow, E. M., Biernat, J., Steiner, B., Schroter, C., Gustke, N., Meyer, H. E., and Mandelkow, E. (1992). "Phosphorylation-dependent epitopes of neurofilament antibodies on tau protein and relationship with Alzheimer tau." Proc Natl Acad Sci U S A *89*(12): 5384-8.

Lindwall, G., and Cole, R. D. (1984). "The purification of tau protein and the occurrence of two phosphorylation states of tau in brain." J Biol Chem *259*(19): 12241-5.

Lovestone, S., and Reynolds, C. H. (1997). "The phosphorylation of tau: a critical stage in neurodevelopment and neurodegenerative processes." Neuroscience *78*(2): 309-24.

Mandelkow, E. M., Herrmann, M., and Ruhl, U. (1985). "Tubulin domains probed by limited proteolysis and subunit-specific antibodies." J Mol Biol *185*(2): 311-27.

Mandelkow, E. M., Drewes, G., Biernat, J., Gustke, N., Van Lint, J., Vandenheede, J. R., and Mandelkow, E. (1992). "Glycogen synthase kinase-3 and the Alzheimer-like state of microtubule- associated protein tau." FEBS Lett *314*(3): 315-21.

Mandelkow, E. M., and Mandelkow, E. (1998). "Tau in Alzheimer's disease." Trends Cell Biol *8*(11): 425-427.

Matsudaira, P. T., and Burgess, D. R. (1978). "SDS microslab linear gradient polyacrylamide gel electrophoresis." Anal Biochem *87*(2): 386-96.

McLaurin, J., Franklin, T., Zhang, X., Deng, J., and Fraser, P. E. (1999). "Interactions of Alzheimer amyloid-beta peptides with glycosaminoglycans effects on fibril nucleation and growth." Eur J Biochem *266*(3): 1101-10.

Moller, H. J. (1999). "Reappraising neurotransmitter-based strategies." Eur Neuropsychopharmacol *9 Suppl 2*: S53-9.

Murrell, J. R., Spillantini, M. G., Zolo, P., Guazzelli, M., Smith, M. J., Hasegawa, M., Redi, F., Crowther, R. A., Pietrini, P., Ghetti, B., and Goedert, M. (1999). "Tau gene mutation G389R causes a tauopathy with abundant pick body-like inclusions and axonal deposits." J Neuropathol Exp Neurol *58*(12): 1207-26.

Nagy, Z., Vatter-Bittner, B., Braak, H., Braak, E., Yilmazer, D. M., Schultz, C., and Hanke, J. (1997). "Staging of Alzheimer-type pathology: an interrater-intrarater study." Dement Geriatr Cogn Disord *8*(4): 248-51.

Nelson, P. T., Stefansson, K., Gulcher, J., and Saper, C. B. (1996). "Molecular evolution of tau-protein - implications for Alzheimer's-disease." Journal of Neurochemistry *67*(4)): 1622-1632.

Neve, R. L., Selkoe, D. J., Kurnit, D. M., and Kosik, K. S. (1986). "A cDNA for a human microtubule associated protein 2 epitope in the Alzheimer neurofibrillary tangle." Brain Res *387*(2): 193-6.

Nicolau, C., Greferath, R., Balaban, T. S., Lazarte, J. E., and Hopkins, R. J. (2002). "A liposome-based therapeutic vaccine against beta -amyloid plaques on the pancreas of transgenic NORBA mice." Proc Natl Acad Sci U S A *99*(4): 2332-7.

Nixon, R. A., and Sihag, R. K. (1991). "Neurofilament phosphorylation: a new look at regulation and function." Trends Neurosci *14*(11): 501-6.

Novak, M., Kabat, J., and Wischik, C. M. (1993). "Molecular characterization of the minimal protease resistant tau-unit of the Alzheimer's-disease paired helical filament." EMBO J. *12*: 365-370.

Peretz, D., Williamson, R. A., Matsunaga, Y., Serban, H., Pinilla, C., Bastidas, R. B., Rozenshteyn, R., James, T. L., Houghten, R. A., Cohen, F. E., Prusiner, S. B., and Burton, D. R. (1997). "A conformational transition at the N terminus of the prion protein features in formation of the scrapie isoform." J Mol Biol *273*(3): 614-22.

Perez, M., Valpuesta, J. M., Medina, M., Montejo de Garcini, E., and Avila, J. (1996). "Polymerization of tau into filaments in the presence of heparin: the minimal sequence required for tau-tau interaction." J Neurochem *67*(3): 1183-90.

Perry, G., Siedlak, S. L., Richey, P., Kawai, M., Cras, P., Kalaria, R. N., Galloway, P. G., Scardina, J. M., Cordell, B., Greenberg, B. D. (1991). "Association of heparan sulfate proteoglycan with the neurofibrillary tangles of Alzheimer's disease." J Neurosci *11*(11): 3679-3683.

Pike, C. J., Walencewicz-Wasserman, A. J., Kosmoski, J., Cribbs, D. H., Glabe, C. G., and Cotman, C. W. (1995). "Structure-activity analyses of beta-amyloid peptides: contributions of the beta 25-35 region to aggregation and neurotoxicity." J Neurochem *64*(1): 253-65.

Pitschke, M., Prior, R., Haupt, M., and Riesner, D. (1998). "Detection of single amyloid beta-protein aggregates in the cerebrospinal fluid of Alzheimer's patients by fluorescence correlation spectroscopy." Nat Med *4*(7): 832-4.

Poorkaj, P., Bird, T. D., Wijsman, E., Nemens, E., Garruto, R. M., Anderson, L., Andreadis, A., Wiederholt, W. C., Raskind, M., and Schellenberg, G. D. (1998). "Tau is a candidate gene for chromosome 17 frontotemporal dementia." Ann Neurol *43*(6): 815-25.

Prusiner, S. B. (1998). "Prions." Proc Natl Acad Sci U S A *95*(23): 13363-83.

Reszka, A. A., Seger, R., Diltz, C. D., Krebs, E. G., and Fischer, E. H. (1995). "Association of mitogen-activated protein-kinase with the microtubule cytoskeleton." Proc. Natl. Acad. Sci. USA *92*: 8881-8885.

Reynolds, C. H., Utton, M. A., Gibb, G. M., Yates, A., and Anderton, B. H. (1997). "Stress-activated protein kinase/c-jun N-terminal kinase phosphorylates tau protein." J Neurochem *68*(4): 1736-44.

Ritchie, K., and Touchon, J. (2000). "Mild cognitive impairment: conceptual basis and current nosological status." Lancet *355*(9199): 225-8.

Rizzu, P., Van Swieten, J. C., Joosse, M., Hasegawa, M., Stevens, M., Tibben, A., Niermeijer, M. F., Hillebrand, M., Ravid, R., Oostra, B. A., Goedert, M., van Duijn, C. M., and Heutink, P. (1999). "High prevalence of mutations in the microtubule-associated protein tau in a population study of frontotemporal dementia in the Netherlands." Am J Hum Genet *64*(2): 414-21.

Rochet, J. C., and Lansbury, P. T., Jr. (2000). "Amyloid fibrillogenesis: themes and variations." Curr Opin Struct Biol *10*(1): 60-8.

Roher, A., Palmer, K., Chau, V., and Ball, M. (1988). "Isolation and chemical characterization of Alzheimer's disease paired helical filament cytoskeletons: Differentiation from amyloid plaque core protein." J. Cell Biol. *107*: 2703-2716.

Ropson, I. J., and Dalessio, P. M. (1997). "Fluorescence spectral changes during the folding of intestinal fatty acid binding protein." Biochemistry *36*(28): 8594-601.

Samuel, W., Galasko, D., Masliah, E., and Hansen, L. A. (1996). "Neocortical lewy body counts correlate with dementia in the Lewy body variant of Alzheimer's disease." J Neuropathol Exp Neurol *55*(1): 44-52.

Samuel, W., Crowder, R., Hofstetter, C. R., and Hansen, L. (1997). "Neuritic plaques in the Lewy body variant of Alzheimer disease lack paired helical filaments." Neurosci Lett *223*(2): 73-6.

Sanger, F., Nicklen, S., and Coulson, A. R. (1977). "DNA sequencing with chain-terminating inhibitors." Proc Natl Acad Sci U S A *74*(12): 5463-7.

Sauder, J. M., Arthur, J. W., and Dunbrack, R. L., Jr. (2000). "Modeling of substrate specificity of the Alzheimer's disease amyloid precursor protein beta-secretase." J Mol Biol *300*(2): 241-8.

Schenk, D., Barbour, R., Dunn, W., Gordon, G., Grajeda, H., Guido, T., Hu, K., Huang, J., Johnson-Wood, K., Khan, K., Kholodenko, D., Lee, M., Liao, Z., Lieberburg, I., Motter, R., Mutter, L., Soriano, F., Shopp, G., Vasquez, N., Vandevert, C., Walker, S., Wogulis, M., Yednock, T., Games, D., and Seubert, P. (1999). "Immunization with amyloid-beta attenuates Alzheimer-disease-like pathology in the PDAPP mouse." Nature *400*(6740): 173-7.

Schneider, A., Biernat, J., von Bergen, M., Mandelkow, E., and Mandelkow, E. M. (1999). "Phosphorylation that detaches tau protein from microtubules (Ser262, Ser214) also protects it against aggregation into Alzheimer paired helical filaments." Biochemistry *38*(12): 3549-3558.

Schweers, O., Schonbrunn-Hanebeck, E., Marx, A., and Mandelkow, E. (1994). "Structural studies of tau protein and Alzheimer paired helical filaments show no evidence for beta-structure." J Biol Chem *269*(39): 24290-7.

Schweers, O., Mandelkow, E. M., Biernat, J., and Mandelkow, E. (1995). "Oxidation of cysteine-322 in the repeat domain of microtubule- associated protein tau controls the in vitro assembly of paired helical filaments." Proc Natl Acad Sci U S A *92*(18): 8463-7.

Selkoe, D. J. (2001). "Alzheimer's disease: genes, proteins, and therapy." Physiol Rev *81*(2): 741-66.

Serpell, L. C., Fraser, P. E., and Sunde, M. (1999). "X-ray fiber diffraction of amyloid fibrils." Methods Enzymol *309*: 526-36.

Shastry, B. S., and Giblin, F. J. (1999). "Genes and susceptible loci of Alzheimer's disease." Brain Res Bull *48*(2): 121-7.

Shopova, M. and Genov, N. (1983). "Protonated form of histidine 238 quenches the fluorscence of tryptophan 241 in subtilisin novo." Int. J. Peptide Protein Res. *21*: 475-478.

Shortle, D., Meeker, A. K., and Gerring, S. L. (1989). "Effects of denaturants at low concentrations on the reversible denaturation of staphylococcal nuclease." Arch Biochem Biophys *272*(1): 103-13.

Sirvio, J. (1999). "Strategies that support declining cholinergic neurotransmission in Alzheimer's disease patients." Gerontology *45*(Suppl 1): 3-14.

Snow, A. D., Lara, S., Nochlin, D., and Wight, T. N. (1989). "Cationic dyes reveal proteoglycans structurally integrated within the characteristic lesions of Alzheimer's disease." Acta Neuropathol *78*(2): 113-123.

Snow, A. D., Mar, H., Nochlin, D., Sekiguchi, R. T., Kimata, K., Koike, Y., and Wight, T. N. (1990). "Early accumulation of heparan sulfate in neurons and in the beta-amyloid protein-containing lesions of Alzheimer's disease and Down's syndrome." Am J Pathol *137*(5): 1253-1270.

Sontag, E., Nunbhakdi-Craig, V., Lee, G., Bloom, G. S., and Mumby, M. C. (1996). "Regulation of the phosphorylation state and microtubule-binding activity of Tau by protein phosphatase 2A." Neuron *17*(6): 1201-1207.

Sorbi, S., Forleo, P., Tedde, A., Cellini, E., Ciantelli, M., Bagnoli, S., and Nacmias, B. (2001). "Genetic risk factors in familial Alzheimer's disease." Mech Ageing Dev *122*(16): 1951-60.

Spillantini, M. G., Goedert, M., Jakes, R., and Klug, A. (1990). "Topographical relationship between beta-amyloid and tau protein epitopes in tangle-bearing cells in Alzheimer disease." Proc Natl Acad Sci U S A *87*(10): 3952-6.

Spillantini, M. G., Goedert, M., Crowther, R. A., Murrell, J. R., Farlow, M. R., and Ghetti, B. (1997). "Familial multiple system tauopathy with presenile dementia: a disease with abundant neuronal and glial tau filaments." Proc Natl Acad Sci U S A **94**(8): 4113-8.

Spillantini, M. G., Murrell, J. R., Goedert, M., Farlow, M. R., Klug, A., and Ghetti, B. (1998). "Mutation in the tau gene in familial multiple system tauopathy with presenile dementia." Proc Natl Acad Sci U S A **95**(13): 7737-41.

Steiner, B., Mandelkow, E. M., Biernat, J., Gustke, N., Meyer, H. E., Schmidt, B., Mieskes, G., Soling, H. D., Drechsel, D., Kirschner, M. W. (1990). "Phosphorylation of microtubule-associated protein tau: identification of the site for Ca2(+)-calmodulin dependent kinase and relationship with tau phosphorylation in Alzheimer tangles." EMBO J **9**(11): 3539-44.

Studier, F. W., Rosenberg, A. H., Dunn, J. J., and Dubendorff, J. W. (1990). "Use of T7 RNA polymerase to direct expression of cloned genes." Methods Enzymol **185**: 60-89.

Surewicz, W. K., Mantsch, H. H., and Chapman, D. (1993). "Determination of protein secondary structure by Fourier transform infrared spectroscopy: a critical assessment." Biochemistry **32**(2): 389-94.

Susi, H., and Byler, D. M. (1983). "Protein structure by Fourier transform infrared spectroscopy: second derivative spectra." Biochem Biophys Res Commun **115**(1): 391-7.

Takano, K., Funahashi, J., and Yutani, K. (2001). "The stability and folding process of amyloidogenic mutant human lysozymes." Eur J Biochem **268**(1): 155-9.

Trinczek, B., Biernat, J., Baumann, K., Mandelkow, E. M., and Mandelkow, E. (1995). "Domains of tau protein, differential phosphorylation, and dynamic instability of microtubules." Mol Biol Cell **6**(12): 1887-902.

Vanier, M. T., Neuville, P., Michalik, L., and Launay, J. F. (1998). "Expression of specific tau exons in normal and tumoral pancreatic acinar cells." J Cell Sci **111**(Pt 10): 1419-32.

Vehmas, A. K., Borchelt, D. R., Price, D. L., McCarthy, D., Wills-Karp, M., Peper, M. J., Rudow, G., Luyinbazi, J., Siew, L. T., and Troncoso, J. C. (2001). "beta-Amyloid peptide vaccination results in marked changes in serum and brain Abeta levels in APPswe/PS1DeltaE9 mice, as detected by SELDI-TOF- based ProteinChip technology." DNA Cell Biol **20**(11): 713-21.

Vickers, J. C., Dickson, T. C., Adlard, P. A., Saunders, H. L., King, C. E., and McCormack, G. (2000). "The cause of neuronal degeneration in Alzheimer's disease." Prog Neurobiol **60**(2): 139-65.

Virginia M-Y Lee, M. G., and John Q Trojanowski (2001). "Neurodegenerative tauopathies." Annu. Rev. Neurosci. **24**: 1121-159.

von Bergen, M., Friedhoff, P., Biernat, J., Heberle, J., Mandelkow, E. M., and Mandelkow, E. (2000). "Assembly of tau protein into Alzheimer paired helical filaments depends on a local sequence motif ((306)VQIVYK(311)) forming beta structure." Proc Natl Acad Sci U S A *97*(10): 5129-34.

von Bergen, M., Barghorn, S., Li, L., Marx, A., Biernat, J., Mandelkow, E. M., and Mandelkow, E. (2001). "Mutations of tau protein in frontotemporal dementia promote aggregation of paired helical filaments by enhancing local beta-structure." J Biol Chem *276*(21): 48165-74.

Wallon, G., Rappsilber, J., Mann, M., and Serrano, L. (2000). "Model for stathmin/OP18 binding to tubulin." EMBO J *19*(2): 213-22.

Walsh, D. M., Klyubin, I., Fadeeva, J. V., Cullen, W. K., Anwyl, R., Wolfe, M. S., Rowan, M. J., and Selkoe, D. J. (2002). "Naturally secreted oligomers of amyloid beta protein potently inhibit hippocampal long-term potentiation in vivo." Nature *416*(6880): 535-9.

Wanker, E. E. (2000). "Protein aggregation and pathogenesis of Huntington's disease: mechanisms and correlations." Biol Chem *381*(9-10): 937-42.

Weingarten, M. D., Lockwood, A. H., Hwo, S. Y., and Kirschner, M. W. (1975). "A protein factor essential for microtubule assembly." Proc Natl Acad Sci U S A *72*(5): 1858-62.

Wille, H., Drewes, G., Biernat, J., Mandelkow, E. M., and Mandelkow, E. (1992). "Alzheimer-like paired helical filaments and antiparallel dimers formed from microtubule-associated protein tau in vitro." J. Cell Biol. *118*: 573-584.

Wilson, D. M., and Binder, L. I. (1997). "Free fatty acids stimulate the polymerization of tau and amyloid beta peptides. In vitro evidence for a common effector of pathogenesis in Alzheimer's disease." Am J Pathol *150*(6): 2181-95.

Wischik, C. M., Novak, M., Edwards, P. C., Klug, A., Tichelaar, W., and Crowther, R. A. (1988a). "Structural characterization of the core of the paired helical filament of Alzheimer disease." Proc Natl Acad Sci U S A *85*(13): 4884-8.

Wischik, C., Novak, M., Thogersen, H., Edwards, P., Runswick, M., Jakes, R., Walker, J., Milstein, C., Roth, M., and Klug, A. (1988b). "Isolation of a fragment of tau derived from the core of the paired helical filament of Alzheimer disease." Proc. Natl. Acad. Sci. U.S.A. *85*: 4506-4510.

Wood, S. J., Wetzel, R., Martin, J. D., and Hurle, M. R. (1995). "Prolines and amyloidogenicity in fragments of the Alzheimer's peptide beta/A4." Biochemistry *34*(3): 724-30.

VII. Appendices

1. Abbreviations

Aβ	Amyloid β-peptide
AD	Alzheimer's disease
ApoE	Apoliprotein E
APP	β-amyloid precursor protein
bp	Base pair
BSA	Bovine serum albumin
CBD	Corticobasal degeneration
CD	Circular dichroism spectroscopy
DNA	Desoxyribonucleic acid
DTT	Dithiothreitol
E.coli	*Escherichia coli*
EDTA	Ethylene diaminetetraacetic acid
EGTA	Ethylenglycol-bis-(2-aminoethyl-ether)-N,N,N,N,-tetraacetic acid
EM	Electron microscopy
FAD	Familial Alzheimer's disease
FRET	Fluorescence resonance energy transfer
FTDP-17	Frontotemporal dementia and parkinsonism linked to chromosome 17
FTIR	Fourier transform infrared spectroscopy
GuHCl	Guanidine hydrochloride
HEPES	N-2-hydroxyethylpiperazine-N'-2-ethanesulfonic acid
HPLC	High performance liquid chromatography
htau	Human tau
IPTG	Isopropyl-β, D-thiogalacto-pyranoside
kb	Kilobase
kDa	Kilodalton
LB	Luria Bertani
MAP	Microtubule associated protein

MARK	Microtubule affinity regulating kinase
MES	2-(N-morpholino) ethanesulfonic acid
MOPS	3-(N-morpholino) propanesulfonic acid
mRNA	Messenger ribonucleic acid
MT	Microtubule
MW	Molecular weight
NFT	Neuro fibrillary tangle
OD	Optical density
PAGE	Polyacrylamide gel electrophoresis
PBS	Phosphate buffered saline
PCR	Polymerase chain reaction
Phe	Phenylalanine
PHF	Paired helical filaments
PiD	Pick's disease
PMSF	Phenylmethylsulfonyl fluorid
Pro	Proline
PS1	Presenilin 1
PS2	Presenilin 2
rpm	Revolution per minute
SDS	Sodium dodecyl sulfate
TEMED	N, N, N', N'-tetra methylethylene diamine
ThS	Thioflavine S
TP/SP	Threonine-Proline/Serine-Proline
Trp	Tryptophan
Tris	Tris (hydroxymethyl) aminomethane
Tyr	Tyrosine
v/v	Volume/volume
w/v	Weight/volume
wt	Wild type

2. Primer sequences for the mutations of tau protein

ΔK280:

5'   GGAAGGTGCAGATAATTAACAAGCTGGATCTTAGCAACG   3'

3'   CCTTCCACGTCTATTAATTGTTCGACCTAGAATCGTTGC   5'

I277P:

5'   GCGGGAAGGTGCAGCCAATTAATAAGAAGCTTGATCTTAGCAACGTC   3'

3'   GACGTTGCTAAGATCAAGCTTCTTATTAATTGGCTGCACCTTCCCGC   5'

I308P:

5'   GGAGGGAAGGTGCAACCAGTCTACAAACCAGTCGACCTGAGCAAGGTG   3'

3'   CACCTTGCTCAGGTCGACTGGTTTGTAGACTGGTTGCACCTTCCCGCC   5'

ΔK280-I277P:

5'   GCGGGAAGGTGCAGCCAATTAACAAGCTTGATCTTAGCAACGTC   3'

3'   GACGTTGCTAAGATCAAGCTTGTTAATTGGCTGCACCTTCCCGC   5'

ΔK280-I308P:

5'   GGCGGCAGTGTGCAACCAGTCTACAAACCAGTCGACCTGAGCAAGGTG   3'

3'   CACCTTGCTCAGGTCGACTGGTTTGTAGACTGGTTGCACACTGCCGCC   5'

Q244W:

5'   CTTTAAGAAGGAGATATTCATATGTGGACAGCCCCCGTGCCCATGCCAGAC   3'

3'   GTCTGGCATGGGCACGGGGGCTGTCCACATATGGATATCTCCTTCTTAAAG   5'

L266W:

5'   GCCTCCCGGCTGGTGCTTCCAGTTCTCAGTCGACCCGATCTTGGACTTGAC   3'

3'   GTCAAGTCCAAGATCGGGTCGACTGAGAACTGGAAGCACCAGCCGGGAGGC   5'

<u>I297W:</u>

5'   CACACTGCCGCCTCCGGGGACGTGTTTCCAATTATCCTTTGAGCCACA   3'

3'   TGTGGCTCAAAGGATAATTGGAAACACGTCCCCGGAGGCGGCAGTGTG   5'

<u>I328W:</u>

5'   TACTTCCACCTGGCCACCTCCTGGTTTATGATGGATGTTGCCTAATGAGCCACA   3'

3'   TGTGGCTCATTAGGCAACATCCATCATAAACCAGGAGGTGGCCAGGTGGAAGTA   5'

<u>F346W:</u>

5'   AATCTTCGACTGGACTCTATCCTTCCAGTCAAGCTTCTCAGATTT   3'

3'   AAATCTGAGAAGCTTGACTGGAAGGATAGAGTCCAGTCGAAGATT   5'

<u>I360W:</u>

5'   TCGAAGATTGGGTCCCTGGACAATTGGACCCACGTCCCGGGCGGAGGAAAT   3'

3'   ATTTCCTCCGCCCGGGACGTGGGTCCAATTGTCCAGGGACCCAATCTTCGA   5'

<u>Y310W:</u>

5'   GTGCAAATAGTCTGGAAACCAGTCGACCTGAGCAAGGTG   3'

3'   CACCTTGCTCAGGTCGACTGGTTTCCAGACTATTTGCAC   5'

3. List of the figures

4. List of the tables

5. Curriculum Vitae

Personal data:

Name: Li Li

Born: 04.08.1971 **in**: Jilin, China

Family status: married

University education:

1989-1993: Study of Natural Pharmacochemistry at the *Changchun college of Traditional Chinese Medicine. China.* Finished with Bachelor degree.
Thesis title "Pharmacological research of Chinese medicine – Meng chong".

1993-1997: Study of Biology at the *Jinan University, Guangzhou, China.* Finished with Master degree.
Thesis title "High-level expression in Pichia pastoris and purification of recombinant β-subunit of human chorionic gonadotropin".

1999-2002: PhD-student at the *Max-Planck-Unit for Structural Molecular Biology* in Hamburg.
Thesis title "Tryptophan and proline scanning mutagenesis: A tool to study the aggregation of tau protein into Alzheimer-PHFs".

6. Declaration (Erklärung)

I declare that I have carried out this thesis by myself and have not used external help except where explicitly indicated.

This thesis was not submitted to any other university.

I did not make any earlier attempt to submit this work as a doctoral thesis.

Hamburg, 07, Nov. 2002

Hiermit erkläre ich, daß ich die vorliegende Arbeit selbständig und ohne fremde Hilfe verfaßt, andere als die angegebenen Quellen und Hilfsmittel nicht benutzt und die den verwendeten Werken wörtlich oder inhaltlich entnommenen Stellen als solche kenntlich gemacht habe.

Ferner versichere ich, daß ich diese Dissertation noch an keiner anderen Universität eingereicht habe, um ein Promotionsverfahren eröffnen zu lassen.

Hiermit erkläre ich auch, daß ich keine anderen früheren Versuche gemacht habe, die Arbeit zur Promotion einzureichen.

Hamburg, 07, Nov. 2002